

The evolution of subsurface urban heat islands under the circumstances of climate change

**Dissertation
zur Erlangung des
Doktorgrades der Naturwissenschaften (Dr. rer. nat.)**

der

Naturwissenschaftlichen Fakultät III
Agrar- und Ernährungswissenschaften,
Geowissenschaften und Informatik

der Martin-Luther-Universität Halle-Wittenberg

vorgelegt von

Herrn Hemmerle, Hannes
Geb. am 23.06.1991 in Bamberg

Gutachter

Prof. Dr. Peter Bayer
PD Dr. Jannis Epting

Tag der Verteidigung: 27. Juli 2023

Abstract

The temperature of the shallow subsurface exhibits recent changes that are caused by climate change at the surface and local anthropogenic heat sources. The typical rise in temperature can trigger detrimental changes in groundwater quality and stress on underground and dependent ecosystems. Contrarily, an elevated ground temperature benefits the utilization of shallow geothermal energy for heating purposes. Both, the subsurface temperature rise and the demand for space heating are most pronounced under urban agglomerations. Often temperatures in associated subsurface urban heat islands are several degrees higher compared to natural conditions. Especially in mixed rural-urban environments the temperature rise caused by direct anthropogenic heat emission and climate change mingles, which makes it hard to differentiate between climate driven and local anthropogenic effects. Typically, monitoring networks are not designed to capture the heterogeneity of urban (thermal) ground conditions, which results in poor data availability especially over longer time periods and thus a lack of studies in this field. In this work, a unique dataset for the City of Cologne is utilized to describe the evolution of a subsurface urban heat island over the past five decades. This overarching objective is complemented by an estimation method for groundwater temperature in data-sparse areas and a case study on isolated climate change effects in exclusively natural environments. The estimation of subsurface temperature in mixed rural-urban environments is applied to the cities of Paris and Cologne at an average error of below 1 K. However, due to the coarse ground resolution (approx. 1km), this approach suffers to resolve local variability at district scale and below. The isolated climate change in natural environments was quantified based on repeated temperature logs for a set of wells located in Bavaria. Compared to the rate of change in air temperature, the temperature rise at 20 m depth is roughly 20% lower, and is further decreasing towards greater depths. In Cologne, the temperature underneath the outskirts and outer city shows a comparable trend, whereas the groundwater temperature rise underneath the urban centre significantly exceeds the rise in above ground temperatures. For Cologne, this rise in temperature translates to a heat gain of the aquifer in the magnitude of 1% of the city's heating demand per year.

Zusammenfassung

Die Temperatur des oberflächennahen Untergrunds weist in jüngster Zeit Veränderungen auf, die global durch den Klimawandel und lokal durch anthropogene Effekte ausgelöst werden. Die typischerweise ansteigenden Temperaturen können negative Auswirkungen auf die Grundwasserqualität, sowie auf unterirdische und vom Grundwasser abhängige Ökosysteme, haben. Umgekehrt begünstigt eine erhöhte Untergrundtemperatur die Nutzung der oberflächennahen Geothermie zu Heizzwecken. Sowohl der Anstieg der Untergrundtemperatur als auch der Raumwärmebedarf sind in städtischen Ballungsräumen am stärksten ausgeprägt. In den damit verbundenen urbanen Wärmeinseln im Untergrund sind die Grundwassertemperaturen oft um mehrere Grad wärmer als unter natürlichen Bedingungen im Umland. Insbesondere am Übergang zwischen dem ländlichen und städtischen Raum vermischen sich direkt anthropogene Wärmeemissionen mit dem durch den Klimawandel verursachten graduellen Temperaturanstieg, so dass es schwierig ist, zwischen klimabedingten und lokalen Auswirkungen zu unterscheiden. Das bestehende Grundwassermonitoring ist nicht darauf ausgelegt, diese Heterogenität des städtischen Untergrundes zu erfassen. Auf Grund der schlechten Datenverfügbarkeit gibt es, vor allem über Zeiträume von mehr als 10 Jahren, nur wenige Studien in diesem Bereich. Ziel dieser Arbeit ist es die Entwicklung einer urbanen Wärmeinsel im Untergrund über die letzten fünf Jahrzehnte, anhand eines einzigartigen Datensatzes für die Stadt Köln, zu beschreiben. Daneben werden diese Erkenntnisse durch eine Fernerkundungsmethode zur Abschätzung der Grundwassertemperatur in datenarmen Gebieten, sowie eine Fallstudie zu den Auswirkungen des Klimawandels in ausschließlich natürlichen Umgebungen, ergänzt. Das Abschätzungsverfahren zur Grundwassertemperatur liefert, für die gemischt ländlich-städtischen Metropolregionen Paris und Köln, einen durchschnittliche Prognosefehler von unter 1 K. Aufgrund der groben räumlichen Auflösung (ca. 1 km) ist dieser Ansatz jedoch nicht in der Lage, lokale Schwankungen auf Bezirksebene und darunter aufzulösen. Der Klimawandel im Untergrund in natürlichen Umgebungen wurde anhand von Temperatur-Tiefen-Profilen in Bayern quantifiziert. Verglichen mit der Änderungsrate der Lufttemperatur ist der Temperaturanstieg in 20 m Tiefe etwa 20 % geringer und nimmt mit zunehmender Tiefe weiter ab. In Köln zeigt die ländliche Umgebung einen vergleichbaren Trend, während unterhalb des Stadtzentrums der Grundwassertemperaturanstieg den Anstieg der Lufttemperatur deutlich überschreitet.

Für Köln bedeutet dieser Temperaturanstieg einen Wärmegewinn des Grundwasserleiters in der Größenordnung von 1 % des jährlichen Raumwärmebedarfs.

Table of Contents

Abstract	iii
Zusammenfassung	iv
Table of Contents	vi
List of Abbreviations	viii
Publications	x
Author contribution statement	x
Motivation	xi
Acknowledgements	xi
1 Introduction	1
1.1 Temperature of the shallow subsurface	1
1.1.1 Seasonal patterns under stationary surface conditions.....	1
1.1.2 Response to surface warming	4
1.1.3 Response to anthropogenic heat sources	6
1.2 Urban heat island effects	6
1.3 Research questions and objectives	9
2 Estimation of groundwater temperatures in Paris, France	13
2.1 Publication abstract	13
2.2 Introduction	13
2.3 Method and Data	15
2.3.1 Geographical setting, geology, climate and hydrology	15
2.3.2 Measured groundwater temperatures	16
2.3.3 Satellite-based estimation of groundwater temperatures	17
2.3.4 Misfit and correlation	21
2.4 Results and Discussion	22
2.4.1 Spatial and vertical distribution of GWT	22
2.4.2 Comparison of measured and estimated GWT	24
2.4.3 Impact of urban and rural estimation approach on GWTs.....	26
2.5 Conclusions	28
3 Climate change yields groundwater warming in Bavaria, Germany .	30
3.1 Publication abstract	30
3.2 Introduction	30
3.3 Methods and data	32
3.3.1 Groundwater temperature data	32
3.3.2 Air temperature data.....	35
3.3.3 Theoretical geothermal potential	35
3.4 Results and discussion	36

3.4.1	Recent variations in air temperature	36
3.4.2	Recent variations in groundwater temperature	36
3.4.3	Correlation between air and groundwater temperature change rates	38
3.4.4	Shallow geothermal potential of recent temperature variations	40
3.5	Conclusions	41
4	The Evolution of the Geothermal Potential of a Subsurface Urban	
	Heat Island	43
4.1	Publication Abstract.....	43
4.2	Introduction.....	43
4.3	Materials and Methods	46
4.3.1	Hydrogeology and aquifer structure	46
4.3.2	Groundwater data.....	47
4.3.3	Theoretical geothermal potential	48
4.3.4	Spatial interpolation and time resolution	49
4.3.5	Comparative Data	49
4.4	Results and discussion.....	50
4.4.1	Aquifer temperature.....	50
4.4.2	Theoretical geothermal potential of shallow urban groundwater	53
4.4.3	Further implications	57
4.5	Conclusions	58
5	Subsurface warming in response to anthropogenic drivers	60
5.1	Synopsis.....	60
5.2	Outlook	63
6	Appendix	67
6.1	Chapter 3 - Climate change yields groundwater warming in Bavaria, Germany.	67
6.2	Chapter 4 - The Evolution of the Geothermal Potential of a Subsurface Urban	
	Heat Island.....	71
7	References	74
	Curriculum Vitae.....	88
	Declaration	89

List of Abbreviations

α	thermal diffusivity
asl	above sea level
AT	air temperature
<i>BD</i>	building density
bgl	below ground level
<i>BT</i>	basement temperature
<i>c</i>	volumetric heat capacity
<i>d</i>	saturated thickness
<i>DEM</i>	digital elevation model
DWD	Deutscher Wetterdienst
K/dec	Kelvin per decade
ΔT_{10}	decadal temperature change
<i>eGWT</i>	estimated groundwater temperature
<i>ET</i>	evapotranspiration
<i>GWL</i>	groundwater level
GWT	groundwater temperature
<i>h</i>	heat transfer coefficient
IQR	Interquartile range
λ	thermal conductivity
<i>LST</i>	land surface temperature
MAE	mean absolute error
ME	mean error
<i>P</i>	Period length
<i>q</i>	heat flux
q_w	groundwater flux
<i>QTB</i>	<i>Quaternary-Tertiary boundary</i>
RMSE	root mean squared error
<i>SD</i>	snow cover
SUHI	subsurface urban heat island
<i>t</i>	time

<i>T</i>	temperature
<i>TGP</i>	theoretical geothermal potential
<i>U</i>	thermal plume velocity
UHI	urban heat island

Publications

This thesis has been written as a cumulative thesis and synthesizes the following three publications:

Section 2 has been published in Hemmerle H., Hale S., Dressel I., Benz S. A., Attard G., Blum P. and Bayer P. (2019) Estimation of Groundwater Temperatures in Paris, France. *Geofluids* **2019**.

Section 3 has been published in Hemmerle H. and Bayer P. (2020) Climate Change Yields Groundwater Warming in Bavaria, Germany. *Frontiers in Earth Science* **8**.

Section 4 has been published in Hemmerle H., Ferguson G., Blum P. and Bayer P. (2022) The evolution of the geothermal potential of a subsurface urban heat island. *Environmental Research Letters* **17**, 084018.

Author contribution statement

The following author contributions are based on the CRediT (Contributor Roles Taxonomy) system.

Hemmerle et al. (2019), Section 2; **Hannes Hemmerle**: Methodology, software, formal analysis, data curation, writing – original draft, writing – review & editing, visualization. **Sina Hale**: Methodology, writing – review & editing. **Ingo Dressel**: Writing – review & editing. **Susanne Benz**: Conceptualization, writing – review & editing. **Guillaume Attard**: Writing – review & editing, visualization. **Philipp Blum**: Writing – review & editing, supervision. **Peter Bayer**: Writing – review & editing, supervision, funding acquisition.

Hemmerle and Bayer (2020), Section 3; **Hannes Hemmerle**: Conceptualization, methodology, software, formal analysis, data curation, writing – original draft, writing – review & editing, visualization. **Peter Bayer**: Writing – review & editing, supervision, funding acquisition.

Hemmerle et al. (2022b), Section 4; **Hannes Hemmerle**: Conceptualization, methodology, software, formal analysis, data curation, writing – original draft, writing – review & editing, visualization. **Grant Ferguson**: Writing – review & editing. **Philipp Blum**: Writing – review & editing. **Peter Bayer**: Writing – review & editing, supervision, funding acquisition.

Motivation

One of (if not the) most pressing challenge we face is providing sustainable and politically independent energy. Utilizing the energy inherent in the shallow subsurface can fill this role and has the potential to boost the energy transition in the slowly adapting buildings sector by providing local and independent climatization. However, efficient and sustainable exploitation of thermal subsurface resources requires exact characterization. This thesis will shed a new light on how anthropogenic heat emission and climate change alter the temperature of the shallow subsurface. I hope that by supporting the understanding of how subsurface warming occurs, this thesis can also assist and hopefully trigger an increased recycling of subsurface excess heat with geothermal heat pumps, and hereby reverse or at least make use of the anthropogenic heating of the subsurface.

Acknowledgements

I would first like to thank everybody who helped collect the field and historic data that have been the basis for this thesis. This includes Leonhard Zimmerer, Rafael Meinhardt, and Johannes Granzow, who greatly supported the measurement campaigns and shared their good moods in the field in all kinds of weather. I would also like to thank the Erftverband, the Rheinenergie, the municipality of the city of Cologne, as well as the staff members from many Wasserwirtschaftsämter in Bavaria that were providing groundwater data, granting access to monitoring wells, and for their time spent on the investigative work of finding abandoned wells.

I would also like to express a big thank you to all my colleagues and friends at work who supported me during the writing process for keeping up my motivation and for the enjoyable office, home office, and after office times. This also includes my supervisor, Peter Bayer, who mastered the fine line between giving me the necessary freedom to test and play with different methodologies and topics, but also ensuring to finish things at just the right time. Lastly, my biggest thank you goes to my family and dear friends for being by my side and their unconditional support.

The research of this thesis was funded by the German Research Foundation (grant number BA2850/3-1).

1 Introduction

1.1 Temperature of the shallow subsurface

The thermal conditions of the shallow subsurface are governed by heat transfer from the atmosphere at the earth's surface, the terrestrial heat flow from the earth's interior, as well as the thermal properties of the subsurface. Under the assumption that both the terrestrial heat flux and the ground's properties are constant in time scales where humans are able to monitor subsurface temperature, recorded temperature changes of the subsurface can be attributed to a variation of surface conditions.

1.1.1 Seasonal patterns under stationary surface conditions

Diurnal and seasonal cycles in atmospheric temperature, solar radiation, and surface heat fluxes are the main driver for temperature changes at the earth's surface (Allen, 2009). These short-phased surface patterns propagate slowly downward into the underlying soil and rocks by diffusion and advection and change the thermal regime of the subsurface (Bense and Kooi, 2004). However, the earth's surface temperature depends on a complex series of factors that include climatic variables, land cover and vegetation, as well as soil properties (Jiang and Tian, 2010). The temperature of the shallow subsurface and near surface air are incorporated as parameters in most weather data monitoring routines. These typically include air temperature data measured at 2 m above ground and soil temperature at 5 cm depth and below. As an illustrative example, the temperature difference between deeper soil layers and air temperature with respect to the temperature at 5 cm below ground level (bgl) is given in Figure 1.1 for monitoring stations (n=199) with continuous data between 2000 and 2019 (CDC, 2021). For this set of monitoring stations in Germany, soil surface temperature (at 5 cm bgl) exceeds air temperature by 1.4 K on average with the highest difference during the warm period and periods with low cloud cover. This general relation is in line with observations from the US (Gallo et al., 2011), Switzerland (Stauffer et al., 2013), and Korea (Lee, 2006). Molnar (2022) quantified this effect for different land covers and vegetation types and found a major discrepancy between vegetation dense land covers (e.g. forests and wetlands at 1 K) and arid climates with bare surfaces (e.g. desert at 4-6 K).

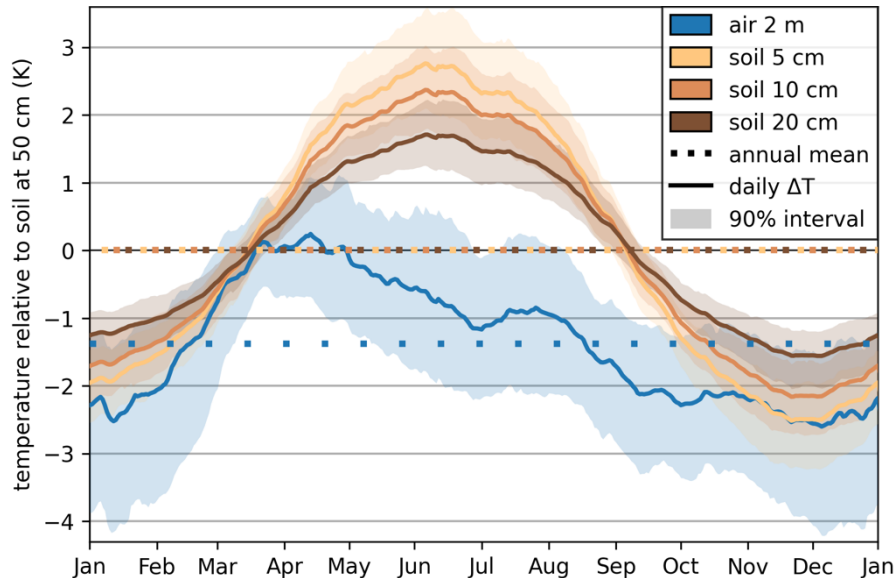


Figure 1.1: Temperature of air and soil at different depths for 199 weather stations in Germany between 2000 and 2019. Temperature is given as difference to the soil temperature at 50 cm bgl. The average annual mean of the temperature difference is given as dotted line. The solid line represents the mean of all stations and the shaded area indicates the 5% to 95% quantile range. Data was obtained from the climate data center (CDC, 2021), which is maintained by Deutscher Wetterdienst (DWD).

Towards deeper soil layers the seasonal amplitude of the surface signal is dampened in response to the slow heat transport in the subsurface. This causes a temporal shift of the peak temperatures (Figure 1.1).

A general analytical expression describing these seasonal effects can be obtained by simplifying the seasonal oscillation into a harmonic wave and calculating the dampening of this wave with increasing depth. The time (t) dependency of lands surface temperature (LST) is then given as a sinusoidal function, $LST(t) = LST_0 + A_{LST} * \cos(\omega t)$, around the annual mean temperature (LST_0), the temperature amplitude (A_{LST}), and a period length (P) of one year, where $\omega = 2\pi/P$. The downward propagation of the thermal signal based on depth (z) can then be described as a dampened wave equation:

$$T(t, z) = LST_0 + A_{LST} \exp(-az) \cos(\omega t - az) \quad (1.1)$$

where $a = \sqrt{\omega/2\alpha}$, and α is the thermal diffusivity (Bodri and Cermak, 2011; Taylor and Stefan, 2009). The relative dampening seasonal temperature variations of this solution based on the thermal diffusivity is displayed in Figure 1.2. For typical rock and soil compositions the seasonal temperature amplitude is dampened below 1 K in the top 10 to 15 m bgl, that is typically referred to as seasonal (Kurylyk et al., 2019) or surficial zone (Anderson, 2005; Parsons, 1970).

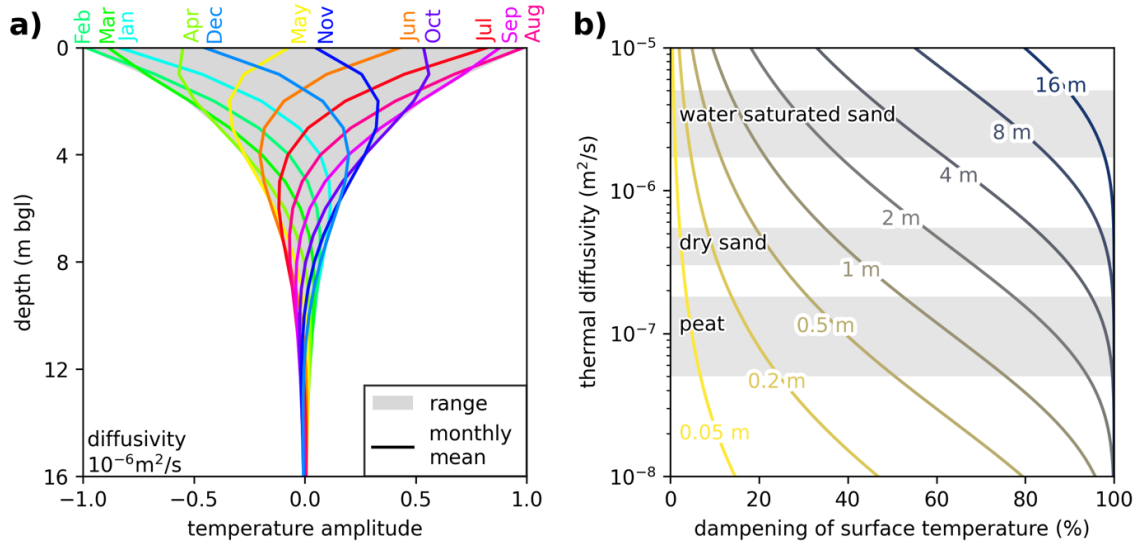


Figure 1.2: (a) Dampening of seasonal temperature oscillation by depth. (b) Dampening of surface temperature by thermal diffusivity for selected depths (lines). Typical value ranges for example rock types are displayed as shaded area (Andújar Márquez et al., 2016).

Underneath this seasonal zone, temperature conditions are projected to be stable and transition towards steady thermal conditions that mirror a gradual increase in temperature according to the local geothermal heat flow. For continental crust the average heat flow is between 64 and 67 mW m^{-2} (Davies, 2013; Limberger et al., 2018; Lucazeau, 2019; Pollack et al., 1993). Under steady conditions and assuming a homogeneous subsurface as well as zero vertical groundwater flow, the temperature profile can then be estimated as (Kappelmeyer and Haenel, 1974)

$$T(z) = LST_0 + q\left(\frac{1}{h} + \frac{z}{\lambda}\right) \quad (1.2)$$

where q is the geothermal heat flux, h is the heat transfer coefficient at the surface, and λ is the bulk thermal conductivity of the soil. Analytical or numerical solutions of the heat diffusion equation can be applied to on an initial temperature profile to superimpose seasonal variations or changes at the top boundary condition (cf. Sections 1.1.2, 1.1.3). Figure 1.3 shows the results of a numerical model that simulates the seasonal behaviour based on the average soil temperature at 5 cm depth (cf. data in Figure 1.1), using typical values for the bulk thermal conductivity ($\lambda = 1.7 \text{ W m}^{-1} \text{ K}^{-1}$) and geothermal heat flux ($q = 65 \text{ mW m}^{-2}$). The exponential dampening of temperature leads to a characteristic lag and decrease of the seasonal amplitude that can be used to estimate thermal parameters or to derive empirical estimation methods for groundwater temperature (GWT) (Kurylyk et al., 2014).

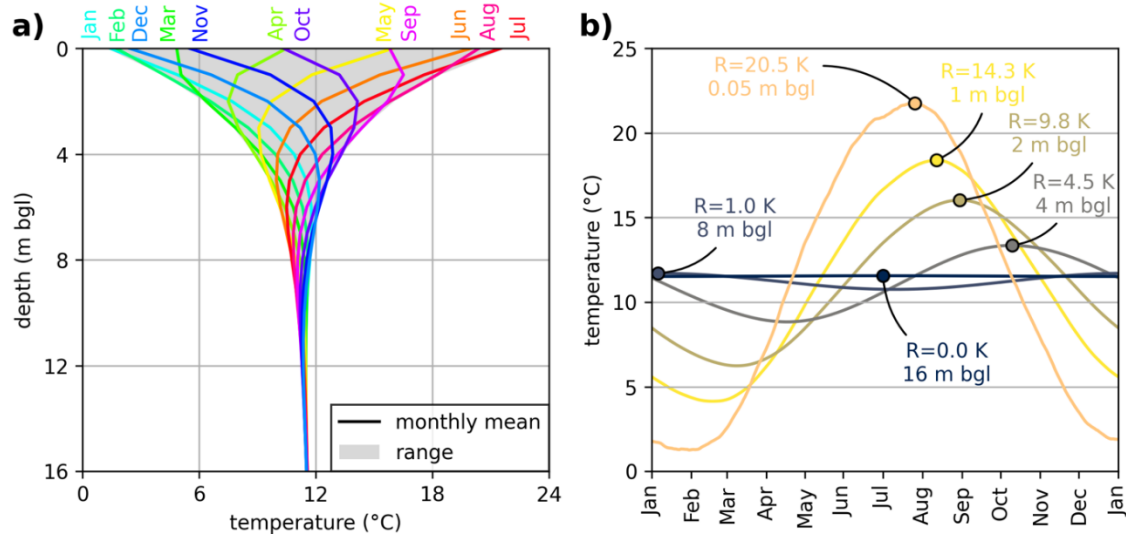


Figure 1.3: (a) Modelled monthly mean temperature depth profiles considering 1D heat diffusion. (b) Daily mean temperature of the modelled heat transport at different depths. The points represent the maximum temperature and the labels give the maximum-minimum temperature range (R) of an annual cycle.

1.1.2 Response to surface warming

Surface temperature witnesses short phased year-to-year variations and long-term changes in response to global climate change. According to the net gain in the global energy inventory modelled in CMIP6, warming of the earth's surface occurs at a rate between 0.55 and 0.89 W m^{-2} for the period of 1993-2018 (Forster et al., 2021). Compared to the terrestrial heat fluxes, this warming rate is roughly one magnitude higher and occurs in the opposite direction (Sec. 1.1.1). By hindering the cooling of the earth due to surface warming, the heat budget of the shallow subsurface increases in both the upper and lower boundaries. This imbalance in the thermal regime results in a net heat gain and subsequent increase in temperature of the shallow subsurface, leading to a bending of temperature depth profiles that integrates the accumulated heat. Unfortunately, temperature log data is scarce especially in historic times as it is not a component of most groundwater monitoring routines. Therefore, evaluating climate change effects based on repeated temperature logs is often not possible.

A variety of analytical, numerical and empirical models and inversion techniques are used in the field of borehole climatology (Bodri and Cermak, 2011; Kurylyk et al., 2019). Such models typically solve the one-dimensional (1D) heat transport equation for conduction and advection based on temperature logs and ground thermal properties (Bodri and Cermak, 2011; Kurylyk et al., 2019). The governing partial differential

equation for conductive and advective heat transport that equate for thermal storage can be written as (Domenico and Schwartz, 1998):

$$\alpha \cdot \frac{\partial^2 T}{\partial z^2} - U \frac{\partial T}{\partial z} = \frac{\partial T}{\partial t} \quad (1.3)$$

where U is the thermal plume velocity defined by the volumetric heat capacities (c) of the solid (c_s) and water (c_w), and the groundwater (Darcy) flux (q_w): $U = q_w c_w / c_s$. A review on analytical solutions of this equation is given by Kurylyk et al. (2019). A simple and straightforward method was developed by Menberg et al. (2014) that calculates the incremental change of a temperature profile per time step based on the surface temperature boundary condition, which is then added to the initial profile (cf. Figure 1.4). This method was developed for equilibrated initial conditions and assumes isotropic thermal characteristics and constant groundwater flow. Subsurface thermal response though is strongly affected by local hydraulic conditions like recharge, and vertical or horizontal groundwater flow. These are known to vary in time and depth and also adjust to climate change (Smerdon, 2017; Wunsch et al., 2022). Additionally, the assumption of homogeneous thermal parameters is mostly not valid as the thermal characteristics change with the strata and particularly water saturation of the soil.

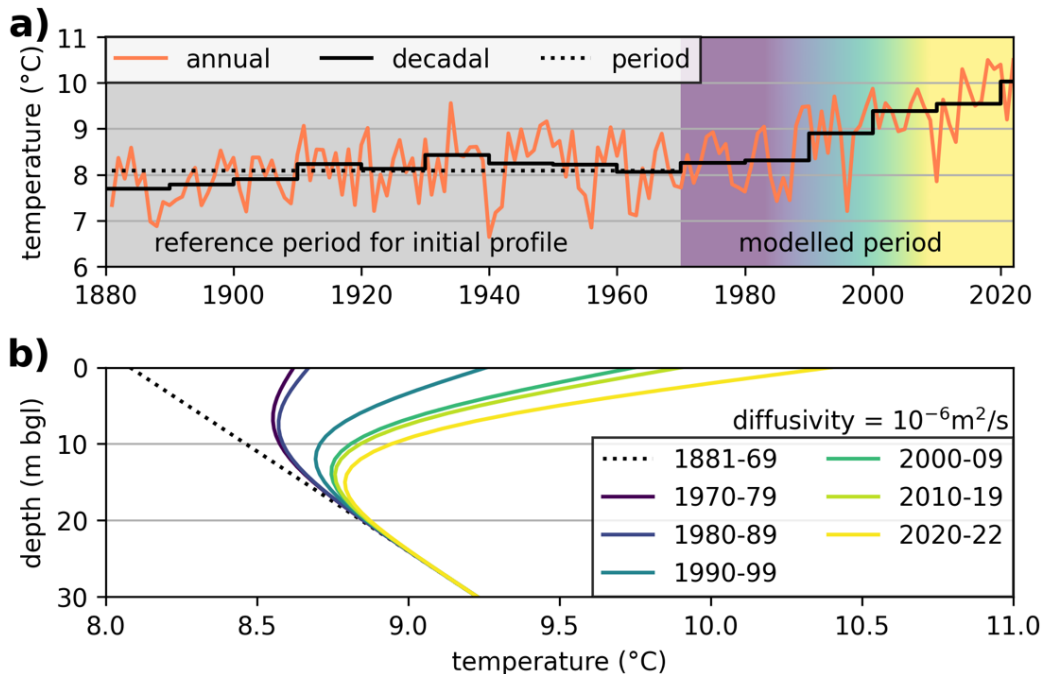


Figure 1.4: Generic example of a subsurface thermal response to surface temperature changes. **(a)** History of mean air temperature in Germany. Data are taken from CDC (2021). **(b)** Idealized change of subsurface temperature assuming that the geothermal heat flow was initially equilibrated with the period mean between 1881 and 1969. Lines represent the average temperature of each period.

1.1.3 Response to anthropogenic heat sources

Alongside climatic variations, the shallow subsurface also responds to heating and cooling by direct anthropogenic sources. In moderate climates, anthropogenic sources typically heat the subsurface, which leads to *positive* local ground(water) temperature anomalies. In Central Europe, two thirds of such anomalies underneath artificial surfaces have an intensity higher than 6 K (Tissen et al., 2019). The diversity of anthropogenic heat sources that impact the subsurface thermal conditions have recently been classified and reviewed in Noethen et al. (2022). Many of these anthropogenic heat sources act as mesoscale modifications of the land surface. This includes mainly basements and surface sealing for traffic and public areas. The effects of such heat sources can be quantified using the analytical solutions for advective-conductive heat transport (Bayer et al., 2016). Especially underground structures in regions with significant horizontal groundwater flow can impact local hydraulic conditions (Attard et al., 2016b) and cause large thermal plumes downstream (Attard et al., 2016a).

The subsurface response to heat sources strongly varies along their thermal signature and geometry. For instance, surface sealing by asphalted surfaces will increase the temperature at the surface while still showing major seasonal variations (Cermak et al., 2017). Contrarily, subsurface structures like tunnels have low seasonal temperature amplitudes and heat (or cool) the subsurface from the inside (Barla and Di Donna, 2018).

The heat flux (q) originating from these heat sources into an underlying aquifer can be calculated by the Fourier equation:

$$q = \lambda \frac{\Delta T}{\Delta z} \quad (1.4)$$

where ΔT is the temperature difference, Δz is the distance between the heat source and the aquifer, and λ is the thermal conductivity.

1.2 Urban heat island effects

Elevated air temperatures in urban centres were first reported at the beginning of the 19th century (Howard, 1818). Stewart (2019) gives a comprehensive review on historic research dedicated to atmospheric urban heat islands (UHI). Following pioneering work in the 19th century the word *städtische Wärmeinsel* (urban heat island) was likely first introduced by Pepler (1929) for the city of Karlsruhe. Pepler and Schmidt (1927) also advanced UHI research from point-based measurements to area-based assessments by

interpolating air temperature cross-sections measured on automobile surveys. Starting in the 1950s, research on UHIs intensified both in the number of cities where heat islands were described and in the amount of collected data. This allowed to scrutinize assumptions on city zoning of diurnal and seasonal patterns and to delineate physical processes. By 1980 the scientific basis enabling generalizations of the atmospheric canopy layer UHI was achieved (Stewart, 2019). This includes the estimation of timing and magnitude of the UHI phenomenon based on local climate, diurnal and seasonal variations, and practical implications, as well as areal zoning and differentiation based on land cover and use, population, and microclimate. The UHI at and above ground is typically classified in atmospheric layers (boundary- and canopy-layer) and the actual land surface UHI.

In the subsurface the first temperature monitoring (starting in 1775) was performed in a cellar in Paris at a depth of 28 m bgl. The temperature in this cellar saw a major gradual increase of around 1.5 K between 1900 and 1970 (Dettwiller, 1970) that exceeded the temperature increase in close-by air temperature stations. Kobus and Söll (1987) report several early studies on the city-scale subsurface urban heat islands (SUHI) phenomenon in Cologne (Balke, 1974, 1977; Balke and Kley, 1981), Karlsruhe (Lofi, 1977), Munich (Dohr, 1989; Höllein et al., 1983), Duisburg (Heitfeld et al., 1981), Strasbourg (Merheb, 1984). These early works are based on city-wide monitoring of temperature logs in groundwater. In these studies, point data are converted into isotherm maps by manual linear interpolation either at certain depths below the surface or below the groundwater table. These pioneer studies also calculate subsidiary effects like the recoverable heat with groundwater heat pumps (Balke, 1977), the contribution of heat sources (e.g. basements, sewer system, infiltration, district heating pipes) to the subsurface energy budget (Lofi, 1977), and future projections of the thermal field (Balke and Kley, 1981). Above named studies were published in German and French in scientific outlets with limited visibility such as theses, governmental reports or specialized journals and have not received international reception. However, these studies were conducted roughly 20 years prior to the major visible studies that indicate anthropogenic warming of the subsurface associated to UHI effects (Allen et al., 2003; Ferguson and Woodbury, 2004; Taniguchi et al., 1999).

Today, the SUHI phenomenon has been reported for more than 50 cities. The research on the individual cities does not typically use a uniform methodology to assess the

intensity of a SUHI. Often the SUHI effect is quantified as a side-effect that occurs to impact groundwater quality or geothermal suitability mapping and modelling. Furthermore, studies on SUHIs describe the temperature almost exclusively in either the soil layer (unsaturated zone < 5 m bgl) or the saturated zone (typically > 10 m bgl). Within this thesis, the term SUHI refers to the conditions in the saturated zone or in other words the groundwater SUHI. Four different approaches are commonly applied to quantify the intensity of SUHIs: (i) the *maximum* approach between the warmest temperature and either the coldest temperature sensed in the monitoring or a rural average background temperature (Öngen et al., 2021; Zhu et al., 2015), (ii) the difference between the *urban average* and a rural background temperature (Bucci et al., 2017; Epting and Huggenberger, 2013; Visser et al., 2020) that represents natural conditions, (iii) the *geothermal gradient offset* that indicates bending of temperature logs compared to extrapolated temperature depth profiles (Taniguchi et al., 2005), and (iv) *statistical* approaches based on all collected data that define a quantile range, i. e. between the 10% and 90% quantile of all measured or computed data (Menberg et al., 2013b). All of these approaches suffer from data scarcity and the erratic distribution of monitoring wells in urban environments. While the maximum temperature differences can easily exceed 10 K, SUHIs are typically understood as large scale heat anomalies at a city-scale. Distinct peaks are often found around local heat sources and underneath the most urbanized areas, where the large scale anomaly (rural-urban difference) ranges from 4 to 7 K (Menberg et al., 2013b). To mitigate the impact of seasonal temperature variations, the SUHI intensity is typically quantified a couple of meters below the seasonal zone underneath 15 m bgl (Banks, 2012). Though most studies do not report seasonal effects, much more rely on the general assumption that seasonal effects wear off below 10 or 15 m, which often is site-specific (Böttcher and Zosseder, 2022). The maximum approach is by definition very sensitive to outliers that are in the proximity to intense anthropogenic heat sources and has a very limited transferability from city to city. The statistical approach tries to decrease the effect of outliers by cutting of the extreme positive and negative values, but suffers from uneven monitoring well distribution. This can be mitigated by areal weighting, modelling, or interpolation of the data, but has not been proposed thus far. The rural-urban approach is also used in assessing the UHI intensity at the surface or in the canopy layer but is impacted by defining a rural

background temperature and the aggregation of an adequate representation of the urban temperature.

1.3 Research questions and objectives

The research of this thesis comprises how temperature can be sensed in complex urban environments that do not feature a rich set of observations (Sec. 2), how climate change heats the shallow subsurface (Sec. 3), and how temperature in an urban setting evolves over time and which implications this growing heat source has for exploitation with geothermal heat pumps (Sec. 4). This yields four major research objectives which are addressed in this thesis and are outlined as follows:

- (O1) Develop a prediction technique that can estimate GWT for large scale metropolitan areas that is applicable for artificial and natural land covers.
- (O2) Quantify the depth resolved change in subsurface thermal conditions in response to atmospheric and surface climate change under natural conditions.
- (O3) Quantify the change of subsurface thermal conditions in urban regions, where the response to climate change mingles with direct heating by anthropogenic heat sources and SUHI effects.
- (O4) Draw implications to what extent the excess heat mapped in O1-3 represents a thermal reservoir and the feasibility of recycling this (waste) heat with shallow geothermal systems.

Objective 1) Groundwater temperature estimation: Especially in urban environments, data scarcity and a lack of monitoring wells often lead to poor data coverage of subsurface conditions. This challenges scientists to provide estimation techniques that can complement monitoring and ease the characterization and mapping of the thermal conditions of the subsurface. Previous studies showed that soil and GWTs can be approximated from abundant satellite data (Benz et al., 2017a; Benz et al., 2016; Huang et al., 2020; Zhan et al., 2014). It was established that ground(water) temperature can be estimated from *LST* considering natural drivers such as snow cover and evapotranspiration under natural conditions (Benz et al., 2017a), and land cover data in urban environments (Benz et al., 2016). The spatial overlap of anthropogenic heat sources in the subsurface and higher surface temperature in cities in response to UHI related processes is promising. This raises the question whether and at what accuracy ground(water) temperature can be estimated in urbanized areas that have both dense

urban fabric and natural surfaces like parks, forested areas, and flood plains. How well do estimation approaches resolve the transition between urban and rural land cover, and is this methodology suitable for local calibration and more accurate than standard interpolation methods? A combination of existing estimation approaches is developed and applied to the metropolitan area of Paris, where the SUHI phenomenon is now described for the first time in Sec. 2.

Objective 2) Subsurface climate change in natural environments: The deviation between measured temperature depth profiles from the local geothermal gradient is known to integrate regional surface temperature increase (Pollack and Chapman, 1993; Wang and Lewis, 1992). The inversion of such deep temperature logs (> 100 m bgl) can provide information on low frequency temperature variations of roughly the past five centuries, but struggles to resolve local effects such as groundwater flow, complex air-ground coupling and trends shorter than 10 years (González-Rouco et al., 2009; Melo-Aguilar et al., 2018). Especially since the 1970s, surface temperature witnesses a strong increase in response to climate change that is reported by a variety of studies in Central Europe (Noethen et al., 2022). However, many of these studies that describe temperature trends do not consider depth-dependent effects or give warming rates at single depths using temperature data gathered during groundwater quality monitoring while pumping (Benz et al., 2018a; Bloomfield et al., 2013; Figura et al., 2011; Menberg et al., 2014; Riedel, 2019). Others resolve trends from installed data loggers at only one specific depth (Egidio et al., 2022), while timeseries recorded at multiple depths at one station (Cermak et al., 2014) are rare. If in-situ data at multiple depths are not available, deriving the warming by repeated temperature logging can provide an alternative for quantifying the heating integrated over a specific period of time. As historic temperature log data are typically scarce, this option has not received broader attention. To fill this gap, a straightforward approach to quantify this climate change effect is developed. This is applied to a rich data set of repeated temperature logs recorded in the early 1990s and 2019 in Bavaria (Germany) in Sec. 3.

Objective 3) Evolution of a subsurface urban heat island: The SUHI phenomenon has been reported for more than 50 cities by now. Being a fairly new field of research, studies typically struggle with a lack of monitoring data in the past and the majority of available studies present only static descriptions of the temperature in the urban subsurface. Rotta Loria et al. (2022) inspected 76 studies on SUHIs and found only three studies that tackle

long-term temperature trends in urban soil (Changnon, 1999; Ichinose and Liu, 2018; Lokoshchenko and Korneva, 2015) and three that quantify changes of ground deeper than 1 m bgl and groundwater (Abe et al., 2014; Menberg et al., 2013a; Watson and Westaway, 2020). Studies that quantify groundwater warming in urbanized regions typically find an elevated rise of temperature in the urban centre compared to the rural surrounding or typical rates of surface warming in response to climate change (listed in Table 1.1).

Table 1.1: Groundwater warming rates in cities. Trend is given in Kelvin per year (K/a).

city	period	groundwater temperature trend	citation
Milano	2016-2020	urban: +0.4 K/a; average: +0.15K/a	Previati and Crosta (2021)
Nuremberg	2015-2020	urban: +0.08 K/a; rural: +0.03 K/a	Schweighofer et al. (2021b)
Basel	1994-2013	average: +0.05 K/a	Epting et al. (2017a)
Nagaoka	1977-2009	urban: +0.05 K/a; rural: +0.02 K/a	Abe et al. (2014)

Especially Previati and Crosta (2021) report extremely steep gradients at 4 K/dec (Kelvin per decade) in the city centre (of Milan, Italy) that could reflect short-phased trends due to the limited time period of only four years of observation. Although there are indications of an elevated temperature rise with increasing urbanization, there is a lack of studies on GWT rise forced by atmospheric climate change, local anthropogenic heat sources, and above ground UHIs. To fill this research gap, the insights from depth dependent climate change under natural land covers (Objective 2) is related to research on subsurface temperature change over time in an urban environment. This will provide a first reference study about how the change under artificial surfaces relates to temperature response under natural surfaces, and how this temperature rise appears with respect to different city zones from the city centre, inner city, to the suburbs and rural surroundings.

Objective 4) Accumulating shallow geothermal potential in response to ground warming: UHIs in the subsurface and groundwater are known to provide a vast potential for space heating by accessing the stored excess heat with shallow geothermal heat pumps (Zhu et al., 2010). While a variety of mapping approaches exist for geothermal potential mapping, the anthropogenic heat that is trapped underneath cities can theoretically meet the residential heating demand of cities from 0.5 to more than 50 years (Bayer et al., 2019). Another approach of defining the theoretically available

anthropogenic heat is to quantify the thermal recharge instead of quantifying the energy in the thermal reservoir (Benz et al., 2015; Menberg et al., 2013a). These studies calculate the amount of energy that can be (sustainably) extracted from the aquifer by imposing conductive heat transport between various surface temperatures based on land use and the groundwater at a certain depth. However, there is no evidence of long-term in-situ thermal storage of heat in urban ground(water). Based on the mapped temperature distributions in O1-3 the corresponding extractable heat that can be harnessed with shallow geothermal systems is quantified. This excess or waste heat resulting from the coexistence of climate change and direct anthropogenic warming can mainly be utilized for heat extraction. However, regardless of the application (cooling, heating, or thermal storage), tapping the energetic potential of urban subsurface provides a local, renewable and politically independent way of meeting the thermal demand of cities (Kammen and Sunter, 2016).

2 Estimation of groundwater temperatures in Paris, France

2.1 Publication abstract

Subsurface temperature data is usually only accessible as point information with a very limited number of observations. To spatialize these isolated insights in the underground we usually rely on interpolation methods. Unfortunately, these conventional tools are in many cases not suitable to be applied to areas with high local variability, like densely populated areas, and in addition are very vulnerable to uneven distributions of wells. Since thermal conditions of surface and shallow subsurface are coupled we can utilize this relationship to estimate shallow GWTs from satellite-derived land surface temperatures. Here we propose an estimation approach that provides spatial GWT data and can be applied to natural, urban as well as mixed environments. To achieve this, we combine land surface temperatures with anthropogenic and natural processes, such as downward heat transfer from buildings, insulation through snow coverage and latent heat flux in form of evapotranspiration. This is demonstrated for the city of Paris, where measurements from as early as 1977 reveal the existence of a substantial SUHI with a maximum GWT anomaly of around 7 K. It is demonstrated that GWTs in Paris can be well predicted with a root mean squared error of below 1 K by means of satellite-derived land surface images. This combined approach is shown to improve existing estimation procedures that are either focused on rural or on urban conditions. While they do not detect local hotspots caused by small-scaled heat sources located underground (e.g. sewage systems and tunnels), the findings for the city of Paris for estimation of large-scale thermal anomalies in the subsurface are promising. The new estimation procedure thus may also be suitable for other cities to obtain a more reliable insight into the spatial distribution of urban ground and GWTs.

2.2 Introduction

Natural in-situ temperatures usually do not substantially vary at a depth of more than 10-20 m. Here, ground and groundwater temperatures are close to the annual mean values in the atmosphere, and commonly only a marginal attenuated influence of the coupled seasonal temperature variation in the atmosphere can be detected (Stauffer et al., 2013). During recent years, attention has been growing to the thermal conditions

beneath cities, which revealed to be completely different when compared to the undisturbed rural surrounding (Benz et al., 2017b; Bucci et al., 2017; Eggleston and McCoy, 2015; Ferguson and Woodbury, 2007; Gunawardhana et al., 2011; Menberg et al., 2013b; Reiter, 2007; Taniguchi et al., 2007). However, the knowledge of the spatial and temporal variability of temperature in urban ground is crucial for proper planning of geothermal energy use. Elevated temperatures offer enhanced opportunities for geothermal heating applications, whereas warmer groundwater is less useful for cooling applications (Bayer et al., 2019; Beyer et al., 2016; Epting et al., 2013; Marschalko et al., 2018; Menberg et al., 2013a; Rivera et al., 2017; Schneider et al., 2016; Zhu et al., 2010). Aside from its role for the geothermal potential, thermal anomalies can influence chemical transport in shallow urban groundwater that often serves as a freshwater resource (Bonte et al., 2013; García-Gil et al., 2016). Finally, anthropogenic accumulation of heat threatens the stability of groundwater ecosystems (Briemann et al., 2011; Griebler et al., 2016).

In most studied cases, temperature in urban ground and groundwater is elevated, which manifests in a large-scale heat carpet underneath a city. This so-called SUHI is highly case-specific, often with highest temperatures beneath city centres and strong local spatial variations (Arola and Korkka-Niemi, 2014; Benz et al., 2018b; Lokoshchenko and Korneva, 2015; Menberg et al., 2013b; Müller et al., 2014; Shi et al., 2012; Taniguchi et al., 2009; Zhu et al., 2015). Ferguson and Woodbury (2004) demonstrated that elevated GWTs below cities are mainly caused by heat losses from buildings. Accordingly, the investigation of SUHIs enables a determination of the initial period of urbanization in a certain region (Bayer et al., 2016; Yamano et al., 2009). In addition to building basements groundwater flow, surface cover and man-made climate change influence GWTs (Bense and Beltrami, 2007; Benz et al., 2015; Epting et al., 2017b; García-Gil et al., 2014; Molina-Giraldo et al., 2011). Additionally, anthropogenic heat sources like subsurface infrastructure, power plants, landfills or geothermal installations can have an impact on the spatial distribution of subsurface temperatures (Menberg et al., 2013a).

Various studies have reported SUHIs below large cities worldwide, for example in Moscow (Lokoshchenko and Korneva, 2015), London (Headon et al., 2009), Cologne (Benz et al., 2016; Menberg et al., 2013b; Zhu et al., 2015), Osaka (Huang et al., 2009; Jago-on et al., 2009; Taniguchi et al., 2009) and Ankara (Turkoglu, 2010). Within these

cities temperatures are measured in a limited number of boreholes or groundwater wells and commonly are several degrees higher than in surrounding rural soil and pristine groundwater bodies. In the city of Paris, measurements from the 18th century onward are reported in a 28 m deep cellar at the city centre (Dettwiller, 1970; Perrier et al., 2005). The long-term temperature increase of 0.1 - 0.7 K/dec is attributed to global warming and the developing atmospheric UHI in Paris. Related studies such as by Pal et al. (2012) primarily focus on the atmospheric and surface layer of Paris' UHI. An analysis of surface temperatures shows that the intensity of Paris' UHI, which is the difference between temperatures in the city and undisturbed conditions, can be up to 6 K (Sarkar and De Ridder, 2011). Escourrou (1990) confirms the presence of a strong atmospheric heat island in Paris and its effect on the local climate (e.g. influence on the rainfall regime, the occurrence of local winds). Cantat (2004) underlines that the size and intensity of Paris' UHI depends on various factors such as seasonal variability, climate or weather conditions.

In this work, the focus is set on the shallow subsurface thermal regime in the metropolitan area of Paris. The objective is to examine the SUHI of Paris spatially based on repeated temperature measurements in wells located in and around the city. Due to the low well density within the studied urban area, especially within the city centre, we investigate the auxiliary use of satellite-derived land surface temperatures to estimate spatial GWT distribution. In the following, first the measured GWT data is described in detail. This information is contrasted to the satellite-based land surface temperatures for the city. Based on this, a new spatial estimation procedure for GWTs in urban, rural and mixed environments is explained and applied to the case study of Paris.

2.3 Method and Data

2.3.1 Geographical setting, geology, climate and hydrology

Paris is the capital of France and located in the northern part of the country in the region Île-de-France (Figure 2.1a). The focus of investigation here is the entire metropolitan area of Paris, which includes the city centre district, the suburbs and the surrounding rural areas. Paris has a circumference of nearly 55 km and also includes the two huge woodlands: Vincennes in the east and Boulogne in the west. The average elevation of the city is 30 m asl (above sea level) The Seine River with a total length of 13 km inside

of Paris crosses the city from northwest to southeast, dividing it into two sections (Chaussé et al., 2008).

In general, Paris' city climate is moderate with relatively warm summers and mild winters. The mean annual air temperature is 10.8 °C. Temperatures within Paris are slightly higher compared to the suburbs and the surrounding rural areas; the temperature difference typically amounts to 1-2 K. Elevated temperatures within the city centre are caused by the increasing urbanization (e.g. higher building density (*BD*)) of the capital (Cantat, 2004; Koukoku-Arnaud et al., 2014).

Paris is eponymous for the Paris basin (French: Bassin parisien). The Paris basin is an elliptical geological basin filled with continental, epicontinental and marine Mesozoic and Tertiary sediments. Postvariscan crustal extension caused subsidence processes during the Permian that formed the Paris Basin alongside other central-European basins. It is present in the northeast of France, in the west of Belgium and in the southeast of England. The centre of the basin is located 80 km east of Paris. Aquiferous formations in the Paris Basin are mainly built up by sandstones, limestones, chalk and carbonates. The aquifer units are intermitted by less permeable claystone and marl layers which results in a complex layered aquifer system (Thierry et al., 2009).

2.3.2 Measured groundwater temperatures

There have been several groundwater measurement campaigns in the metropolitan area of Paris. Data from 1990 to 2015 were measured by local authorities in wells of the Paris metropolitan area and are available in the French national database on groundwater resources (ADES, 2018). The well coordinates and measuring depths are accessible at InfoTerre (2018). Even though a rich data set of 3018 GWT measurements exists, the records are heterogeneous, often incomplete over time and information on the specific sampling methods is sparse. The majority of GWT data were measured on-site while pumping. The given depths, therefore, represent the mean depth of the screened well interval. During pre-processing, we excluded outliers exceeding a 6 K offset to the median for a single well location for further analysis. Moreover, measured values with an offset above 2.5 times the interquartile range (IQR) were expelled if the IQR was above 1 K. This was necessary to exclude outliers most probably caused by poor handling during sampling and typos. In addition, four outliers that are directly influenced by a waste disposal site north of Paris were eliminated. A total of 74 outliers (2.3 % of

the available data) was removed from the data pool. The remaining data covers 377 sampling wells in the outer and inner suburbs of Paris. The derived spatial coverage is nonuniform and there are no data points in the city centre (Figure 2.1).

Diffre et al. (1977) provide GWT data, that include measurements in the city centre from February 1977. As the corresponding coordinates of the observation wells were not given in that report, they had to be extracted from the online database InfoTerre (2018). Unfortunately, none of the wells measured in 1977 are listed in the ADES (2018) database (Figure 2.1b). The 1977 GWTs focus on the inner suburbs and the city centre, while the more recent ones reveal the thermal conditions in the surrounding.

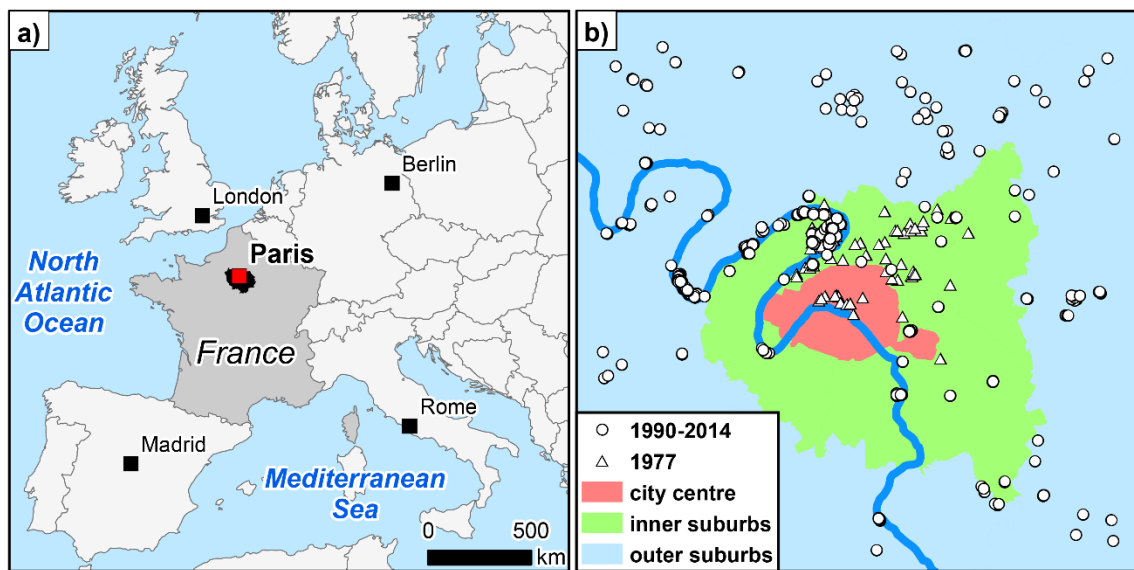


Figure 2.1: (a) Location of Paris in Western Europe. (b) Map of the observation points in Paris with a separation into outer suburbs, inner suburbs and city centre. The blue line marks the river Seine crossing Paris.

2.3.3 Satellite-based estimation of groundwater temperatures

Recently, satellite data was suggested to investigate the thermal ground conditions in cities and SUHIs. Zhan et al. (2014) estimated ground temperatures in Beijing, China, from MODIS land surface temperatures. The results were compared with recorded temperatures (measuring depths of 0.05 m, 0.40 m and 3.20 m). A time delay between the maximum temperatures of the atmosphere and the ground was detected depending on the measuring depth. Hafner and Kidder (1999) used Advanced Very High-Resolution Radiometer (AVHRR) satellite data to determine the albedo of the land surface as well as soil thermal and moisture properties around Atlanta, USA. These parameters were utilized for numerical simulation of Atlanta's atmospheric temperature dynamics. The spatial extension and intensity of atmospheric UHIs in 18 Asian

megacities was analysed by Tran et al. (2006) using satellite-derived *LST* data. This study demonstrated that the spatial heterogeneity of the investigated heat islands mainly depends on vegetation cover and *BD*, whereas its total extent and intensity is related to the population size.

Benz et al. (2016) analysed whether the spatial distribution of interpolated GWT is linked to the spatial distribution of satellite-derived *LST*. In this context, the four German cities Berlin, Munich, Cologne and Karlsruhe were analysed. In order to quantify the relation between GWT and *LST*, the Spearman correlation coefficient was determined and correlations of up to 80% were found. Benz et al. (2016) also propose a method for calculating GWTs with the help of mean annual *LST*, *BD* and basement temperature (*BT*). This reflects that accelerated ground heat flux in cities is not only caused by land surface changes and modified above-ground temperatures as detected from satellites, but also by other heat sources such as heat release from basements, buildings and underground networks.

Even for undisturbed rural areas, *LSTs* are generally colder than adjacent GWT. This offset is caused by a variety of processes in the soil transition zone and varies with local climate, biological activity and the hydrogeological setting (Kollet et al., 2009; Mann and Schmidt, 2003). Benz et al. (2017a) introduce an approach to calculate this offset on a global scale. This approach empirically relates evapotranspiration (*ET*) and the number of days with snow cover (*SD*) to the offset between *LST* and GWT. For a global GWT dataset, they could reduce the root mean squared error (RMSE) of prediction by 0.5 K to 1.4 K and increased the squared spearman correlation coefficient by 0.5 to 0.95 compared to a prediction relying solely on *LST*.

Due to the fact that we have a strong spatial variety of our measured GWT in Paris, in the following, we combine the individual approaches of Benz et al. (2016) and Benz et al. (2017a) to estimate GWT in the region of Paris, both for rural and urban areas at the same time (Figure 2.2). This combined approach has been suggested by Benz (2016) for German cities and it has the specific advantage of covering natural and urban processes within one estimate.

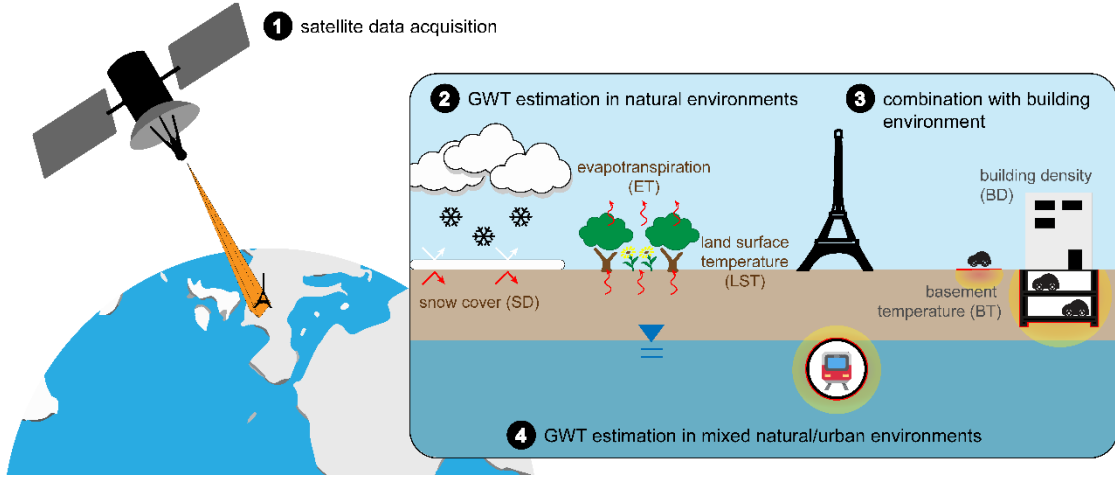


Figure 2.2: Schematic visualization of the combined estimation method.

Estimated groundwater temperatures ($eGWT$) are calculated in three steps:

$$eGWT_{rur} = LST + (3.5 \pm 0.2) * 10^4 K \frac{m^2 \cdot s}{kg} \cdot ET + (6.6 \pm 0.3) K \cdot SD \quad (2.1)$$

$$eGWT_{urb} = \max \left\{ \begin{array}{l} LST \\ LST \cdot (1 - BD) + BT \cdot BD \end{array} \right. \quad (2.2)$$

$$eGWT_c = \max \left\{ \begin{array}{l} eGWT_{rur} \\ eGWT_{rur} \cdot (1 - BD) + BT \cdot BD \end{array} \right. \quad (2.3)$$

The first step consists of estimating GWT in rural areas. Here, the offset between LST and GWT is dominated by latent heat flux cooling down the surface in form of evapotranspiration and by snow cover insulating the subsurface during the winter period. An empirical best-fit approximation for estimating rural groundwater temperatures ($eGWT_{rur}$) from satellite-derived data on a global scale is given by Equation (2.1) (Benz et al., 2017b). The second step is estimating groundwater temperatures in urban environments ($eGWT_{urb}$) by Equation (2.2, which takes into account BD and BT (Benz et al., 2016). The third step combines rural and urban estimations by replacing LST by $eGWT_{rur}$ in Equation (2.2). The resulting Equation (2.3 is intended to estimate groundwater temperatures in rural, urban and mixed settings ($eGWT_c$).

Building densities were calculated at a resolution of $1 \text{ km} \times 1 \text{ km}$ from OpenStreetMap (2018) building polygons. BT s were estimated to be $17.5 \pm 2.5 \text{ }^\circ\text{C}$ following guidelines by the International Organization for Standardization (ISO, 2007) and assuming similar conditions for Central Europe. This value range is also consistent with average BT s

obtained from borehole temperature profile inversion in the area of Zurich, Switzerland (Bayer et al., 2016).

Satellite-derived data represent the decadal mean from 2005 to 2014 and include land surface temperatures, evapotranspiration and the percentage of snow days. Data was retrieved and processed with Google Earth Engine according to the procedure that is explained in detail in Benz et al. (2017a). The MODIS Aqua and Terra *LST* and Snow Cover Daily Global 500 m products were retrieved from Google Earth Engine, courtesy of the NASA EOSDIS Land Processes Distributed Active Archive Center (LP DAAC), USGS/Earth Resources Observation and Science (EROS) Center, Sioux Falls, South Dakota (Hall and Riggs, 2016; MODIS, 2018). In contrast to Benz et al. (2017a), the updated MODIS data version 6 was used for determining *LST* values. Snow days were computed with MODIS version 5 due to different snow cover algorithms and product availability in the version 6 data, which could not be used with the empirical variables in Equation 2.1 without biasing $eGWT_{\text{rur}}$. For a detailed discussion of the given raster data, we refer to Benz et al. (2017a). Estimated groundwater temperatures were computed by Equations 2.1, 2.2, 2.3 using ArcPy and ArcMap 10.5.1 (ESRI, 2011). Note that extracted raster data on point locations were bilinearly interpolated between the middle of adjacent raster cells. All raster data was exported at a resolution of approximately $1 \text{ km} \times 1 \text{ km}$ (Figure 2.3).

LSTs range from $10.4 \text{ }^\circ\text{C}$ in the outer suburbs to $14.9 \text{ }^\circ\text{C}$ within the city centre (Figure 3a). This dataset exhibits two central *LST* cold spots (12.7 and $12.5 \text{ }^\circ\text{C}$), caused by the two large forests in the eastern and western part of the city centre. The annual percentage of snow days (*SD*) ranges from 0 to 7.3% and as expected *SDs* are more frequent in the outer suburbs than in the city centre. Again, the two forests manifest as anomalies in the spatial *SD* distribution (Figure 3b). In contrast to the *LST* and *SD*, the data on *ET* has a lower resolution of $0.25^\circ \times 0.25^\circ$ (approx. $28 \text{ km} \times 28 \text{ km}$). The city centre is almost fully covered by one cell of low *ET* with a value of $10 \text{ mg m}^{-2} \text{ s}^{-1}$. Towards the rural areas, the *ET* increases up to $17 \text{ mg m}^{-2} \text{ s}^{-1}$ (Figure 2.3c). Finally, *BD* is calculated from building polygons of OpenStreetMap at a resolution of $1 \text{ km} \times 1 \text{ km}$. The *BD* is highest in the city centre (up to 60%) and decreases towards suburbs to nearly zero in areas of low population.

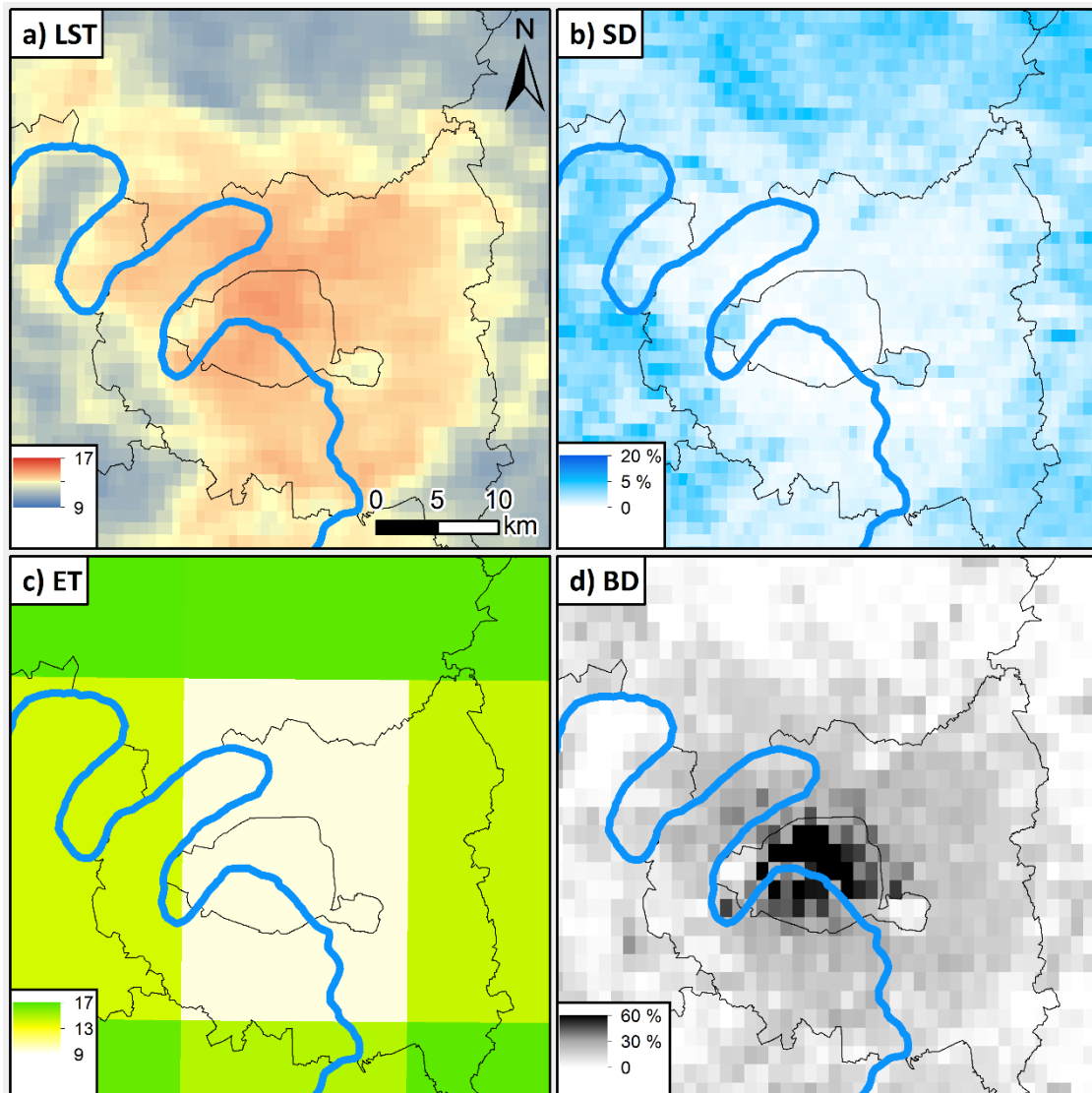


Figure 2.3: (a) Land surface temperature (*LST*) in °C, (b) percentage of snow days (*SD*), (c) evapotranspiration (*ET*) in $\text{mg m}^{-2} \text{s}^{-1}$, and (d) building density (*BD*) in percent within the research area. Black lines indicate governmental districts of Paris. The river *Seine* is displayed in blue.

2.3.4 Misfit and correlation

The estimate of GWT is assessed by calculating the root mean squared error (RMSE), mean absolute errors (MAE) and the mean error (ME) between measured and estimated GWT. RMSE and MAE are used to evaluate the misfit of the predicted GWT. Calculating the RMSE is probably the most common way to evaluate the predictive capabilities of a model. However, it is more sensitive than the MAE to large prediction errors or outliers, because errors are squared before being averaged. The ME is used to describe the error orientation, as positive and negative errors cancel each other out when calculating the ME. It is thus useful to test if observed values are over- or underestimated by the prediction. In addition, a linear least square regression is performed to correlate

measured and estimated GWTs by using the Spearman method. Hereby, the obtained Spearman correlation coefficients (r) quantify the link between estimated and measured GWTs, but are less useful as (mis)fit measures.

2.4 Results and Discussion

2.4.1 Spatial and vertical distribution of GWT

In a first step, we characterize the spatial and vertical distribution of GWTs based on the measured data (Figure 2.4). For this, the available early measurements from 1977, which focused on the city centre, and averages from the years 1990 to 2015 for the greater Paris region, were spatially combined.

In February 1977, the reported GWT beneath the city centre ranged between 14.1 °C and 18.3 °C. Towards the suburbs, the measured temperatures decreased yielding a temperature range from 12.2 °C to 16.6 °C. The measurement depths range from 17 m to 100 m below ground level. For the shallower measurements, a slight seasonal bias can be expected. For the 87 observation wells measured in February 1977, no repeated or more recent GWT measurements are available. From the period between 1990 and 2015, a total of 297 sampling points are located above a depth of 80 m below ground level showing a temperature range between 9.6 °C to 22.8 °C. Above 15 m below ground level, GWTs are strongly affected by seasonal influences. Here they show a standard deviation of 2.82 K compared to a standard deviation of 1.23 K for measurements between 15 m and 80 m. For the latter interval temperatures in the inner suburbs range between 11.8 °C and 18.1 °C and between 11.7 °C and 17.2 °C in the outer suburbs.

While no clear spatial trend can be deduced for the shown data, the lower limit of GWT clearly declines towards the outskirts. Nevertheless, the lower limit of 14.1 °C for the GWTs in the city centre in 1977 is remarkable, being more than 3 K higher than the average air temperature of 10.8 °C during that time. On average they are also warmer than temperatures in the inner and outer suburbs. If we ignore any temporal and or vertical effects, the maximum temperature in the city centre (measured in 1977) is exceeding rural GWTs (measured after 1990) by 5 to 6 K. This offset is typical for SUHIs in Western Europe and on the upper end of observed intensities in previously studied Germany cities (Menberg et al., 2013b).

The vertical resolution of the measured data is depicted in Figure 2.4. Most sampling points were obtained in shallow depths of a few tens of meters, with some measurements

also taken in depths of more than 100 m. However, no clear evidence of the geothermal gradient can be observed. Still, for the comparison between satellite-derived *LST* and the measured GWT, the lower depth limit for this analysis is set to 80 m in order to zoom-in on the regime influenced by land surface effects. Additionally, the shallowest 15 m of the subsurface are disregarded to avoid any influence of seasonal atmospheric temperature variation. The usual seasonal temperature variation in a humid climate is below 1 K for depths of more than 10 m (Stauffer et al., 2013).

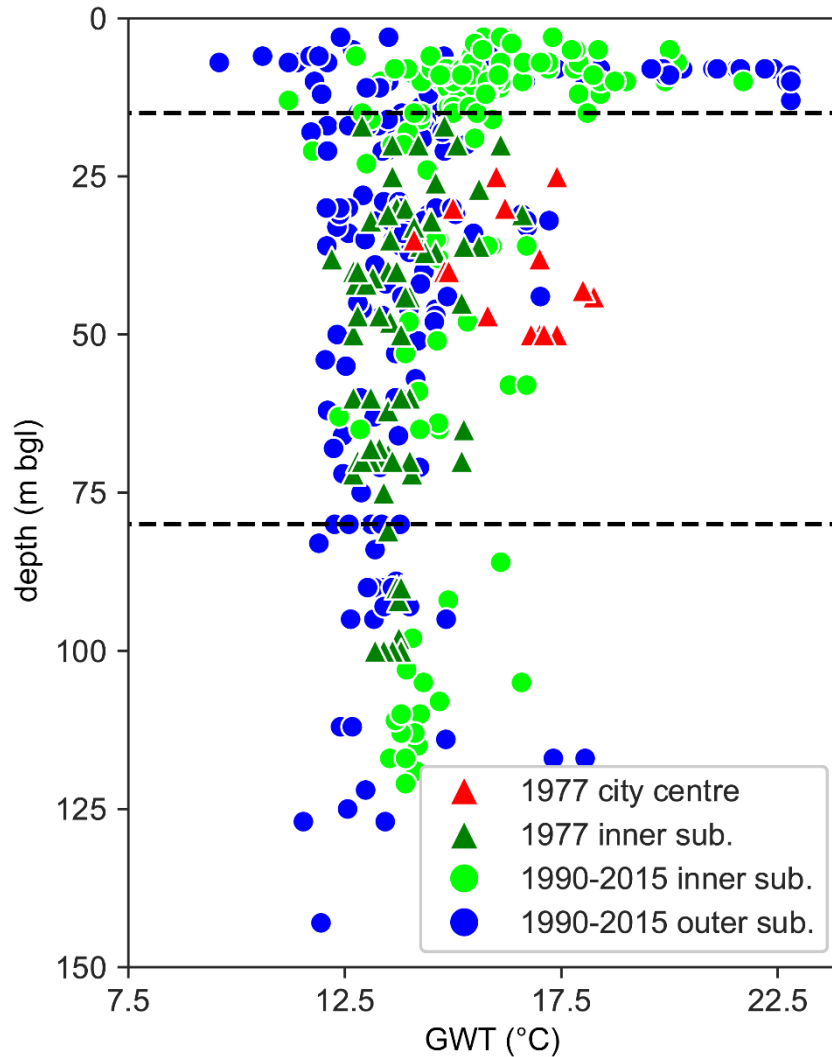


Figure 2.4: Temperature-depth scatter plot with 1977 data and mean values from 1990 to 2015. Horizontal dashed lines at 15 m and 80 m depths define the depth interval considered for correlation analysis and estimation of groundwater temperatures.

In the next step, Equation 2.3 is applied to estimate groundwater temperatures using the combined method, $eGWT_c$. This resulting map in Figure 2.5b represents the $eGWT_c$ at shallow depths with a temperature range of 11.3 °C to 16.6 °C. Consistent with the

available GWT measurements from different points in time, the city centre is characterized by warm temperatures, which are decreasing towards the suburbs.

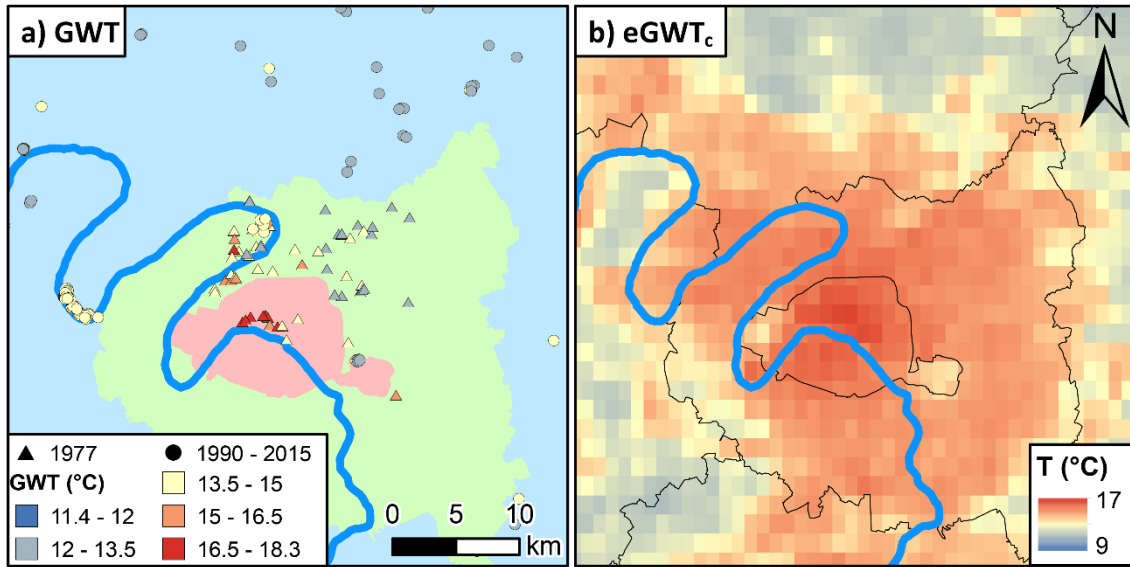


Figure 2.5: (a) Measured and (b) estimated groundwater temperatures in Paris. Depth of groundwater temperatures ranges from 15 to 80 m. Colors in the left figure represent city centre (red), inner suburbs (green) and outer suburbs (blue) of Paris.

2.4.2 Comparison of measured and estimated GWT

To assess the quality of predicted groundwater temperatures from satellite imagery, $eGWT_c$, they are compared with well measurements in the field. It is important to note the time difference: data in the city centre was only observed in 1977, about three decades earlier than the satellite data considered for calculating $eGWT_c$. However, as GWTs are expected to have increased during that time (Bayer et al., 2016; Kurylyk et al., 2014; Menberg et al., 2014), these measurements are included in the following comparison viewing them as minimum values. In order to inspect the role of temporal variability and trends, we separately compare measured GWTs from (i) 1977, (ii) 1990 - 2015, and (iii) 2005 - 2015 with satellite-derived estimates. The latter GWT subset is extracted as it covers roughly the same time period as the satellite-based product. Since satellite data covers the time period from 2005/01 till 2014/12 and GWTs are recorded till 2015/11, the data contains a negligibly small amount of 85 unsynchronized single measurements (4.4 % of the single measurements between 2005 and 2015).

Figure 2.6 shows the measured GWTs versus LST and $eGWT_c$ along with misfit and Spearman correlation indices. The city centre wells measured in 1977 (Figure 2.6a) yield misfits (RMSE, MAE) between $eGWT_c$ and measured GWTs around 0.5 K higher than the error observed between LST and GWT. Additionally, the ME is higher (Figure

2.6a,d) when comparing measured groundwater data with $eGWT_c$ (1.27 K) than with just LST (0.09 K). This means that subsurface temperatures are overestimated by $eGWT_c$ when using recent values of LST and old well temperatures in equation (3). As LST is expected to have increased by around 1 K from the 1970s to the period between 2005 to 2015 due to climate change and atmospheric urban heating this is not surprising. At the same time GWTs in 1977 were as high as 18.3 °C, which is warmer than the assumed BT of 17.5 °C. Therefore, other heat sources such as heat release from subsurface infrastructures may play a significant role but cannot be reproduced by this method. This is supported by the low sensitivity of the measured GWT to the LST as revealed by Figure 2.6a.

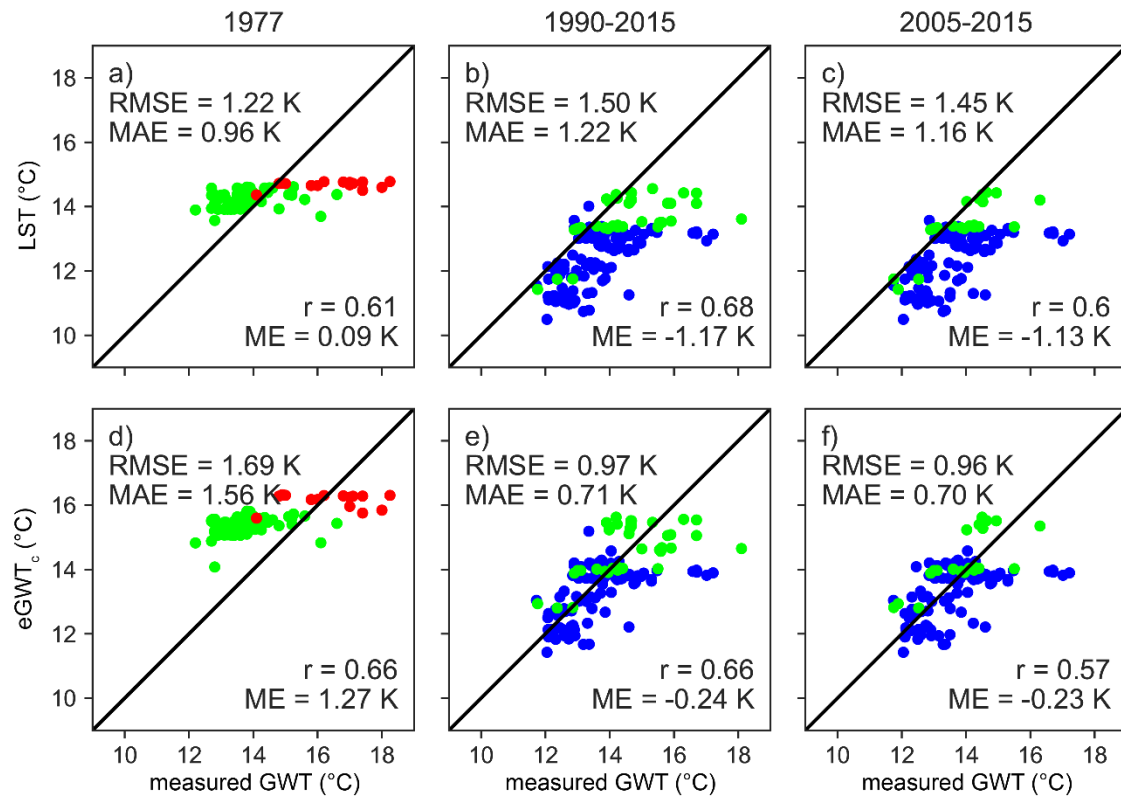


Figure 2.6: (a-c) Land surface (LST) and (d-f) estimated groundwater temperatures ($eGWT_c$) versus measured GWTs for time periods 1977, 1990 to 2015, and 2005 to 2015. Red, green and blue dots represent city centre, inner and outer the suburbs, respectively.

The picture is different when analyzing the recent datasets from 1990 to 2015 and 2005 to 2015: when using $eGWT_c$ instead of LST RMSEs decrease by 0.53 K and 0.49 K and the MAE decreases by 0.51 K and 0.46 K for the time periods of 1990 to 2015 and 2005 to 2015, respectively (Figure 2.6b,c,e,f). The RMSE and MAE relative to $eGWT_c$ are below 1 K for both time periods, with both misfit values of the reference time period (2005 to 2014) being slightly lower compared to the entire dataset from 1990 to 2015.

We can therefore conclude that the estimation approach is most applicable for overlapping time periods between subsurface and satellite measurements.

Overall, the combined approach as given in Equation 2.3 delivered groundwater temperature estimates with a RMSE below 1 K. However, even for this time period, extreme temperature anomalies cannot be predicted. It is very likely that these wells are impacted by local heat sources other than buildings. When applying this method to the German cities of Berlin, Cologne and Karlsruhe, Benz (2016) found similar results with RMSEs between $eGWT_c$ and GWT of 0.96, 0.86 and 0.82 K, respectively.

2.4.3 Impact of urban and rural estimation approach on GWTs

To evaluate the suitability of the different GWT estimation procedures (Equation 2.1-3 and LST only), we use the correlation coefficient (r), RMSE, MAE and ME. Figure 2.7 shows the correlation to measured GWT of the different equations for calculating $eGWT_{urb}$, $eGWT_{rur}$, $eGWT_c$ and the sole use of LST .

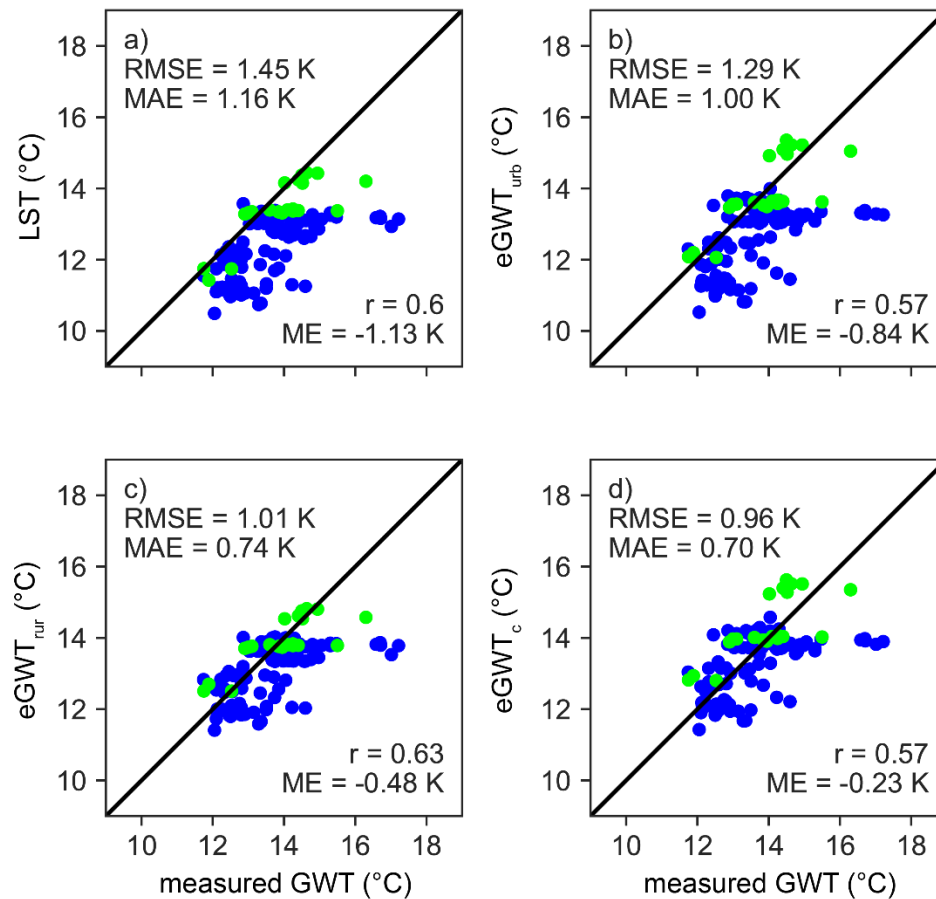


Figure 2.7: Comparison of LST (a), $eGWT_{urb}$ (b), $eGWT_{rur}$ (c), and $eGWT_c$ (d) for GWT and satellite data with measured GWTs within the years 2005 to 2015. Green and blue dots represent inner and outer suburbs, accordingly.

While RMSE and MAE are lowest for the combined method, indicating an improvement of the estimation accuracy, correlation is highest for $eGWT_{\text{rur}}$. According to these results, this approach which estimates naturally occurring offsets also has a higher impact on the predicted groundwater temperatures than the urban approach ($eGWT_{\text{urb}}$). This is a consequence of the location of the observations points that are solely in the inner and outer suburbs of Paris and have BD values below 0.3. In the city centre, BD values are more than doubled, which also doubles the amount of positive temperature correction (Equation 2.3). At the same time, the $eGWT_{\text{rur}}$ has a lower impact on the city centre because both SD and ET are significantly lower (Figure 2.3).

All predictions underestimate measured GWTs with a minimum ME of -0.23 K for $eGWT_{\text{c}}$. However, we could improve the negative offset by 0.9 K compared to the misfit between measured GWTs and LST . In contrast, Benz (2016) found that the combined method overestimates temperatures in the city centres of Karlsruhe, Cologne and Berlin. This overestimation can in part be attributed to insulation of basements, which is not considered in this estimation. Overall, we expect $eGWT_{\text{c}}$ to work best in city centres of larger urban areas, due to higher BD and lower ET and SD values. For the given groundwater data in the outskirts of Paris, $eGWT_{\text{c}}$ is only slightly favorable over the use of $eGWT_{\text{rur}}$.

Although the comparison between the results of the individual equations correlates well with measured groundwater, the used approach also has some limitations. Particularly, local thermal disturbances caused by underground anthropogenic heat sources (e.g. geothermal devices, sewer networks and underground constructions) cannot be detected from above ground data or their thermal footprints are too small to be resolved by the resolution of $1 \text{ km} \times 1 \text{ km}$ of $eGWT_{\text{c}}$. Moreover, the resolution of the ET data set is very coarse (about 28 km) and cannot detect small-scale or even city-scale features. Applying the combined method to Karlsruhe and Cologne in Germany, the ET dataset did not display the reduction of ET commonly associated with urban areas, which added to an overestimation of GWTs in those areas (Benz, 2016). Unfortunately, no recent GWTs within the Paris city centre are available here and these observations can thus not be tested for such a large-scale city. However, future measurement campaigns could help to eliminate this limitation.

Another limitation of the method used is that the *LST* as primary input data already indicates a heat anomaly in the city centre, and the data used for *ET* and *SD* are also affected by urbanization. Accordingly, it cannot be differentiated between natural and anthropogenic thermal contributions by the use of this method, whereas the processes itself can fairly easily be attributed to one or the other.

2.5 Conclusions

For the first time, the large-scale SUHI in the groundwater of Paris is spatially investigated. The minimum and maximum GWTs are 11.4 °C and 17.2 °C measured between 2005 and 2015 for the shallow subsurface at depths between 15 m and 80 m. These GWTs represent the inner and outer suburbs of Paris. They should be interpreted as regional trends and are not meant to represent local temperature disturbances caused by anthropogenic heat sources which may be of a much greater magnitude. The minimum and maximum GWT observed in 1977 below the city centre ranges between 14.1 °C to 18.3 °C. Despite the temporal gap of 28 years between the two measurement campaigns, this indicates a characteristic difference between the centre and suburbs. Based on the examined data, the maximum GWT anomaly reaches 6.9 K in Paris.

In the present study, an approach is applied that estimates groundwater temperatures ($eGWT_c$) from satellite-derived data and building footprints combining existing methods for estimating rural ($eGWT_{\text{rur}}$) and urban ($eGWT_{\text{urb}}$) groundwater temperatures. Estimates are validated with temperatures measured in the wells of Paris. Predicted GWT have a very good fit ($RMSE < 1$ K) and only slightly underestimate measured GWT with a mean error of -0.23 K. In addition to that, a coherent spatial estimation of the SUHI of Paris is obtained. Even so, measured extreme GWT that cannot be reproduced as subsurface heat sources other than in basements are not considered. In an ideal case, the estimation techniques displayed here would supplement existing temperature measurements in wells, which would allow use of this method as a tool to spatially connect point information obtained from wells.

In future studies, the presented procedure needs to be further validated by estimating GWTs in other rural and urban environments. This is ideally accomplished in regions, where GWT data with a very dense spatiotemporal resolution is available. When applying this approach to other cities, it should be kept in mind that the anthropogenic

fingerprint varies among different regions, countries and climates. The role of this variability will be scrutinized by comparison of different case studies in the future.

3 Climate change yields groundwater warming in Bavaria, Germany

3.1 Publication abstract

Thermodynamic coupling between atmosphere and ground yields increasing aquifer temperatures as a consequence of global warming. While this is expected to manifest as a gradual warming in GWT time series, such continuous long-term recordings are scarce. As an alternative, the present work examines the use of repeated temperature-depth profiles of 32 wells in southern Germany, that were logged during campaigns in the early 1990s and in 2019. It is revealed that the temperatures have increased in nearly all cases. We find a moderate to good depth-dependent correlation to trends in air temperature, which however is strongly influenced by local hydrogeological and climate conditions. While during the last three decades, air temperatures have increased by a rate of 0.35 K/dec on average, the temperature increase in the subsurface is decreasing with depth, with median values of 0.28 K/dec in 20 m and only of 0.09 K/dec in 60 m depth. Still, the slow and damped warming of the groundwater bodies are remarkable, especially considering naturally very minor temperature changes in pristine groundwater bodies and predictions of atmospheric temperatures. This entails implications for temperature-dependent ecological and hydro-chemical processes, and also for the heat stored in the shallow ground. Moreover, it is demonstrated that the annual heat gain in the groundwater bodies below 15 m due to climate change is in the range of one third of the state's heat demand, which underlines the geothermal potential associated with the change in natural heat fluxes at the ground surface.

3.2 Introduction

Global warming is one of the most pressing challenges in the 21st century. Atmospheric climate and temperature variations are excessively studied, and a gigantic amount of climate data are continuously collected to delineate past warming trends and to predict future impacts of greenhouse gas accumulation. There is much less attention to the subsurface thermal regime, which is thermodynamically coupled with the atmosphere and thus also influenced by climate change. In fact, borehole temperature depth-profiles that deviate from the normal geothermal gradient served as early witnesses of regional atmospheric temperature increase (Pollack and Chapman, 1993; Wang and Lewis,

1992). This has in particular been studied in boreholes where vertical conduction is the dominant heat transport process and groundwater flow can be neglected. In contrast, temperature profiles recorded in wells are favoured to infer the role and intensity of vertical groundwater flow (Bense et al., 2017; Bredehoeft and Papaopulos, 1965; Kurylyk and Irvine, 2019; Kurylyk et al., 2019; Li et al., 2019; Sorey, 1971; Taniguchi, 1993; Taniguchi et al., 1999). The use of natural temperature variations in aquifers has also been recognized as a precious tracer to understand groundwater flow systems, in particular when interacting with surface waters (Coluccio and Morgan, 2019; Constantz, 2008; Kaandorp et al., 2019; Molina-Giraldo et al., 2011; Rau et al., 2010; Saar, 2011).

Temperature profiles measured in wells reflect spatially and temporally varying heat inputs in aquifers from the surface and thus can be used to examine thermal coupling at the ground surface (Bense and Kurylyk, 2017; Burns et al., 2016; Gunawardhana and Kazama, 2011; Kurylyk et al., 2013). Especially when the shallow subsurface is dominated by horizontal flow, changes in atmospheric temperatures and land use represent thermal signals that are conducted to the aquifer and become visible in well-logs. These changes are pronounced in cities, where accelerated heat flux from urban warming, sealed ground and buried infrastructures yields large scale SUHIs (Bayer et al., 2019; Benz et al., 2016; Epting et al., 2017b; Ferguson and Woodbury, 2004; Hemmerle et al., 2019; Menberg et al., 2013b; Zhu et al., 2015), and urban, industrial and waste sites are revealed to cause the most prominent local heat anomalies in Central European aquifers (Tissen et al., 2019). In less-disturbed rural areas, GWTs are reported to slowly increase as well, which is obviously the response of the shallow ground to recent climate change (Bloomfield et al., 2013; Colombani et al., 2016; Kurylyk et al., 2014; Maxwell and Kollet, 2008; Menberg et al., 2014). In comparison to atmospheric temperature recordings, however, continuously monitored long-term time series of GWTs are scarce, often strongly superimposed by local effects and thus our current picture of subsurface warming due to climate change is not very clear. As alternative means, repeated transient temperature logs in wells can be used (Bense and Kurylyk, 2017; Benz et al., 2018b). Conductive heat transport through the ground and aquifer is slow, however, the time period between two measurements has to be in the order of years and ideally decades.

In this study, the main objective is to reveal subsurface temperature variations. We report the findings of rare well temperature profiles measured again after more than 25 years.

Focus is set on a large spatial coverage with several wells in order to reveal regional groundwater warming and to minimize the fingerprint of local effects. The wells are all located in the country of Bavaria in southern Germany, where climate change effects on groundwater are broadly discussed. As in many other countries, aquifers represent the major source of freshwater and thus any factors that impair groundwater reservoirs are of prime hydrological interest. Therefore, related work and recent reviews of groundwater climate change focus mainly on change of groundwater recharge and availability (Alam et al., 2019; Bloomfield et al., 2019; Earman and Dettinger, 2011; Green et al., 2011; Stoll et al., 2011; Zhang et al., 2020). Potential hydrochemical effects from climate-driven shifts in groundwater levels on contaminant mobilization are stressed by Jarsjö et al. (2020). The consequences of ongoing shallow groundwater warming are only rarely discussed but manifold (Riedel, 2019). Among these are fundamental changes to microbial activity and ecosystems in groundwater that rely on long-term stable thermal conditions (Griebler et al., 2019; Kløve et al., 2014), as well as potential threads on spring and cave ecosystems (Jyväsjärvi et al., 2015; Mammola et al., 2019). Leonhardt et al. (2017) emphasize for the springs in the Bavarian National Parks that climate change effects are most critical, and just recently therefore a program of long-term monitoring of biotic and abiotic data including temperature at 15 of these springs has been initiated by the authorities.

In the following, we describe the temperature profile measurements in Bavarian wells, which serve as the basis of this work. The presented data preparation is tailored to the purpose of this study, which is on quantifying the long-term thermal evolution of the aquifers on the country scale. This is examined by including available air temperature records and comparing the changes in the atmosphere with those found in the subsurface. Furthermore, in order to elucidate the heat accumulation associated with climate induced warming of the subsurface, also the change of the regional geothermal potential is assessed.

3.3 Methods and data

3.3.1 Groundwater temperature data

GWT data is recorded in Bavaria by logging temperatures in observation wells using a water level meter with a temperature sensor. Data was gathered during the period from 1992 to 1994 and in 2019. During the 1992-4 period, wells were sampled every 3 months

on an irregular basis within one year, so that up to four measurements were obtained for each well. These measurements were performed by the Landesamt für Umwelt Bayern (LfU Bayern), which is the environmental state office of the federal state of Bavaria in Germany. In 2019, the same set of wells were measured in April and July/August field campaigns using a water level meter type 120 – LTC from HT Hydrotechnik GmbH. For the 2019 dataset, precision and accuracy of the temperature sensor is 0.1 K. For the 1992-4 sampling campaign, the precision is also 0.1 K. The accuracy for this dataset is assumed to be in the same magnitude, assuming the use of standard devices even though no detailed information on the applied loggers is preserved. The vertical resolution of sampling was highest close to the surface where temperature variations are commonly strongest. Temperatures were recorded in 1 m steps above 20 m, in 2 m steps between 20 and 40 m and in 10 m steps below 40 m for the 1992-4 campaign. In 2019, temperature was sensed at 0.5 m intervals above 10 m, at 1 m intervals between 10 and 40 m, at 2 m intervals between 40 and 60 m and at 5 m intervals below 60 m. For further analysis, all measured temperatures were then interpolated linearly at 1 m resolution.

Initially the data set measured in 1992-4 covered 347 temperature-depth profiles (209 of the wells are shallower than 10 m). From these, 95 wells had a complete seasonal record of four seasonal measurements. Temperature data from these 95 wells have been made available by the LfU Bayern for this study. Out of these, 46 wells were measured again in 2019. The other wells were either shallower than 15 m, have been dismissed from the observation well network (renaturalised), could not be found in the field or could not be accessed (no access permission for wells on private property).

For this study we applied a threshold for seasonal temperature variation of 0.5 K below 20 m. 12 wells that exceeded this threshold were cut for further analysis. These wells showed inconsistencies or clearly revealed the effect of disturbing processes either in the 1992-4 or in the 2019 measurements. In one of the wells abnormal changes of more than 4 K between the 1990s and 2019 period together with an inconsistent signal in 2019 were related to strong superpositioning of local anthropogenic disturbances and thus these measurements were also excluded. At one well, the groundwater table was below 100 m depth, and in one well the probe got stuck in both 2019 measurements after less than 2 m below groundwater level. These two wells have also been excluded for further analysis.

The 32 remaining observation wells are located in different hydrogeological settings and distributed all over Bavaria. A map showing the location of the observation wells and air temperature stations is given in Figure 3.1. Temperature-depth profiles are available as supplementary material to this article and are additionally archived in World Data Center PANGAEA (<https://doi.pangaea.de/10.1594/PANGAEA.923529>).

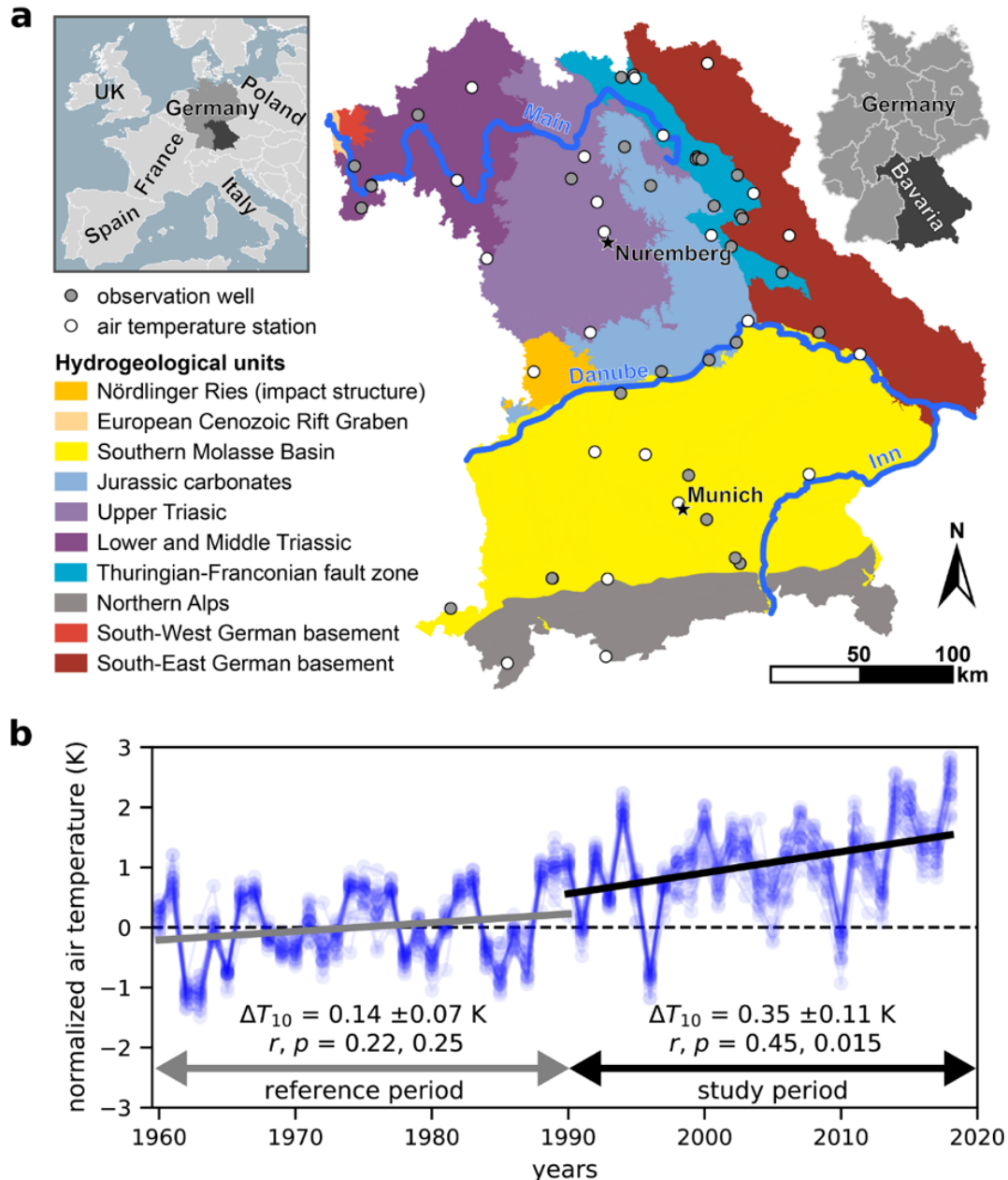


Figure 3.1: (a) Map of the main hydrogeological units and the location of the 32 groundwater temperature (GWT) observation wells and the 23 air temperature (AT) stations selected for this study. Major cities and rivers are indicated by black stars and blue lines, accordingly. (b) Arithmetic annual mean air temperatures from 1960 to 2018 for 23 stations in Bavaria (blue dots and lines). Temperatures are normalized to the respective mean temperature of the period from 1960 to 1989 for each station. ΔT_{10} is the decadal temperature change calculated by a linear least square regression with the Pearson correlation coefficient (r) and p-value (p).

3.3.2 Air temperature data

To derive atmospheric temperature trends, we used arithmetic annual mean values from 23 air temperature stations in Bavaria. These data are provided by the Climate Data Center (CDC) run by the Deutscher Wetterdienst (DWD). According to recommendation of the World Meteorological Organization (2017) air temperature data was split into two 30-year periods. Herein after referred to as reference period 1960-1989, and study period 1990-2019. Air temperature stations were selected for having consistent, gap-free records from 1960 onwards. Detailed descriptions and metadata for each weather station can be found on the accessed FTP server by the DWD.

3.3.3 Theoretical geothermal potential

Temperature variations in the subsurface also change the total thermal energy stored in the subsurface. From the perspective of shallow geothermal energy utilization, this energy determines the theoretical geothermal potential (Bayer et al., 2019). This represents the heat in place and can be calculated based on the caloric equation of state for a water saturated homogeneous solid:

$$E = [n \cdot c_w + (1 - n) \cdot c_s] \cdot V \cdot T \quad (3.1)$$

where n is the porosity of the solid, c_w and c_s in $\text{kJ}(\text{m}^3\text{K})^{-1}$ are the volumetric heat capacities of water and solid, V (m^3) is the reservoir volume and T (K) is the temperature of the reservoir. This equation can be condensed by distinction of a component related to material properties, $m = n \cdot c_w + (1 - n) \cdot c_s$, and a part describing the thermal field of the reservoir, $\tau = V \cdot T$. If we assume a laterally homogeneous reservoir where temperature only varies with depth (z), τ becomes $\tau = A \cdot \int T(z) dz = A \cdot \theta$, where A is the area and θ is the integral of the temperature over depth. Thus, the heat in place is $E = m \cdot A \cdot \theta$. Accordingly, the change of the thermal energy stored in the subsurface with constant material properties can be described as $\Delta E(\tau) = m \cdot A \cdot \Delta\theta$.

We also tested a different approach where the arithmetic mean difference profile is linearly fitted to each observation profile. This approach is based on standard statistical measures, as related spatial temperature profile analysis is scarce, there is no earlier work known following the same approach. In this model, profiles are calibrated for the lowest RMSE between the reference profile and the measured ΔT profiles at each station. This allows for the possibility to get both a spatial and a total depth coverage at each observation well. The resulting profiles were integrated over the depths between 15 and

100 m and afterwards interpolated via inverse distance weighting on a 1 x 1 km grid with a total of 70,610 grid cells for the state of Bavaria.

3.4 Results and discussion

3.4.1 Recent variations in air temperature

Recent trends in air temperature are calculated from annual mean values of 23 air temperature stations, uniformly distributed over Bavaria (Figure 3.1b). Figure 3.1a shows the temperature record since 1960 normalised by the corresponding mean temperature of the reference period from 1960-1989 for each station. Annual mean air temperature records for individual stations exhibit a high year-to-year variability of up to 3 K, but also a high consistency of the trendlines among each other. This indicates that relative air temperature changes behave uniformly within the studied area and are forced by a large-scale climatic regime. Calculating a linear regression over longer periods allows to deduce the decadal temperature change rate (ΔT_{10}), which is the slope of the linear regression per decade. For the study period of 1990-2019, the linear regression of these air temperature stations yields a slope of 0.35 ± 0.11 K/dec. Compared to the linear regression slope of the previous 30 years period of 0.14 ± 0.07 K/dec, the rate of temperature change for the study period is significantly elevated. The change in slope of the linear regression is consistent with the median temperature change of 1.06K between 1990-2019 and the subsequent 30 years (1960-1989), which results in a decadal temperature change of also 0.35 K/dec.

3.4.2 Recent variations in groundwater temperature

To reveal subsurface temperature variations, we will first describe recent GWT variations in the wells individually. Recorded temperature profiles reflect a limited section of the subsurface. This section is limited by the groundwater table towards the top and the drilling depth of the observation well to the bottom. From the seasonal measurements 1992-4 period, we can confer seasonal temperature variation by depth. For depths shallower than 15 m, seasonal variations are higher than 0.1 K and thus measurable. Supplementary Figure S6.1 shows the mean values of the ranges (min-max differences) per depth at the selected 32 stations.

Vertical temperature changes below 15 m commonly follow the local geothermal gradient according to the basal heat flux from the interior of the earth. They also conserve thermal signatures over a longer time period, e.g. from land-surface

temperature changes (e.g. in urban areas (Banks et al., 2009) as well as from changes in regional GWTs – which closely reflects mean annual air temperatures in the recharge area (Burns et al., 2017)). Changes in repeated temperature profiles measured over timeframes of more than a year can therefore reveal long-term temperature variations, such as those related to global warming. The temperature difference, $\Delta T(z)$, between the 1992-4 and the 2019 period is calculated from mean temperature profiles for each time period (cf. Supplementary Figure S6.2). This yields ΔT -profiles for each individual station depicted in Figure 3.2a. To deal with alternating sampling dates in the 1992-4 period and for better comparability, the temperature change is normalised to the ΔT_{10} with respect to the time span between the periods. The decadal temperature change rates per depth are depicted as boxplots in Figure 3.2b. At a depth of 20 m, ΔT_{10} varies between -0.01 and 0.49 with a mean of 0.28 K/dec. Towards greater depths, the mean ΔT_{10} decreases to 0.16, 0.09, 0.07, 0.05 K/dec at 40, 60, 80 and 100 m depth, respectively.

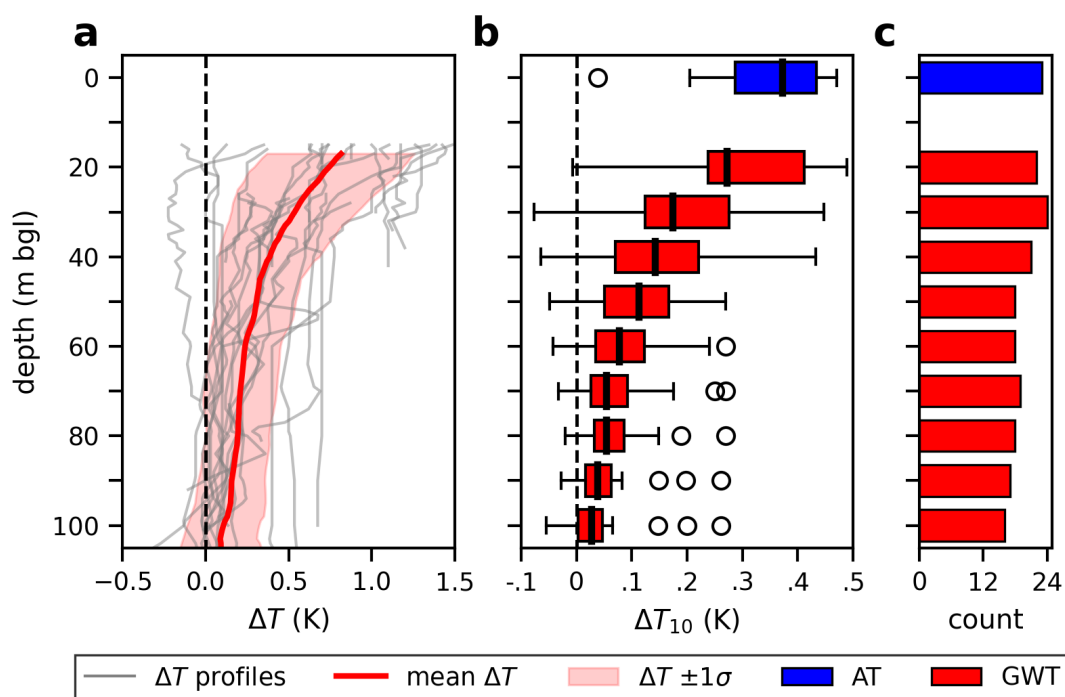


Figure 3.2: (a) Differences (ΔT) between the temperature profiles measured in 2019 versus the mean signal of the time period from 1992-1994 (grey lines). The arithmetic mean difference (red line) is calculated as rolling mean with a window of 5 m and is displayed as red line along with the standard deviation (1σ) as red transparent area. (b) Decadal temperature change rate (ΔT_{10}) for air temperature (AT, blue box) and groundwater temperature at different depths (GWT, red boxes). AT represent the slopes of ordinary least squared regression on annual mean values from 1990-2018. GWT rates are calculated from temperature-depth profiles measured in 2019 and 1992-1994. Whiskers are drawn for values smaller than 1.5 magnitudes of the interquartile range. Outliers are shown as dots. The mean value is given as white bar. (c) Count of measurements at respective depths.

The proposed rates are in line with recent single depth groundwater observations from the western adjacent federal state of Baden-Württemberg and observations in Austria in the south. For Baden-Württemberg, Riedel (2019) reported ΔT_{10} rates of 0.1 to 0.4 K/dec based on a state-wide groundwater quality dataset for the period from 2000 to 2015. Riedel (2019) also found a quasi-depth dependency with temperatures in spring waters averaging at a higher ΔT_{10} rate of 0.3 K/dec over a rate of 0.2 K/dec in groundwater. In Austria, Benz et al. (2018a) observed a slightly higher temperature change rate of 0.7 ± 0.8 K over the 20-year period from 1994 to 2013 ($\Delta T_{10} \sim 0.37 \pm 0.42$ K/dec). In both studies, temperature change rates are not linked to depths. Despite this it has to be noted that the average measurement depth in the Austrian wells is relatively shallow at 7 ± 4 m below ground surface.

3.4.3 Correlation between air and groundwater temperature change rates

To infer the correlation between air and groundwater temperature variations, the air temperature at each observation well is calculated by inverse distance weighting of the five nearest air temperature stations. Figure 3.3 shows the temperature change per decade for each of the 32 observation wells for air temperature and the mean value of 10 m increments of the individual temperature profiles. For the respective depths vs. air temperatures, Pearson correlation coefficients (r) indicate a moderate but robust correlation with values between 0.4 and 0.6. p -values exhibit that statistical significance is increasing with depth despite a high-variability. In general, higher temperature change rates in air temperature are reflected by higher temperature change rates in the subsurface. However, local variations are high both in the penetration depth of the signal and in absolute values. Note that air temperature change rates have a low standard deviation of 0.8 K, which makes it hard to identify distinct variations between temperature stations, as the atmospheric temperature signal is more homogeneous than that in the subsurface. The diffuse signal present in the subsurface is hereby hard to infer with the minor variations in air temperatures (Figure 3.3a). The correlation metrics are highest for the ΔT_{10} at 100 m and inferred air temperature. Assuming a process where the thermal field of the subsurface is mainly altered by a change in ground surface conditions (e.g. for shallow and unconfined aquifers), we would expect the contrary with decreasing metrics at greater depth induced by changing ground surface conditions.

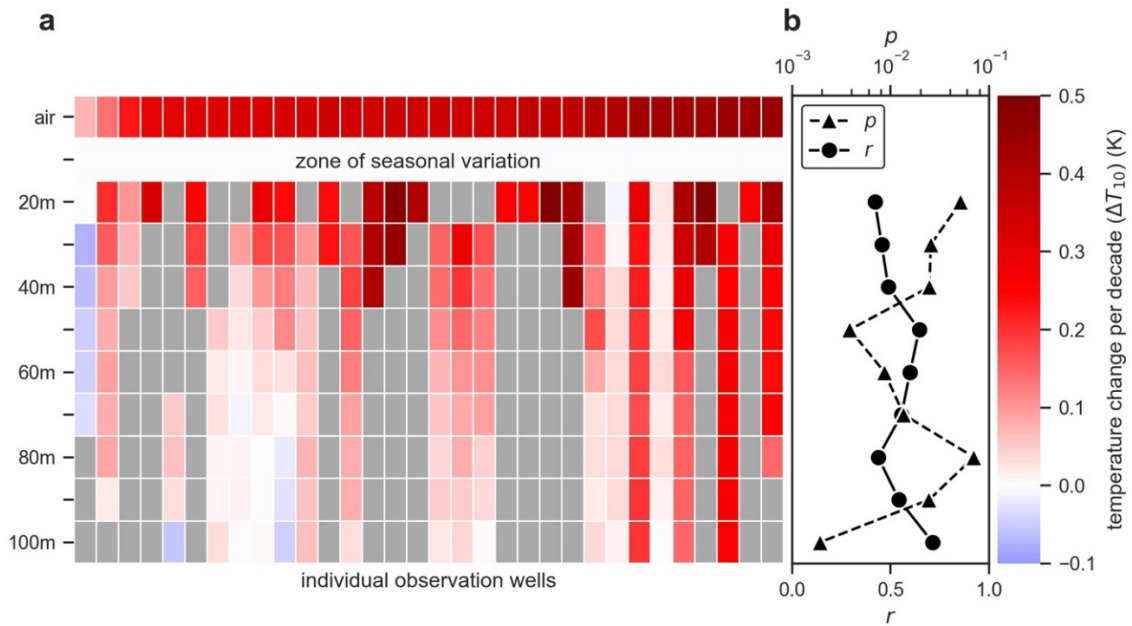


Figure 3.3: (a) Heatmap showing the temperature change per decade (ΔT_{10}) for air temperature (AT) of the period from 1990-2018 and for groundwater temperature (GWT) calculated from temperature-depth profiles measured in 2019 and 1992-1994. Air temperature is inferred for each observation well location. Values at 10 m depth have been masked for showing high seasonal variability. Observation wells are sorted by their AT lapse rates. Empty cells are displayed in grey. (b) Pearson correlation coefficient (r) and p-value (p) for GWT at respective depths.

Obviously, correlating surface or air temperatures directly to subsurface temperatures presumes that changes in the temperature profile are a result of downward vertical heat transfer (advective or diffusive). If this is not the case, temperatures especially at greater depths could be altered by lateral heat transfer associated with the regional groundwater flow regime (Bense et al., 2020; Burns et al., 2016; Taniguchi et al., 1999; Zhu et al., 2015). In this case the temperature profile would carry an integrated signal dominated by annual mean temperatures of the recharge area. However, despite the potential influence of local hydrogeological conditions, it is also possible that the observed discrepancy is an artefact of the statistical analysis as the number of observations decreases with depth (from 24 to 16).

The substantial number of wells included in this study allows robust average estimates. Compared with the corresponding aboveground air temperatures, as expected, the decadal temperature increase is dampened in the subsurface. The median values for Bavaria are $\Delta T_{10} = 0.35$ K for the atmosphere, 0.28 K at 20 m and 0.09 K at 60 m depth. This means that at the deepest level, the changes, however, are close to measurement accuracy. Temperatures in air and subsurface show a moderate to good correlation, with higher scattering of groundwater than air temperatures. Major tendencies of air

temperature are also reflected in the subsurface temperature record. This supports a good statistical basis of the measured data, even without detailed analysis of the site-specific heat transport processes.

3.4.4 Shallow geothermal potential of recent temperature variations

The changes in subsurface temperatures also constitute an increase in thermal energy stored in the subsurface in response to recent shifts in the thermal regime of surface conditions. This additional heat can be accessed via shallow geothermal systems and thus increases the theoretical geothermal potential of the shallow subsurface. To accurately quantify this additional heat, both geological material properties and the thermal field have to be characterized at a high level. However, thermal properties such as heat capacity do not vary over a broad range in geological media (Stauffer et al., 2013).

Table 3.1: Heat content model parameters for the minimum, medium and maximum scenario.

Parameter	Abbrv.	Unit	Min	Median	Max
Area	A	km ²		70,610	
Vol. heat capacity of water	c_w	kJ (m ³ K) ⁻¹		4,190	
Vol. heat capacity of the solid	c_s	kJ (m ³ K) ⁻¹	1,900	2,200	2,500
Porosity	n	-	0.05	0.1	0.15
Energy stored per year	ΔE	PJ	155	184	212
Standard deviation	1σ	PJ	125	149	171
Energy stored per year (spatial IDW)	ΔE	PJ	208	248	285
Root-mean squared error (spatial IDW)	$RMSE$	PJ	40	47	54

If we assume bulk material properties and superimpose an arithmetic mean ΔT profile over the depth interval between 15 and 100 m below surface, we can calculate a rough estimate of the magnitude of the heat flow into the subsurface. Table 3.1 lists the energy stored per year for a minimum, a maximum and median (50%) assumption of porosity (0.5 to 0.15) and volumetric heat capacity of the solid (1900 to 2500 kJ (m³ K)⁻¹). The energy stored per year varies between 155 (± 125) and 212 (± 171) PJ between the minimum and maximum scenarios ($\pm 1\sigma$). For the median scenario the thermal energy stored by climate change in the subsurface per year equals 184 (± 149) PJ. Compared to the primary energy demand (1944 PJ) and the heating demand (669.7 PJ) in 2017 (Ebert and Voigtländer, 2019), the energy stored per year in the subsurface for the median scenario equals 9.5% of the annual primary energy demand or 27.5% of the heating

demand of Bavaria. This simplistic calculation, however, does not consider spatial variations and relies on the arithmetic mean differences of all profiles.

For an alternative approach where the arithmetic mean difference profile is linearly fitted to each observation profile, stored energies for the minimum and maximum scenario are 208 and 285 PJ with RMSEs of 40 and 54 PJ, accordingly. The median scenario yields a thermal energy input of 248 PJ with an RMSE of 47 PJ, which would equal 12.8% of the Bavarian primary energy demand or 37% of the heating demand. Figure S3 and S4 in the supplementary material display the profile fitting and the spatial distribution of interpolated groundwater and air temperatures. Note that the spatial coverage of the observation wells with respect to the area of Bavaria is insufficient to produce fully reliable numbers, but it provides a first rough estimate of the order of magnitude of energy stored in the subsurface annually. Still, the presented spatial approach offers the opportunity to employ more precise regionalised material parameters for heterogeneous hydrogeological facies. In essence, we found the thermal energy stored by climate change in the subsurface per year to be in the magnitude of 10% of the total Bavarian primary energy demand, or one third of the heating demand. This continuous heat transfer represents an enormous replenishing resource that is fuelled by climate change. The results from this local study are expected to be applicable in similar magnitudes on a global scale as observed atmospheric temperature trends in Bavaria are in line with the global trend and the thermal connection between the surface and shallow subsurface has been proven to be robust also on a global scale (Benz et al., 2017a).

3.5 Conclusions

The scope of this study was to extract regional long-term trends of GWT, and for this purpose, well profiles re-measured after up to 27 years were compared to each other. In order to remove as much as possible momentary, local variability, we compared profiles that were obtained as averaged logs from repeated campaigns throughout each year. The total number of suitable wells was 32 which cover broadly the entire state of Bavaria, Germany, and these offered a substantial insight into the shallow thermal regime in the subsurface. Clearly, each profile was different, influenced by the local hydrogeological, climatic and potentially anthropogenic conditions. However, short term variability and seasonality was shown to be marginal for these wells beneath 15 m, and this is where long-term climate change left an observable thermal imprint. Nearly all wells revealed

increasing GWTs. The increase and the discrepancy among the well profiles was largest at shallow depth, and a maximum warming of 1.5 K was observed. Only one well showed a slight cooling by 0.2 K, but on average, 0.7 K warmer groundwater is found at 15 m depth which declines with depth along the profile.

Over the past ~30 years, the warming climate transferred heat in the subsurface at a rate that is estimated roughly more than one quarter of the state's annual heating demand. Rising ground(water) temperatures increase shallow geothermal system efficiency, and accelerated ground heat flux represents a form of thermal recharge of shallow geothermal reservoirs. This ground heat gain thus can be considered as favourable for geothermal use. In contrast, groundwater ecosystems used to nearly static thermal conditions need to adjust and may be under increasing stress. Even if the changes are considered marginal so far, and impacts are considered acceptable, the GWT will further increase as delayed response to the past temperature changes, and are likely to rise further in response to future atmospheric warming.

4 The Evolution of the Geothermal Potential of a Subsurface Urban Heat Island

4.1 Publication Abstract

Meeting the rising energy demands of cities is a global challenge. Exploitation of the additional heat in the subsurface associated with the SUHI has been proposed to address the heating demands. For the sustainable use of this heat it is crucial to understand how SUHIs evolve. To date, there have been no comprehensive studies showing how temperature anomalies beneath cities change over time scales of decades. Here, we reveal the long-term increase of temperatures in the groundwater beneath Cologne, Germany from 1973 to 2020. The rise in GWT trails atmospheric temperature rise in the rural areas and exceeds the rise in atmospheric temperature in the urban centre. However, the amount of heat that is currently stored each year in the thin shallow aquifer reaches only 1% of the annual heating demand. The majority of the anthropogenic heat passes by the vertical extent of the aquifer or is discharged by the adjacent river. Overall the geothermal resource of the urban ground remains largely underused and heat extraction as well as combined heating and cooling could substantially raise the geothermal potential to supply the city's demand.

4.2 Introduction

Emerging urban expansion and densification cause warming in cities. So-called UHIs overprint natural conditions in the atmosphere, at the surface and also in the subsurface (Ferguson and Woodbury, 2007; Oke, 1982). Above ground UHIs have a negative connotation as increased heat stress raises mortality especially during the warm period (Hsu et al., 2021; Lo et al., 2019). Conversely, SUHIs can have beneficial effects on the shallow geothermal potential of urban aquifers (Bayer et al., 2019; Zhu et al., 2010). The rising energy demand for heating and cooling forced by socioeconomic trends and higher cooling loads in response to climate change (IEA, 2018; van Ruijven et al., 2019; Yalew et al., 2020) is amplified in cities as the proportion of people who are living in cities is to rise continuously in the 21st century (Ritchie and Roser, 2018; United Nations and Social Affairs, 2018).

We are facing this rising energy demand under the necessity to mitigate greenhouse gas emissions and to achieve better integration of renewable energies into our cities

(Kammen and Sunter, 2016). Compared to transmission of electric power, transportation and distribution of thermal energy is not feasible at larger scales (Henry et al., 2020). Accessing shallow geothermal energy from urban aquifers yields one of, if not the, most promising alternative to combustion of fossil fuels for thermal applications in cities. Shallow geothermal applications in cities benefit from elevated urban underground temperature in comparison to natural conditions (Couderc, 2017; Rivera et al., 2017). Given the relatively high energy density of soil and groundwater, this significantly elevates the potential of shallow geothermal systems for heating (Arola and Korkka-Niemi, 2014; Bayer et al., 2019; Zhu et al., 2010). Vice versa, elevated temperatures in urban aquifers decrease the potential for space cooling with geothermal energy.

Efficient planning and implementation as well as sustainable operation of shallow geothermal units in urban aquifers requires a detailed conceptual knowledge and understanding of the processes that lead to the formation of SUHIs. While above ground the UHI phenomenon is well studied and monitored, little so can be said for underground conditions even though SUHI effects have been reported in more than 50 cities globally (Figure 4.1)(Allen et al., 2003; Arola and Korkka-Niemi, 2014; Bucci et al., 2017; Buday et al., 2019; Changnon, 1999; Djebebe-Ndjiguim et al., 2013; Eggleston and McCoy, 2015; Epting et al., 2017a; Farr et al., 2017; Ferguson and Woodbury, 2007; Ford and Tellam, 1994; García-Gil et al., 2016; Headon et al., 2009; Hemmerle et al., 2019; Huang et al., 2020; Kazemi, 2011; Klene et al., 2003; Lee and Han, 2013; Lokoshchenko and Korneva, 2015; Marschalko et al., 2018; Menberg et al., 2013b; Morris et al., 2006; Mount and Hernandez, 2002; Müller et al., 2014; Öngen et al., 2021; Previati and Crosta, 2021; Salem et al., 2004; Savva et al., 2010; Schweighofer et al., 2021a, b; Tang et al., 2011; Taniguchi et al., 2005; Taniguchi et al., 2007; Taylor and Stefan, 2009; Tissen et al., 2021; Turkoglu, 2010; Visser et al., 2020; Vranjes et al., 2015; Westaway and Younger, 2016; Yalcin and Yetemen, 2009; Yamano et al., 2009; Yusuf, 2007). SUHIs are formed by anthropogenic surface warming that propagates into the subsurface and is enhanced by buried infrastructures, especially if these reach into the water-saturated zone (Attard et al., 2016a; Bidarmaghz et al., 2019; Epting et al., 2013). In the subsurface, UHIs typically have average temperature increases between 1 to 3 K beneath the entire urbanized area, but with pronounced local hot spots. As heat transfer is much slower in the subsurface, short-phased surface variations, such as the

seasonal signal, fuse into a year-round stable temperature at depths greater than 10 m bgl.

Due to the scarcity in underground temperature monitoring, available studies provide mostly stationary descriptions of the thermal field. Studies that report urban underground temperature over time are extremely rare and typically only comprise few years. Especially in studies covering less than five years, extreme temperature rises that locally exceed +2 K/dec are reported (Lee and Han, 2013; Previati and Crosta, 2021; Schweighofer et al., 2021b), while also average temperature rises are above +0.5 K/dec (Epting et al., 2017a; Previati and Crosta, 2021; Schweighofer et al., 2021b). In many places urban temperature rise more than doubles the expected surface warming in response to climate change (Bayer et al., 2016; Eggleston and McCoy, 2015). Despite these insights, there is a lack of evidence on how urban underground jointly responds to climate change and anthropogenic warming.

To quantify the geothermal potential of cities, most studies assess the theoretical geothermal potential (TGP) (Bayer et al., 2019), which is the available heat in place for a stationary temperature distribution above natural conditions. The TGP is based on depleting the additional energy in the reservoir and it could be shown that it could in theory supply the annual heating demand in cities for multiple years (Zhu et al., 2010).

The objective of this study is to reveal the long-term evolution of the SUHI phenomena and its significance for future shallow geothermal energy supply in cities. We want to fill this research gap by presenting unique city-wide subsurface temperature records for the city of Cologne, starting in 1973 (Balke, 1974). Cologne is one of few cities where extensive GWT monitoring has been performed since the 1970s (Balke, 1974, 1977; Balke and Kley, 1981) with an urban underground temperature anomaly of up to 4 K reported already in 1974. These early works date back more than three decades before the term SUHI was phrased and are backed up by a variety of recent studies (Benz et al., 2015; Benz et al., 2016; Menberg et al., 2014; Menberg et al., 2013b; Meng et al., 2019; Vienken et al., 2019; Zhu et al., 2015; Zhu et al., 2010). We demonstrate how the thermal field develops and how the urban aquifer is charged by anthropogenic heat emission and climate change. These results offer a unique insight into heat storage rates and SUHI evolution based on data monitored over nearly half a century.

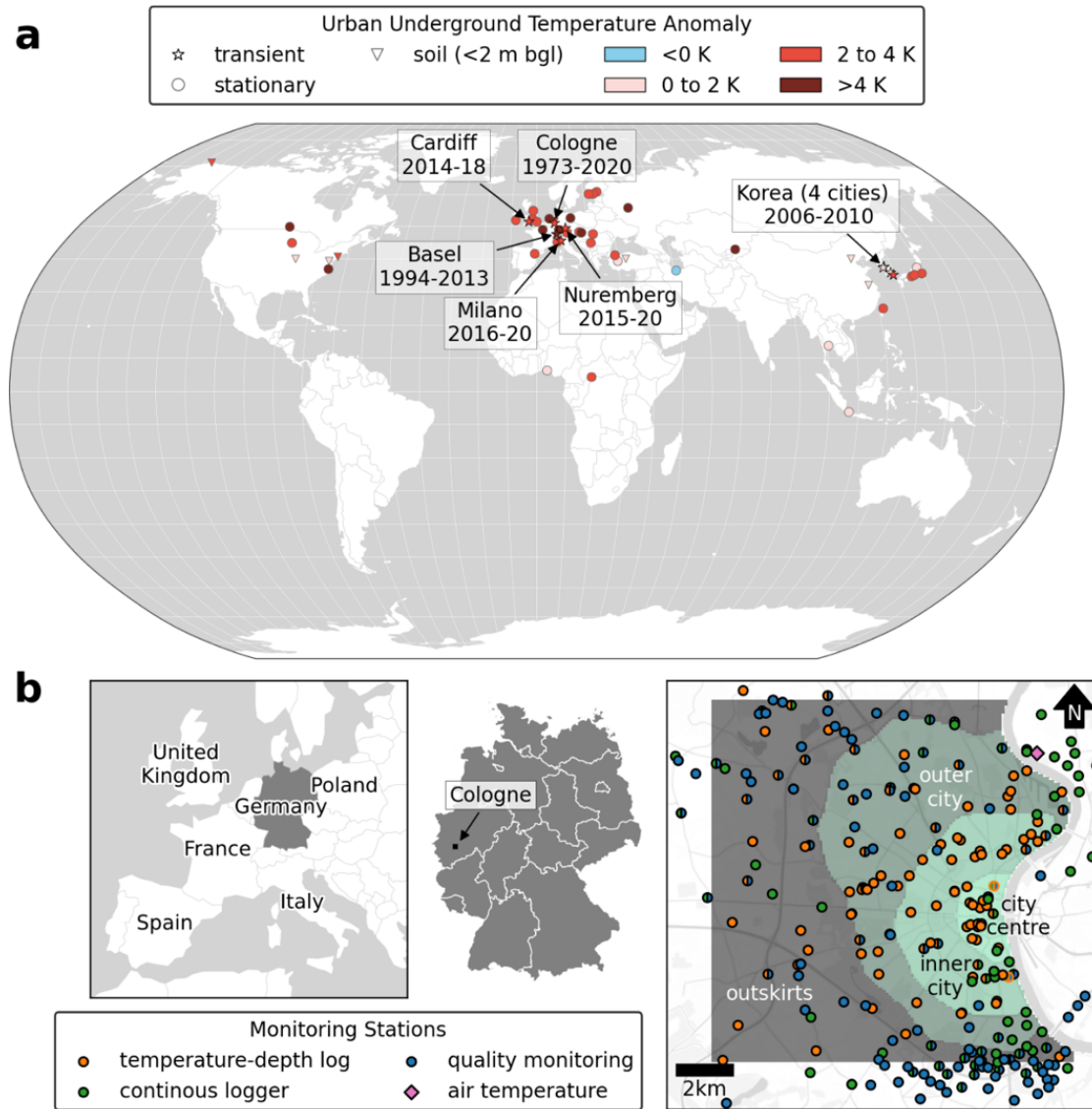


Figure 4.1: (a) Urban underground temperature anomalies. Colours indicate the magnitude of the temperature anomaly in K. Markers represent the studied medium. Triangles represent studies in soils at depths shallower than 2 m bgl. Circles and stars are studies in groundwater that either propose stationary temperatures (circles) or transient analysis (stars with labels of city names and studied time periods). (b) Location of temperature monitoring stations in the greater region of Cologne. City zones (city centre, inner city, outer city and outskirts) are highlighted for the reference area. Base map accessed from maps.stamen.com (2021-05-27).

4.3 Materials and Methods

4.3.1 Hydrogeology and aquifer structure

The region of interest is located south of the Lower Rhine Basin. The shallow subsurface is composed of Quaternary terrace deposits, that are underlain by Tertiary sediments. The Quaternary deposits host an unconfined aquifer that mainly consists of gravels and sands, while the underlying Tertiary clays, silts, lignite and soft coals down to 200 m bgl function as aquitard (Balke and Karrenberg, 1973; Hilden, 1988; Klostermann, 1992;

Zhu et al., 2015). The *Quaternary-Tertiary boundary (QTB)* was used to delineate the bottom of the aquifer. *QTB* depths are composited from 440 depth values from monitoring wells (ELWAS, 2013), 97 public borehole profiles (DABO, 2020), and supported by 676 resolved from the isolines of the Quaternary basis map that was kindly provided by the geological survey of North Rhine-Westphalia. Interpolated *QTB* range between 15 and 81 m asl in the model area. Surface elevation of the public 1 m digital elevation model (*DEM*) tiles (OpenGeoDataNRW, 2021) were composited and resampled to 100 m resolution.

4.3.2 Groundwater data

Groundwater data can be classified into three groups: temperature depth logs, temperature and hydraulic head continuous loggers, and temperature recorded during groundwater quality measurements. In total, 266 wells with temperature monitoring were selected for the analysis.

Temperature depth logs have been performed in 1973 (Balke, 1974), 1977 (Balke and Kley, 1981), in 2009 and 2012 (Zhu et al., 2015; Zhu et al., 2010), and between 2018 and 2020. Temperatures were recorded *in-situ* without pumping as profiles measured from top to bottom. The vertical resolution is increasing towards greater depths and is between 1 and 5 m. Different standard temperature level meters (e.g., SEBA KLL-T) with an accuracy between 0.05 and 0.1 K were used. The drift in absolute temperature between these devices is typically below 0.2 K. For the measurement campaigns in 1973 and 1977 not all recorded profiles were preserved over time. Data from the years 1973 and 1977 are digitized from aquifer temperature maps measured 0.5 m below groundwater level in 1973 and in 15 and 20 m bgl in 1977.

Temperature and hydraulic head continuous loggers are maintained by government institutions (city and district government of Cologne), water suppliers (Rheinenergie AG) and a non-profit public body (Erftverband). Temperature timeseries are available only for 77 stations maintained by the Rheinenergie AG. At these standard groundwater monitoring loggers with temperature accuracy <0.3 K and precision <0.1 K are typically installed less than 5 m bgl. Hydraulic head measurements, both manual and logged, were used from 968 stations (ELWAS, 2013).

GWT recorded during groundwater quality measurements are recorded on-site during pumping. These data have high measurement errors <1 K due to exposure to surface

condition, temperature changes caused during pumping, and differences in the sampling routine. Accuracy and precision of the used probes are below 0.2 K.

In this study we use the term aquifer temperature as a measure for the temperature at depths between 15 and 25 m bgl. This depth interval was cropped from temperature logs and available quality and logger data, because it is typically below the water table, within the vertical extent of the aquifer, and the depth in which historic temperature records are available (Balke, 1974; Balke and Kley, 1981). To resolve the aquifer temperature for each station, annual arithmetic means from the three data groups were calculated separately. Afterwards, the mean of these was calculated where applicable for each station, which resulted in 2999 annual mean values at 253 stations. Gaps in the annual mean values of the aquifer temperature were filled by linear interpolation within the data limits to achieve higher temporal coverage. Hereby, 1662 at 159 stations were filled. The total number of annual mean values for the aquifer is 4661 at 253 stations. In the SW of the region of interest, the aquifer wedges out completely.

Groundwater data are analysed on an annual basis in this study. However, seasonal variations at depths between 15 and 25 m bgl are above the typical temperature range in natural conditions that is below 0.1 K for depths below 15 m bgl. The mean seasonal temperature range observed at 57 stations in quarterly repeated temperature logs between September 2018 and 2019 is 0.5 K at 15 m bgl, 0.2 K at 20 m bgl, and 0.1 K at 30 m bgl. The year-to-year variability or annual reproducibility, expressed by the difference of the September temperature in 2019 and 2018 is around +0.1 K for the entire depth interval. Permanently installed loggers in the area indicate the same seasonal temperature range and year-to-year variability as the quarterly temperature logs.

4.3.3 Theoretical geothermal potential

The TGP defines the additional energy content in a reservoir towards natural conditions, without taking into account technical accessibility, economic feasibility and legislative regulations (Bayer et al., 2019). TGP can be calculated for water saturated porous aquifers by the equation (Balke, 1974; Bayer et al., 2019; Zhu et al., 2010):

$$TGP = ((1 - n) * c_w + n * c_s) * \Delta T * A * d \quad (4.1)$$

where n is the porosity, c_w and c_s are the volumetric heat capacities of the fluid (4.15 MJ K⁻¹ m⁻³) and porous media (2.1 MJ K⁻¹ m⁻³). ΔT (K) is the temperature difference ($\Delta T = T_l - T_0$) between local aquifer temperature (T_l) and the proposed natural

background temperature in 1973 of 10.8 °C (T_0). The TGP was calculated for a respective reservoir volume that was discretized by a 100 x 100 m grid (A) with variable saturated thickness (d). The saturated thickness ($d = \min(\min(GWL, DEM) - QTB, 0)$) was calculated between the groundwater level (GWL), the DEM surface elevation, and the QTB (Figure 4.2).

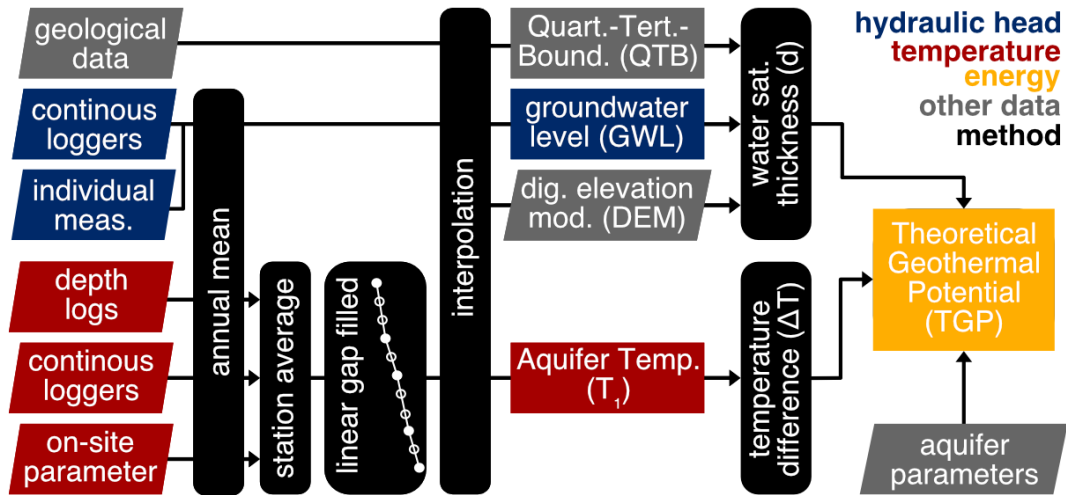


Figure 4.2: Methodology flowchart.

4.3.4 Spatial interpolation and time resolution

TGP, aquifer temperature and hydraulic heads were gathered as annual mean values and calculated for each year from 1973 to 2020. The QTB was assumed to be constant through time and calculated from all available data. All data is interpolated using standard inverse distance weighting on a 100 m x 100 m grid considering the nearest 15 data points and to a power of 1.5. Interpolated surfaces were smoothed by applying a Gaussian filter with 2 standard deviations.

4.3.5 Comparative Data

To compare trends in GWT air temperature data were accessed from the Climate Data Center (CDC, 2021) of the DWD. Data was recorded hourly 2 m above ground, quality controlled, and resampled by the DWD. To relate the resolved TGP to regional residential space heating demand statistics for Germany (BMW, 2020) were projected to the city zones by the number of inhabitants in 2020 of the town quarters (StadtKöln, 2021) and surrounding municipalities (IT.NRW, 2021). To reduce annual variations, the mean of the annual residential space heating demand between 2010 and 2020 was taken as a reference.

4.4 Results and discussion

4.4.1 Aquifer temperature

The GWT in the Cologne area is conditioned by a SUHI phenomenon with the temperature being highest underneath the city centre and gradually decreasing towards the rural areas. The presented temperatures are monitored in the typical depth of the shallow aquifer between 15 and 25 m bgl. We refer to four zones of decreasing age and building density, from the city centre, inner and outer city, to the outskirts. Figure 4.3 delineates the spatial distribution of the aquifer temperature beneath Cologne displayed as mean value of 8-year periods since 1973. In every time period, temperature declines from the city centre area towards the outskirts over the past 48 years. The temperature anomaly between the city centre and the outskirts varies in time and rises by roughly 60% from +1.8 K in the 1973-1980 period to +2.9 K in the 2013-2020 period. Within the city zones temperature rise is highest in the city centre at +2.0 K and significantly lower in the outer city and outskirts at below +1 K difference between the 2013-2020 and the 1973-1980 period (Figure 4.3).

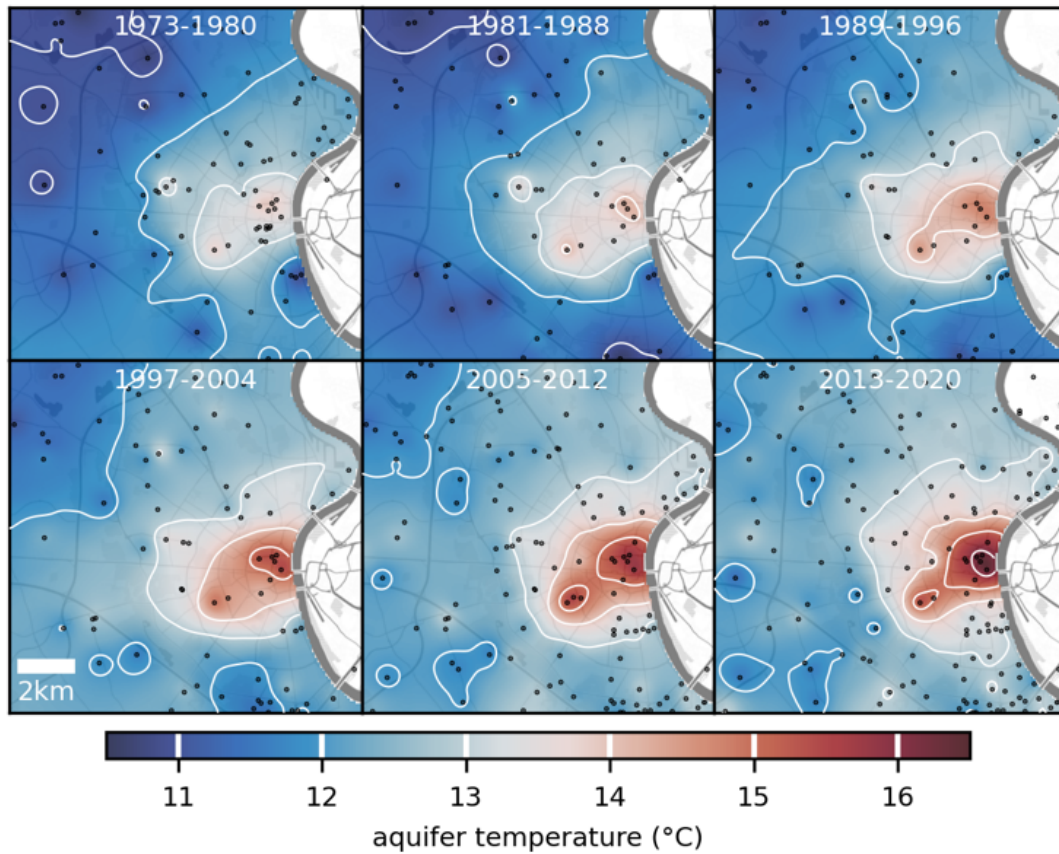


Figure 4.3: Mean aquifer temperature between 15 and 25 m bgl of 8-year periods. Observation wells with data in the respective period are given as black dots. Regional extent is 13 km x 13 km.

To better describe groundwater warming we performed regression analysis of the regional annual mean values of the aquifer in the four city zones, as well as in timeseries sensed at individual wells, and compared these to changes in ambient air temperature. The rate at which aquifer temperature is increasing is displayed versus the temperature in 2020 in Figure 4.4. Assuming a linear behaviour, the annual mean aquifer temperature in the city zones reveals a positive temperature shift of 0.52 ± 0.01 , 0.29 ± 0.01 , 0.22 ± 0.01 , 0.24 ± 0.02 K/dec for the city centre, inner and outer city and outskirts, respectively (Figure 4.4). The annual means of the city zones indicate a strong correlation with time supported by squared Pearson correlation coefficients ranging between 0.97 and 0.84. The city zone values are supported by linear regression results of time series at individual wells, displayed in Figure 4.4, that comprise at least 30 years and have a median slope of 0.37 K/dec. Three of 64 timeseries exceeded a mean squared error towards the regression line of 0.5 K. Two of them are the actual maximum and minimum slopes at 1.06 and -0.37 K/dec. 63 out of the 64 wells indicate a positive temperature trend, and the one well that carries a negative trend is next to a flooded open

pit mine with monitoring starting after reclamation in 1978. The maximum slope is observed directly in the city centre and indicates a high rise in temperature with more than 20 °C measured in 2020 (15-16 °C in 2009, and 17-18 °C in 2018 and 2019).

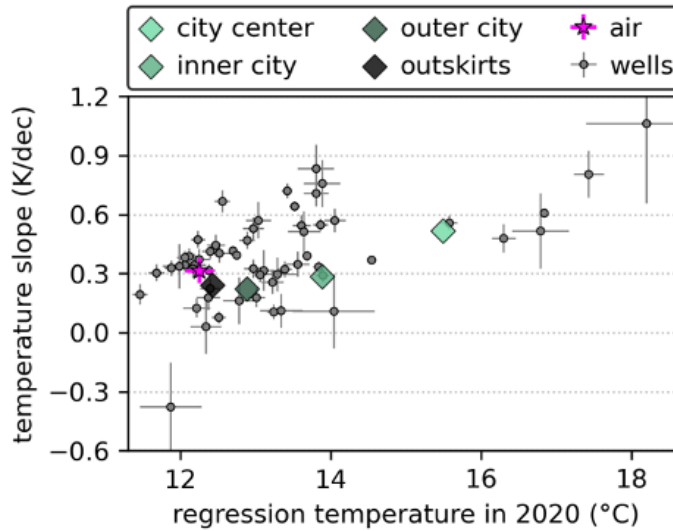


Figure 4.4: Temperature trends of 64 individual wells, regional mean in city zones, and 2 m air temperature. Error bars represent the standard errors of the linear regression.

Between 1973 and 2020, ambient annual air temperature means indicate a rise of 0.31 ± 0.06 K/dec ($R^2=0.34$). Compared to aquifer temperature gradients in the rural parts (outskirts and outer city), the lapse rate in air temperature is about 25% higher. This trailing equals rates that are typically found when comparing temperature in air to the shallow subsurface (Benz et al., 2018a; Hemmerle and Bayer, 2020; Menberg et al., 2014). The underground temperature gradient in the city centre is contrarily exceeding atmospheric temperature rise and can be attributed to higher anthropogenic heat fluxes caused by a higher building density, surface imperviousness, and more underground buildings in this area (Benz et al., 2015). Subsurface temperature shift in the inner city reflects a transition between the rural outskirts and the city centre. It is assumed that the temperature rise in response to heated basements and surfaces is limited as the heat flux is effectively reduced when subsurface temperature is at the same level as the basement temperature. The strongest increase in temperature is observed between the 1980s and the middle of the 2000s, in which the rise in temperature is highest in all areas (cf. Table 4.1). Between the second (1981-1988) and fourth (1997-2004) period, temperature rise per period is highest at roughly +0.5 K in the city centre and +0.3 K in the other city parts. In the past two periods (2005-2012 and 2013-2020) the temperature increase per period is reduced to +0.3 K in the city centre and to around +0.1 K or below in the other

city areas per period and in the same magnitude as between the first two periods (1973-1980 and 1981-1988).

Table 4.1: Mean aquifer temperature of 8-year periods in the different city zones. Temperature is given in °C with the standard deviation in brackets ($\pm 1\sigma$).

city zone	1973-1980	1981-1988	1989-1996	1997-2004	2005-2012	2013-2020
city centre	13.2 (± 0.5)	13.5 (± 0.5)	14.1 (± 0.5)	14.6 (± 0.6)	14.9 (± 0.6)	15.2 (± 0.8)
inner city	12.6 (± 0.5)	12.7 (± 0.6)	13.0 (± 0.6)	13.3 (± 0.7)	13.6 (± 0.7)	13.7 (± 0.6)
outer city	12.0 (± 0.5)	12.0 (± 0.5)	12.3 (± 0.4)	12.6 (± 0.4)	12.7 (± 0.3)	12.7 (± 0.3)
outskirts	11.4 (± 0.4)	11.4 (± 0.3)	11.8 (± 0.4)	12.1 (± 0.4)	12.2 (± 0.3)	12.3 (± 0.3)
total	11.8 (± 0.6)	11.9 (± 0.7)	12.2 (± 0.7)	12.5 (± 0.7)	12.6 (± 0.7)	12.7 (± 0.8)

4.4.2 Theoretical geothermal potential of shallow urban groundwater

We quantified the TGP of the urban aquifer based on the vertical extent of the aquifer, the water saturated thickness, and the aquifer temperature. The TGP mirrors the trends seen in aquifer temperature and is highest in the city centre area in all periods, while increasing over time as illustrated in Figure 4.5. In all city zones, TGP exhibits a strictly increasing trend over time with mean values (± 1 standard deviation) of 117, 83, 49, and 18 TJ km⁻² in the 1973-80 period and 202, 130, 79, and 43 TJ km⁻² in the 2013-20 period in the city centre, inner city, outer city and outskirts, respectively. In the SW of the study area the TGP is zero, because the Quaternary terrace deposits that host the aquifer wedge out in this region.

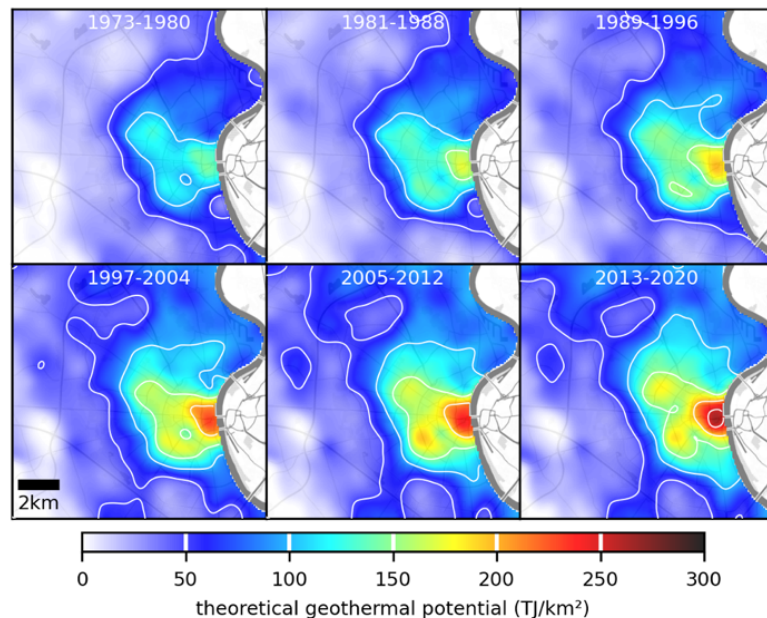


Figure 4.5: Theoretical geothermal potential of 8-year periods. Regional extent is 13 km x 13 km.

While the TGP density is highest in the central parts, the total energy content is actually lowest in the city centre at 936 TJ, due to the small fraction of the city area (cf. Table 4.2). Compared to the estimated residential heating demand for this area, the city centre yields the highest capacity for supplying residential space heating. The additional energy stored in the city centre in the 2013-20 period would equal the demand of about 1 year. In the surrounding city zones this ratio is slightly lower, equalling between 79% and 95% of the annual residential heating demand.

However, this stationary calculation of the TGP as a one-time extractable heat reservoir formed by anthropogenic heating on top of the potential of natural conditions and neglects transient effects and technical accessibility of the energy. To resolve the energy that is constantly stored in the aquifer we performed a linear regression of the annual area means of the four city zones (Figure 4.6). The regression yields a storage rate of 27 mW m⁻² for the total area, and 70, 39, 26, 22 mW m⁻² for the respective city zones (Table 4.2). Even though heat storage is three magnitudes higher in the city centre when compared to the outskirts, the heat stored in the aquifer each year equals only 1% of the thermal demand. These storage rates are also significantly lower than the average anthropogenic heat flux of 390 mW m⁻² from the surface towards the aquifer that was calculated by Benz et al. (2015) using a 1D analytical model for this area.

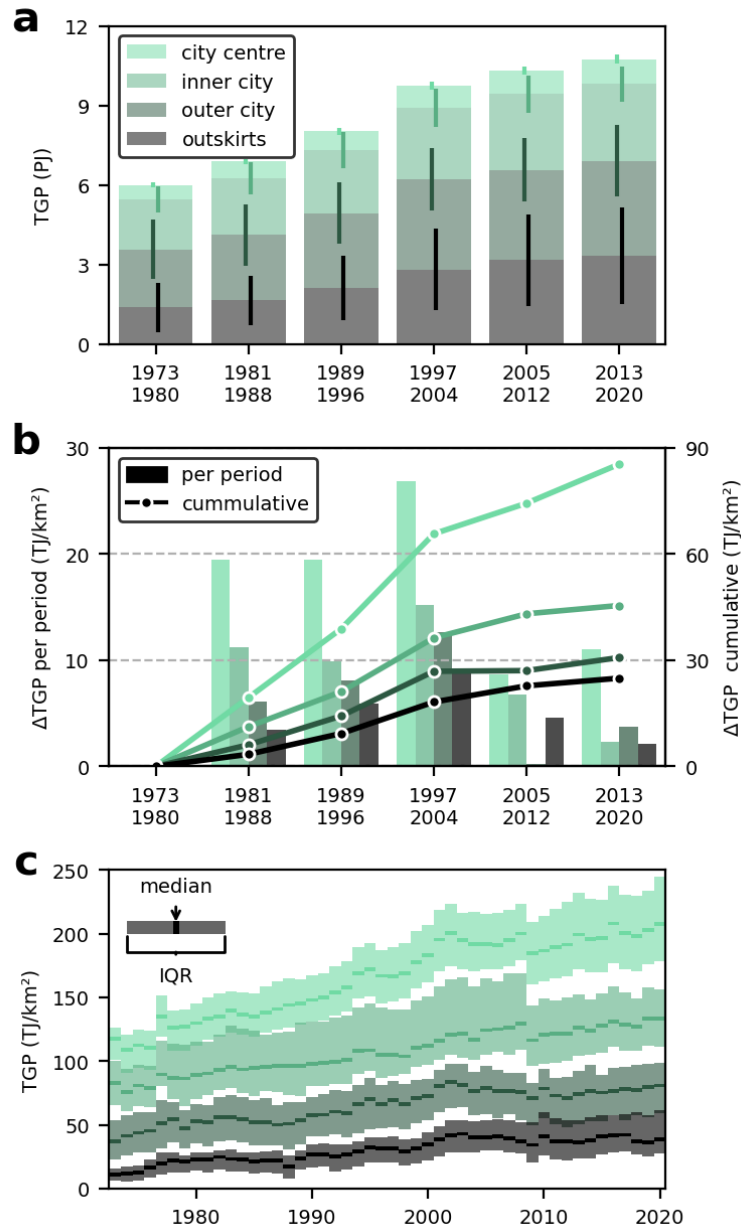


Figure 4.6: (a) Total theoretical geothermal potential (TGP) of city zones for 8-year periods. Error lines indicate standard deviation in zonal distributions. (b) Cumulative and absolute TGP change per period. (c) Interquartile range (IQR) and median TGP per area for city zones.

This implies that only about 5 to 20% of the energy that is released into urban underground is also stored within the aquifer in the form of heat. The calculated shares of the TGP reflect the observed energy growth of the aquifers thermal reservoir in time and are related to an average thermal demand, which either over- or underestimates the potential, as heating loads in Germany have an annual variation of around $\pm 10\%$. In addition, the actual operative potential for shallow geothermal systems will be much higher if we consider mixed heating and cooling applications, transient heat transport, and if a depletion of the of the thermal reservoir is allowed. The thermal conditions in

the aquifer tend to equilibrate from the year 2000 and onwards (Figure 4.6b) and the net heat gain thus declines over time. However, recharge of the shallow ground would dynamically adapt if more energy would be extracted. In order to describe dynamic phenomenons such as groundwater flow, heat loss towards the aquifer boundaries, or changes caused by shallow geothermal systems under specific thermal loads, a numerical model would be needed which is beyond the scope of this study.

Table 4.2: Mean aquifer temperature, theoretical geothermal potential (TGP), and water saturated thickness (d) of 8-year periods in the different city zones. Groundwater temperature (GWT) is given in °C with the standard deviation in brackets ($\pm 1\sigma$).

city zone	pop	area	residential		TGP (2013-20)		TGP cap.	TGP shift	GWT shift	d mean
			space heating demand		TJ	TJ km ⁻²				
<i>unit</i>	<i>k</i>	<i>km²</i>	<i>TJ a⁻¹</i>	<i>W m⁻²</i>	<i>TJ</i>	<i>TJ km⁻²</i>	<i>a</i>	<i>mW m⁻²</i>	<i>K/dec</i>	<i>m</i>
city centre	45	4.6	927	6.39	936	202	1.0	70.2 \pm 2.4	0.52 \pm 0.01	17.6
inner city	180	22.3	3683	5.24	2897	130	0.8	39.4 \pm 1.8	0.29 \pm 0.01	16.3
outer city	185	45.1	3780	2.66	3575	79	1.0	25.7 \pm 1.6	0.22 \pm 0.01	13.7
outskirts	190	78.1	3896	1.58	3332	43	0.9	21.6 \pm 1.0	0.24 \pm 0.02	9.4
total area	600	150.1	12285	2.60	10739	72	0.9	26.9 \pm 1.2	0.25 \pm 0.01	12.0
city area	410	72.0	8389	3.69	7407	103	0.9	32.8 \pm 1.6	0.26 \pm 0.01	14.8

The gross energy which is not stored in the aquifer is transported by groundwater advection outside its vertical or lateral extent. Vertical conductive heat transport towards greater depths in this area is less efficient than lateral advective heat transport by groundwater flow, that is oriented in north-eastern direction towards the receiving stream. Numerical model results of this area suggest that the annual heat loss towards the river is around 610 TJ per year (Zhu et al., 2015), that equals 5% of the total TGP. In vertical direction the shallow aquifer is typically at depths between 10 to 30 m bgl. In this zone, shallow geothermal energy can be effectively harnessed by especially open-loop groundwater heat pump systems. Anthropogenic heat is also stored in the underlying aquitard down to a depth of at least 100 m bgl as is evident from borehole temperature logs and model results (Zhu et al., 2015). Similar penetration depths between 60 and 130 m bgl are reported for other cities (Ferguson and Woodbury, 2004; Taniguchi et al., 2005; Visser et al., 2020). The energy stored in the underlying aquitard could also be accessed using for example borehole heat exchangers in combination with ground source heat pump systems. In addition, the UHI phenomenon affects the unsaturated zone. Analytical simulation shows that under natural and urban green surfaces the heat flux can be reversed and cool the urban subsurface (Benz et al., 2015;

Benz et al., 2018b). Natural surfaces also have major cooling effects on atmospheric UHIs (Aram et al., 2019).

To quantify heat losses and heat fluxes inside and outside the aquifer spatially and temporally, detailed numerical models can be used. Models of comparable urban aquifers containing river boundaries (Attard et al., 2016a; Epting et al., 2017a; García-Gil et al., 2014) revealed that rivers can have a significant effect on the thermal state of urban aquifers by infiltration and exfiltration in the river beds and by flooding events. Such models can also be employed to balance heat fluxes based on implemented surface boundary conditions. Recent modelling results for Cardiff (UK) suggest surface averaged heat fluxes at a rate of 60 mW m⁻² at 20 m bgl (Makasis et al., 2021).

4.4.3 Further implications

Urban subsurface is characterized by temperatures that are anthropogenically altered by continuous heat release over large areas and long periods. The opportunity to extract the accumulated heat is often overlooked, and together with the naturally stored heat, shallow geothermal energy will gain importance for integrated heat supply in cities. Clearly, as demonstrated for the city of Cologne, SUHIs tend to reach a quasi-steady thermal condition that follows atmospheric warming, and the urban heat in place as expressed by the TGP thus will not substantially increase more than elsewhere in the future. However, the geothermal usage potential can substantially be enhanced by active urban-scale subsurface heat extraction, which accelerates the ground heat gain and thus stimulates large-scale urban heat recycling. This means, by concerted application of great numbers of ground source and groundwater heat pump systems (Couderc, 2017; Rivera et al., 2017; Tissen et al., 2021), the urban underground will absorb more energy while losing less heat in-situ by lateral groundwater flow and exfiltration to rivers. Such active subsurface temperature regulation will not only be beneficial for heat supply, but is essential for facilitating effective cooling by utilization of groundwater. This bivalent use of aquifers as heat source and sink is the ideal solution, especially considering that in many cities the thermal stress for shallow aquifers is augmented by residential and industrial cooling demands (Epting et al., 2018). The relative importance of cooling will increase in the future with global warming and improved insulation of buildings.

Active control and regulation of further heat accumulation is necessary not only for optimizing urban subsurface geothermal use. Warming of aquifers deteriorates

groundwater quality by oxygen depletion and enhanced mobilization of contaminants. Warmed groundwater stimulates growth of pathogenic microbes while modifying biodiversity and character of groundwater ecosystems (Blum et al., 2021; Brielmann et al., 2009). For buried structures, there is a need for thermal insulation, and especially the temperature of drinking water is reported to rise in cities due to warming of the buried supply network (Agudelo-Vera et al., 2020).

4.5 Conclusions

Based on five decades of monitoring for the city of Cologne, we found that the shallow aquifer temperature is rising continuously. In the city centre, where urbanization is most dense, temperature rise is highest at a rate of 0.52 K/dec. This decreases towards the outer city and outskirts where it is less than half as high at rates of 0.22 and 0.24 K/dec. Compared to the rise in ambient surface temperature of 0.31 K/dec, rates in the shallow subsurface of the less densely populated areas indicate the expected trailing response to atmospheric climate variations, while in the city centre subsurface warming is increased compared to surface warming. A SUHI is present since the start of recordings but is rising in intensity over time. In the 1970s aquifer temperature in the city centre was elevated by +1.8 K on average towards the rural area. This temperature anomaly expanded by about 60% to +2.9 K in recent years. It is expected that the SUHI phenomenon will continue as a response to atmospheric warming. However, we see a reduction of the rate at which urban subsurface is heated in the past two decades. This suggests that the aquifer is approaching a temperature level at which the steady temperature from buried infrastructure and basements result in reduced thermal gradients and equilibrated heat fluxes.

The elevated temperature translates to additional heat that is stored in the aquifer. Compared to natural conditions in the 1970s, the additional heat stored in the aquifer domain equals the city's residential heating demand of around one year. However, the rate at which energy accumulates is relatively low and equals only about 1% of the residential heating demand. Compared to calculations of the anthropogenic heat flux into the urban subsurface, the rate at which energy is stored in the aquifer domain over time is one magnitude lower. The low storage ratio of the emitted waste heat is attributed to both lateral heat transport towards the adjacent river and vertical surpassing of the depths of the aquifer. This implies that on the one hand, the capacity of using only the

aquifer for sustainable space heating is not promising, and that on the other hand, the heat reaching the groundwater is to a large proportion trespassing the thin aquifer layer and not stored over time.

However, the potential for modern shallow geothermal units that combine heating and cooling is not based on depletion of a thermal reservoir. Sustainable operation of such aquifer thermal energy storage systems relies heavily on balancing heating and cooling loads and achieving constant year-to-year temperature in the reservoir. For these systems, the SUHI phenomenon acts as a regional imbalance and is a major factor to be considered to achieve longevity and sustainability. Especially cooling applications suffer from higher ground temperature but see a rising demand in response to climate, technological and socio-economical change. The observed trend in reduction of the heat accumulation in recent times could be crucial for the availability of urban underground as a promising resource for cooling applications, and a key component in the transition towards renewables.

5 Subsurface warming in response to anthropogenic drivers

The previous chapters addressed the major objectives outlined in Sec. 1.3:

- Sec. 2 proposes a novel approach for estimating groundwater temperature at city scale (Objective 1),
- Sec. 3 quantifies the depth-dependent change of groundwater temperature in the past three decades for natural environments (Objective 2),
- Sec. 4 describes the evolution of the temperature and heat content of an urban aquifer over the past five decades (Objective 3).

The associated heat content (Objective 4) in response to climate change and to the development of a SUHI are quantified in Sec. 3 and Sec. 4. A quantification of the geothermal potential based on the remote sensing estimation technique has been published as a conference proceeding paper (Hemmerle et al., 2021). The results of this work are briefly summarized below.

5.1 Synopsis

The proposed technique (Objective 1) combines two existing methods for the estimation of groundwater temperature under natural and artificial surfaces. It was shown that this combined approach can significantly lower the error of estimation. For the metropolitan area of Paris, the root-mean squared error was below 1 K (RMSE = 0.96 K). This methodology was also applied to the metropolitan area in Cologne in Hemmerle et al. (2021) to benchmark the technique for another city and to test the capability of deriving the theoretical geothermal potential (Objective 4). With the local calibration for the empirical factor of the impact of the building density, a set of 72 observations could be estimated with an RMSE of 0.86 K. Using the estimated temperature and the methodology proposed by Zhu et al. (2010), the additional heat content of the shallow aquifer could be quantified to match the city's space heating demand for 2.8 years. The calculated intensities of the SUHIs of Paris (max. +7 K) and Cologne (max. +5 K) represent typical intensities (Menberg et al., 2013b; Zhu et al., 2010). A shortcoming of the approach is that it does not split data into test and training data, which would allow for testing the approach versus unknown (test) data. Therefore, the technique does not estimate the temperature but uses the local calibration to provide a regionalization

method like other geostatistical methods for spatial interpolation. Given the coarse resolution of estimators, *LST* (roughly 1 km at surface) and *ET* (2.5 arc minutes), this methodology struggles in regions with a high density of observations (like Cologne), where often multiple observation wells lie within one pixel. Instead, it benefits from the general thermal coupling of land surface and shallow subsurface and the low variance of GWT underneath the seasonal zone. Thus, this methodology is best suited for regional to global scale estimates. Despite the promising results this method could not be adopted for the transient simulation of the Cologne area because MODIS data collection does not start before 2000. Likewise, the uncertainty of the estimate represented by the RMSE and also the error that is caused by data gaps in the coverage of the *LST* do not allow for quantification of warming trends with respect to depth or time.

To quantify the change of temperature over depth and time in response to surface warming a comparison of repeated temperature logs can be used. The warming trend for a set of 32 wells in Bavaria, Germany is quantified between the early 1990s and 2019. All of the wells are located in rural areas with no apparent direct anthropogenic heat sources in their vicinity. The wells included in this study were sampled at least 4 times to aggregate an annual mean and to reduce seasonal variations. Conversely, several wells were excluded from the analysis due to very high temperature variations greater than 0.5 K below 20 m. In addition, the resolved rates represent only the median values with data not being continuously available at all depths. The local variability between the wells is significant, especially regarding the rate of temperature increase.

The results show a strong depth dependency of the temperature change compared to the rise in air temperatures of a rate of 0.35 K/dec. This rate is significantly dampened towards greater depth with median values of 0.28 at 20 m and 0.09 K/dec per at 60 m bgl. The attenuation is in line with other studies in Central Europe and the expected thermal response by conductive heat transport from a warming surface (Figure 1.4). Compared to the less urbanized outskirts of Cologne, the trend and dampening is similar at 0.24 K/dec between 1973 and 2020. It was also shown that if temperature logs are directly compared to another, distinct requirements with regard to the seasonal variation have to be taken into account.

In the urban subsurface heat from a plethora of sources accumulates and forms large-scale thermal anomalies (Ferguson and Woodbury, 2007). Compared to the gradual surface warming in response to climate change, the warming by anthropogenic sources

causes thermal boundary conditions to change rapidly either at ground level by surface sealing, at a couple of meters depth for buildings with basements, or within the subsurface by underground buildings and infrastructure (Noethen et al., 2022). The large number of individual heat sources, as a result of increasing urbanization, leads to a superposition of several thermally affected zones. It was shown that the warming rate in the city centre of Cologne (0.52 K/dec) is twice as high as in the outskirts and also exceeds the change in surface air temperature. Furthermore, the temperature trends indicate that the warming rate is decreasing in recent years in the city centre. This could be caused by an approaching equilibration of the GWT in the city centre (15.2 °C on average in the period 2013-2020) with the temperature of heat sources.

In cities with high groundwater flow, advection is the dominant heat transfer mechanism (Böttcher and Zosseder, 2022) and causes significant deviations of the expected geothermal gradient downstream. The advective heat transport in Cologne is directed to the river Rhine that the warmed groundwater is infiltrating in and subsequently leads to a large loss of heat (Zhu et al., 2015). While it was shown that significant amounts of energy are emitted to the urban subsurface (Benz et al., 2015), the energy that is stored over time is one magnitude below the anthropogenic heat release. Compared to the annual residential heating demand of the area, the heat that is stored in the aquifer underneath Cologne per year only has a capacity of around 1% to cover this capacity. The total additional heat stored in the aquifer compared to natural conditions in the 1970s could theoretically match the city's residential space heating of approximately one year. Harnessing this energy in densely urbanized areas faces crucial practical hurdles such as availability of space for drilling and above-ground structures, as well as implementation in the local heat supply of buildings. In addition, the need for space and industrial cooling is increasing especially in cities (Deroubaix et al., 2021; Epting et al., 2018), whereas the approach used here is only capable of estimating the available heat without considering technical feasibility of extraction. However, these insights are still crucial for geothermal exploitation as they indicate an a priori imbalance for designing shallow geothermal units that target both heating or cooling, as well as aquifer thermal energy storage systems (Stemmler et al., 2022).

5.2 Outlook

Heat sources and processes that transport and accumulate heat have been quantified in a variety of studies and verified in different cities. The shape and intensity of SUHIs has been shown to vary with local hydrogeology, climate, and urbanization, to an extent that allows making generalisations and estimating the phenomenon by different parameters such as *LST* or land cover type. However, there is still significant room for improvements in the applied methods and validation with field data, especially with respect to time- and depth-dependent effects. Currently, no commonly agreed upon best-practice approaches exist for sampling and monitoring, quantifying SUHI intensities, climate change effects, or numerical model development. In the following, a set of challenges and starting points for future research is proposed based on the four objectives defined for this study. The topics target at solving some of the previously described shortcomings of the applied methodology of this work, aim at increasing transferability of methods and ease the comparability of studies that deal with subsurface environments, thereby extending the scope of SUHI research from primary temperature related studies in the directions of groundwater quantity and quality.

Objective 1. (i) Current *groundwater temperature estimation* techniques typically do not include depth related effects. A depth resolution of the estimation approaches in this study could significantly reduce the error that arises from temperature variations that typically are similar or even higher than the proposed estimation error. A depth resolution could be achieved by either calibration of the depth effect based on locally available temperature logs or by coupling a simple 1D conductive and advective heat transport model for each pixel. (ii) The estimation method presented in this study uses a local calibration for each city. Calibrating this methodology for multiple cities would provide a more universal tool for estimating subsurface temperature in densely populated regions with intermitting urbanization. A computationally efficient method could replace the building density that is calculated from OpenStreetMap building polygons in this study with impervious built-up raster data provided by the Copernicus Land monitoring services. (iii) The estimated groundwater temperature could be coupled with typical traffic-light-approaches that provide suitability maps for shallow geothermal utilization. In succession this can be used to produce more applicable maps for commissioning and planning of geothermal heat pumps by providing an estimate of the extractable heat and temperature. These would synergize with geological suitability

maps that are already available in many regions in Central Europe, and in combination with depth dependent information, this approach could be utilized for open- and closed-loop system suitability, as well as for aquifer thermal energy storage potential mapping.

Objective 2. (i) A variety of studies report on *subsurface climate change in natural environments* in Central Europe. The data used to quantify the rate of warming comprise temperatures recorded during groundwater quality monitoring while pumping, data loggers installed on multiple or single depth levels, and temperature logs. The type of measurement dictates the sampling frequency, depth allocation, available time period, and error of the measurement itself. Ideally, the data density should be increased to resolve spatial trends at different climatic settings as well as at different depths. (ii) The variability regarding depth and climate should be accompanied by an analysis of local hydrogeological drivers like vertical groundwater flow and thermal ground properties. The statistical analysis of the temperature trends is often not backed up by advective-conductive heat transport models. Such models can assess the impact of surface warming based on different criteria like depth to groundwater table, aquifer and soil type, infiltration, and land cover. (iii) While temperature is not the only parameter that changes with climatic variations, the projections and historic analysis of subsurface temperature should go hand in hand with a likely more severe issue, groundwater quantity. Analysing thermal trends alongside variations in groundwater levels is crucial for thorough future projections of water availability and quality. It is current practice in Germany, that water extraction permits are commissioned based on the groundwater recharge of the past decades. However, the available quantity is unlikely to be constant, given that the surface climate already responds to global climate change and that this trend is projected to continue or even accelerate in the upcoming years.

Objective 3. (i) The Cologne example for the *evolution of subsurface urban heat islands* is currently a unique study reporting on city-wide monitoring continuously over multiple decades. While it was shown that a significant SUHI already accumulated by the 1970s and is growing since then, these findings cannot be generalized due to the lack of comparative data. Historic records in Karlsruhe and Munich suggest a similar evolution but have not been analysed in a comparable way. In Karlsruhe some parts of the city show a decreasing trend which is attributed to the regulation of allowed reinjection temperature of thermal waste water (Menberg et al., 2013a). This exemplifies the local variability and causes of short-term changes in anthropogenic overprinting of natural

conditions. Assuming that most Central European cities have a similar history of urbanization, the start of the anthropogenic heating will date far earlier than any available subsurface temperature records of reasonable quantity or quality. (ii) Based on the limited available data and studies on the topic, the evolution could be simulated with numerical models. However, developing numerical flow and heat transport models in urban areas throughout historic times is challenging with the limited information on underground flow barriers, local groundwater extraction and infiltration, and the complexity of urban groundwater recharge. Integrating simultaneous warming by climate change and direct anthropogenic sources alongside precipitation data could feature climate projections based on the shared socioeconomic pathways to model the future development. This could verify the assumptions that the thermal regime is approaching a thermal equilibrium within the shallow subsurface and that the anthropogenic heat flux in the subsurface will be hereby reduced. (iii) The effects of subsurface warming should ideally be quantified along the trends in groundwater heads in cities. In a variety of cities either rising groundwater levels have been reported that sometimes are counteracted with excessive pumping for either short-phased construction or long-term groundwater drainage. This effect is also affected by artificial recharge in cities and interactions with the sewer network, and is of enormous relevance for cities that use local groundwater resources for their freshwater supply.

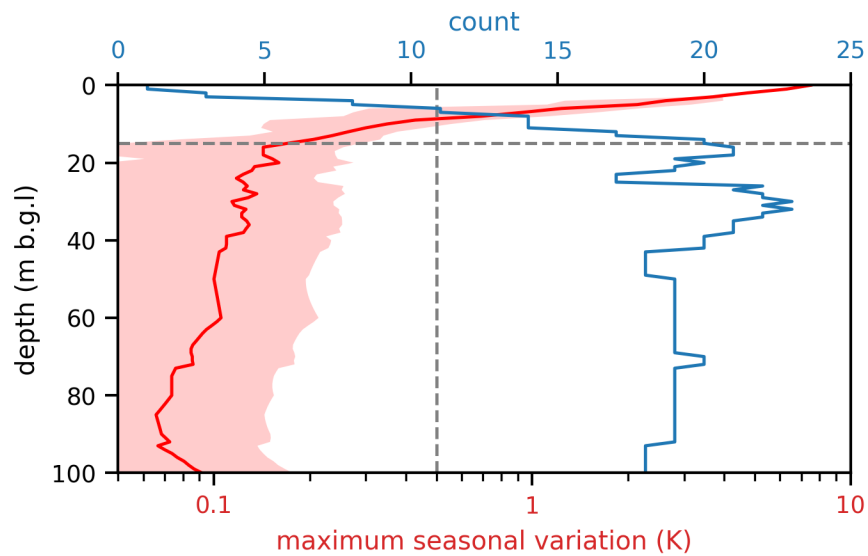
Objective 4. (i) The *accumulating shallow geothermal potential in response to ground warming* could be benchmarked for a set of cities with a standardized methodology. This could also feature a comparison of different methods that discriminate between the theoretical, technical, and economic potential and the variance of the latter from city to city. (ii) Arising by a growing demand for space cooling in moderate climates, the potential of combined cooling and heating solutions should be implemented as a standard in geothermal potential mapping. Whereas a few different approaches already exist, these are typically tailored to the available data at local or national scale. Likewise, installing a high number of units per area will cause an overlap of the thermally affected zones that can lead to a decrease in efficiency. Therefore, it is crucial that in areas with a high density of shallow geothermal systems, these are incorporated in a management framework at city or district scale. (iii) Lastly, the way that we quantify the geothermal potential is based on the energy that can be utilized. Extracting the heat underneath cities at large scale would also lead to a significant cooling of the urban subsurface. Next to

the heating and cooling potential, putting a SUHI on cold feet will change the heat flow and interaction with the surface. This can potentially reduce surface temperature and mitigate a fraction of the UHI phenomenon at the surface. Currently, there is a lack and hereby arising necessity for studies that quantify the possible socioeconomic potential on the quality of urban life.

6 Appendix

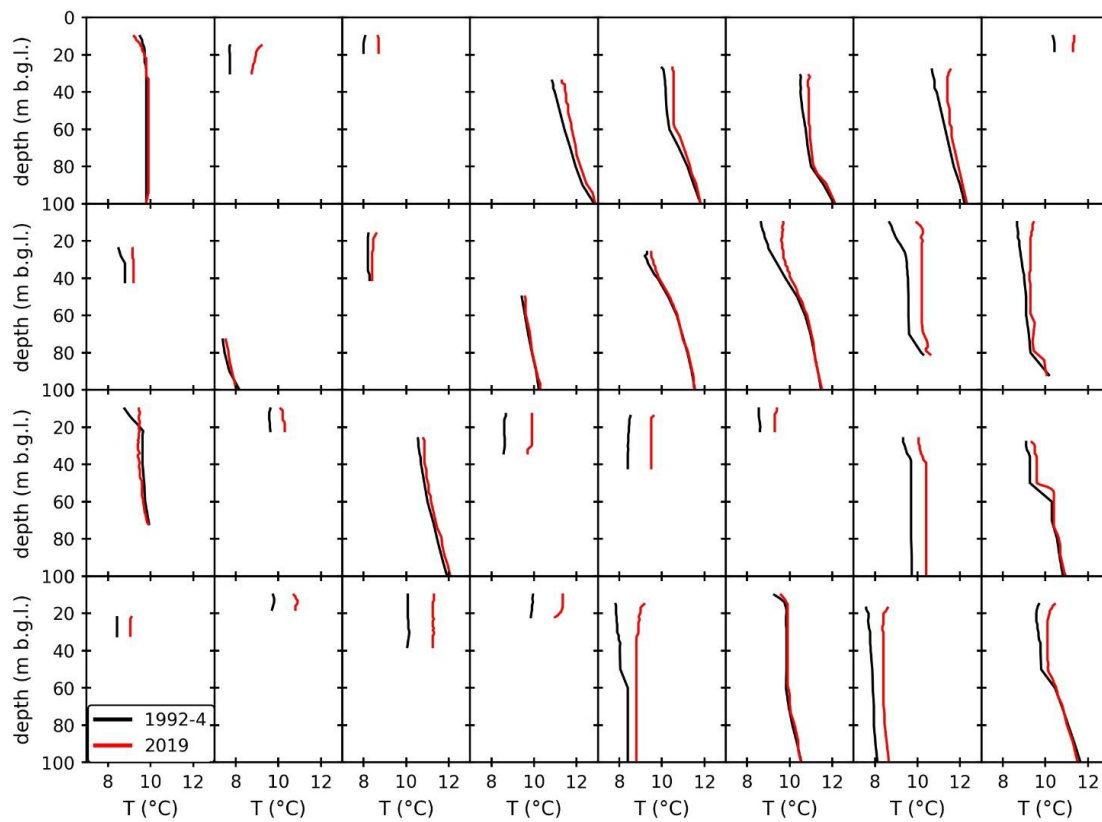
6.1 Chapter 3 - Climate change yields groundwater warming in Bavaria, Germany

Supplementary Figure S6.1 shows the maximum seasonal variation of the 32 observation wells during the 1992-4 period. The maximum seasonal variation has been calculated as maximum-minimum difference out of 4 seasonal measurements at a 1 m depth resolution.



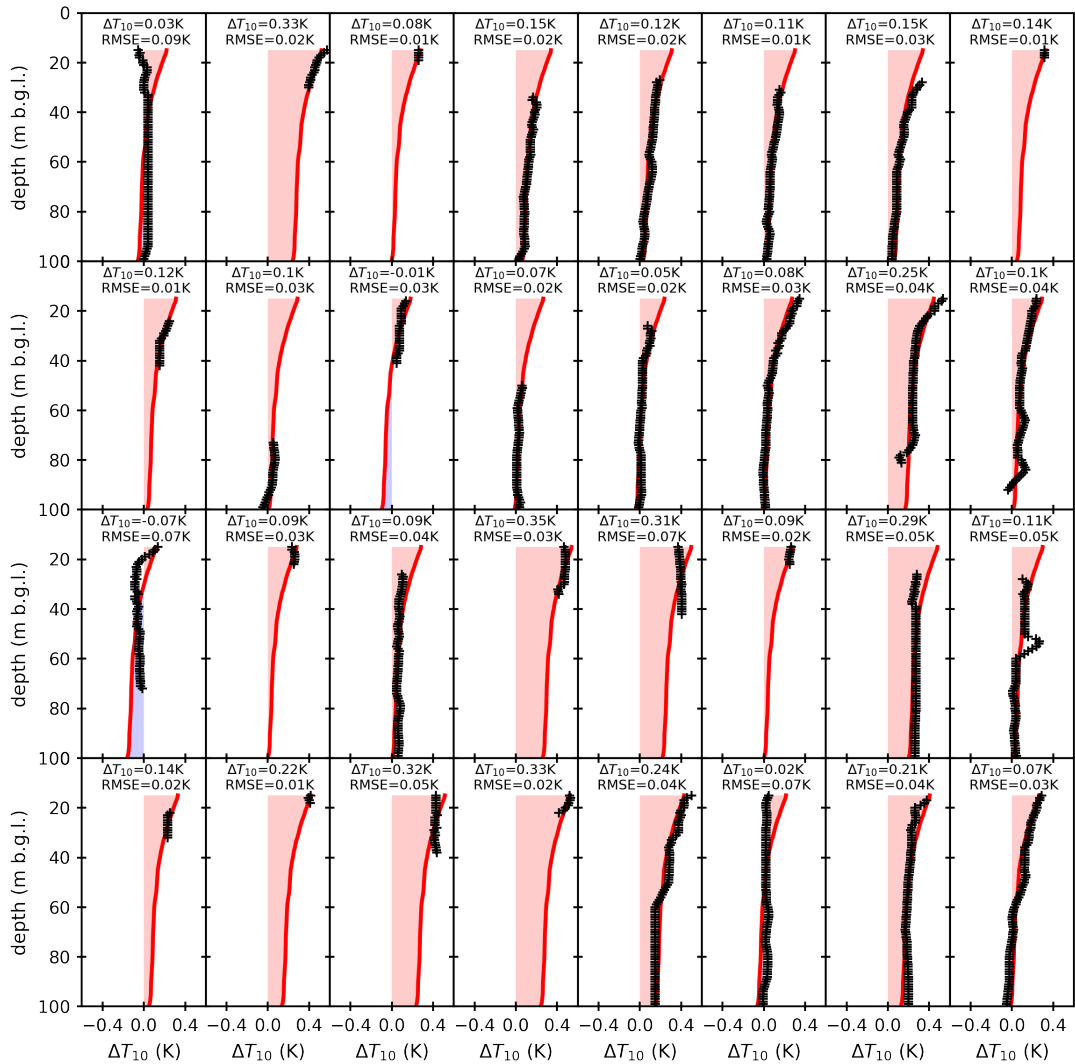
Supplementary Figure S6.1: Mean values of the seasonal maximum minimum difference of the 32 selected observation wells during the 1992-4 period (red line) \pm one standard deviation (red area) and the number of sample values for computing the mean value (count, blue line). The 335 horizontal dashed line (15 m) indicates the depth for separating the seasonally influenced or dominated temperature regimes. The vertical line (0.5 K) is the threshold defined for selecting seasonally undisturbed temperature records.

Supplementary Figure S6.2 shows the mean of the repeated temperature depth profiles of the respective periods from 1992-4 and 2019.



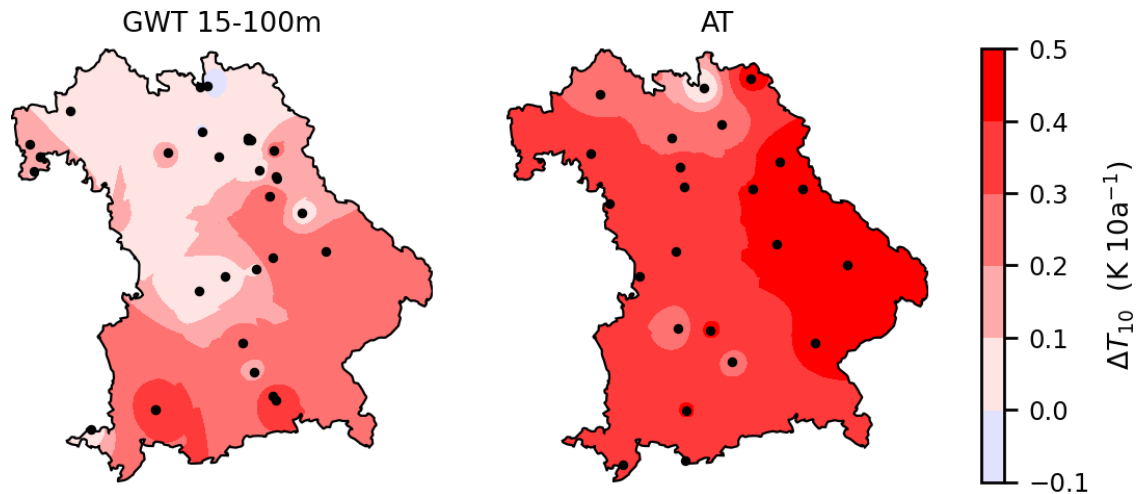
Supplementary Figure S6.2: Mean temperature depth profiles of the repeated measurements of the 1992-4 and 2019 period.

Supplementary Figure S6.3 shows the result of the RMSE based fitting of a reference profile on the measured ΔT profiles at each station. The reference profile is shifted with a step width of 0.001 K. RMSEs are calculated for each step and the step with the lowest RMSE is used as prediction or fitted reference profile and the alternative approach in the main text body.



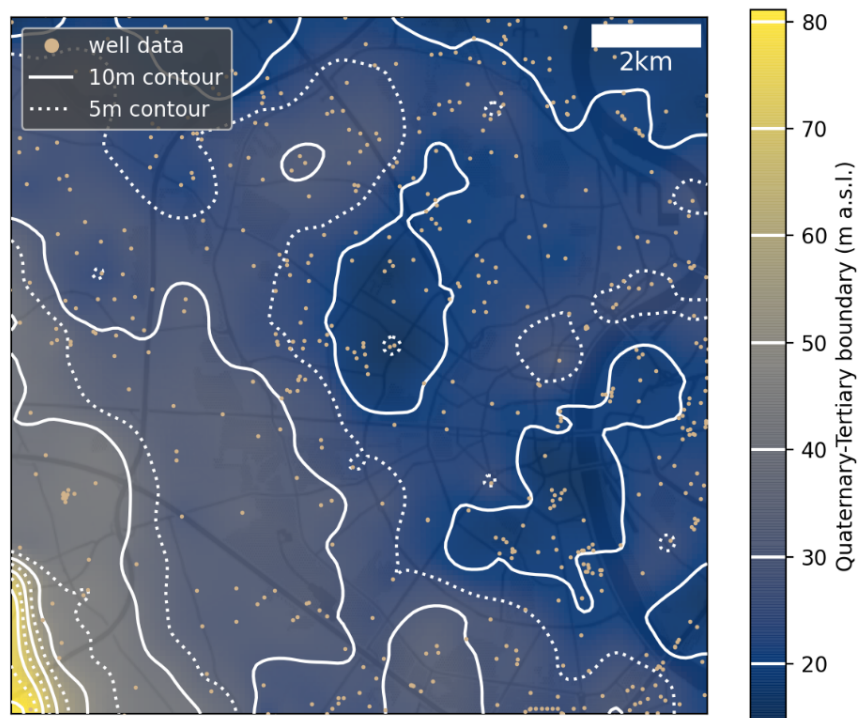
Supplementary Figure S6.3: Fitted (red line) and measured (black crosses) mean temperature differences per decade (ΔT_{10}) of the observation wells. ΔT_{10} values given represent the mean value for each profile. Root mean squared errors (RMSE) reflect the error between the fitted and measured ΔT_{10} data.

Supplementary Figure S6.4 shows an inverse distance weighting interpolation of the mean ΔT_{10} rates in groundwater (GWT, cf. Supplementary Figure S6.3) and air temperature. The spatial distribution of the mean ΔT_{10} rates in groundwater are used as alternative approach for calculating the shallow geothermal potential in the main text body.

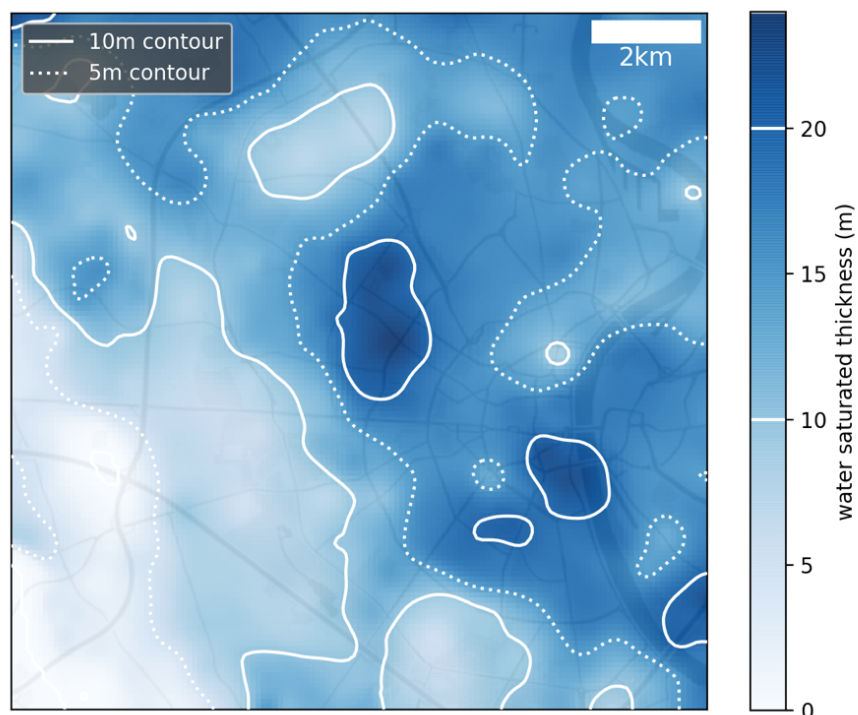


Supplementary Figure S6.4: Interpolated ΔT_{10} rates in groundwater (GWT) and air temperature (AT). Datapoints are indicated by black dots. Groundwater ΔT_{10} rates are given as mean between 15 and 100 m depth. Map is projected in EPSG 31467 and clipped to the outline of the federal state of Bavaria.

6.2 Chapter 4 - The Evolution of the Geothermal Potential of a Subsurface Urban Heat Island



Supplementary Figure S6.5: Quaternary-Tertiary boundary in the model domain. Data within the model domain are displayed. Interpolation was stabilized with data in a 1 km buffer region around the model domain (not displayed, cf. Figure 4.1b).



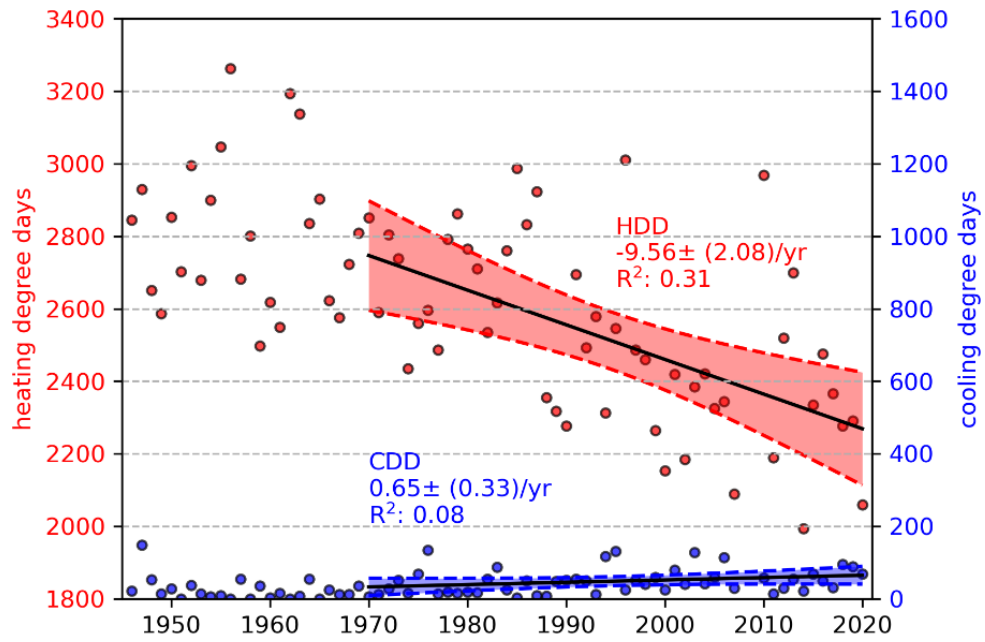
Supplementary Figure S6.6: Mean water saturated thickness between 1973 and 2020 of the aquifer in the model domain.

Supplementary Table 6.1: Zonal TGP statistics by city zones for 8-year periods. City zones represent the city centre (IV), inner city (III), outer city (II), and the outskirts (I).

TGP	city zone	8-year period					
		1973-1980	1981-1988	1989-1996	1997-2004	2005-2012	2013-2020
Total (TJ)	IV	539	630	720	843	882	936
	III	1845	2085	2311	2645	2814	2897
	II	2203	2502	2868	3435	3423	3575
	I	1404	1673	2129	2814	3171	3332
mean $\pm 1\sigma$ (TJ km ⁻²)	IV	117 \pm 23	136 \pm 28	156 \pm 31	183 \pm 35	191 \pm 36	202 \pm 40
	III	83 \pm 24	93 \pm 28	104 \pm 30	119 \pm 33	126 \pm 33	130 \pm 30
	II	49 \pm 26	56 \pm 27	64 \pm 27	76 \pm 28	76 \pm 28	79 \pm 31
	I	18 \pm 12	21 \pm 12	27 \pm 16	36 \pm 20	41 \pm 22	43 \pm 24
min-max (TJ km ⁻²)	IV	57 - 150	68 - 181	76 - 207	89 - 242	97 - 253	104 - 274
	III	19 - 130	28 - 149	33 - 159	40 - 182	48 - 205	54 - 201
	II	6 - 131	10 - 139	18 - 154	21 - 169	26 - 176	25 - 188
	I	0 - 76	0 - 64	0 - 80	0 - 95	0 - 101	0 - 107

Beyond the potential of using the rising energy amount for heating purposes, urban underground resources in moderate climates can play a crucial role for meeting the heating demand. What is more, they can adapt to a transitional shift towards joined heating and cooling applications. In Cologne and in Europe in general¹, the number of cooling degree days (CDD) has been increasing and the number of heating degree days (HDD) has been decreasing during the past decades (see Supplementary Figure S6.7) for trend analysis of CDD/HDD). Regardless of the shift in response to climate change, the HDD are still exceeding CDD (51) by far in the last decade (2010s), and for 2018 about 350 times more energy was used for residential space heating than for residential space cooling in Germany (BMW, 2020).

¹ EUROSTAT. *Energy statistics - cooling and heating degree days*, <ec.europa.eu/eurostat> (2021).



Supplementary Figure S6.7: Heating degree days (HDD) and cooling degree days (CDD) trends based on 2 m air temperature. Annual HDD (red) and CDD (blue) are displayed as points. Linear regression lines are given with statistics and the 99% confidence interval. Methodology for calculating HDD and CDD is adopted from EUROSTAT (2021).

7 References

- Abe H., Tang C. and Kondoh A. (2014) Effect of urban aquifer exploitation on subsurface temperature and water quality. *Groundwater* **52**, 186-194.
- ADES (2018) Portail national d'accès aux données sur les eaux souterraines, www.ades.eaufrance.fr, accessed on 06.11.2018.
- Agudelo-Vera C., Avvedimento S., Boxall J., Creaco E., de Kater H., Di Nardo A., Djukic A., Douterelo I., Fish K. E. and Iglesias Rey P. L. (2020) Drinking water temperature around the globe: understanding, policies, challenges and opportunities. *Water* **12**, 1049.
- Alam S., Gebremichael M., Li R., Dozier J. and Lettenmaier D. P. (2019) Climate change impacts on groundwater storage in the Central Valley, California. *Climatic Change* **157**, 387-406.
- Allen A., Milenic D. and Sikora P. (2003) Shallow gravel aquifers and the urban 'heat island' effect: a source of low enthalpy geothermal energy. *Geothermics* **32**, 569-578.
- Allen P. A. (2009) *Earth surface processes*. John Wiley & Sons.
- Anderson M. P. (2005) Heat as a ground water tracer. *Groundwater* **43**, 951-968.
- Andújar Márquez J. M., Martínez Bohórquez M. and Gómez Melgar S. (2016) Ground Thermal Diffusivity Calculation by Direct Soil Temperature Measurement. Application to very Low Enthalpy Geothermal Energy Systems. *Sensors (Basel)* **16**, 306.
- Aram F., García E. H., Solgi E. and Mansournia S. (2019) Urban green space cooling effect in cities. *Heliyon* **5**, e01339.
- Arola T. and Korkka-Niemi K. (2014) The effect of urban heat islands on geothermal potential: examples from Quaternary aquifers in Finland. *Hydrogeology Journal* **22**, 1953-1967.
- Attard G., Rossier Y., Winiarski T. and Eisenlohr L. (2016a) Deterministic modeling of the impact of underground structures on urban groundwater temperature. *Science of the Total Environment* **572**, 986-994.
- Attard G., Rossier Y., Winiarski T., Cuvillier L. and Eisenlohr L. (2016b) Deterministic modelling of the cumulative impacts of underground structures on urban groundwater flow and the definition of a potential state of urban groundwater flow: example of Lyon, France. *Hydrogeology Journal* **24**, 1213-1229.
- Balke K. (1974) Der thermische Einfluss besiedelter Gebiete auf das Grundwasser, dargestellt am Beispiel der Stadt Köln. *GWF-Wasser/Abwasser* **115**, 117-124.
- Balke K. (1977) Das Grundwasser als Energieträger. *Brennst.-Wärme-Kraft* **29**, 191-194.
- Balke K.-D. and Karrenberg H. (1973) Geothermal and hydrogeological investigations in the southern Lower Rhenish Bight (Geothermische und hydrogeologische Untersuchungen in der-südlichen Niederrheinischen Bucht). *Geologisches Jahrbuch Band C* **5**.
- Balke K.-D. and Kley W. (1981) Die Grundwassertemperaturen in Ballungsgebieten. *Bundesministerium für Forschung und Technologie - Forschungsbericht T* **81-028**.
- Banks D. (2012) *An introduction to thermogeology: ground source heating and cooling*. John Wiley & Sons.

-
- Banks D., Gandy C., Younger P., Withers J. and Underwood C. (2009) Anthropogenic thermogeological ‘anomaly’ in Gateshead, Tyne and Wear, UK. *Quarterly Journal of Engineering Geology and Hydrogeology* **42**, 307-312.
- Barla M. and Di Donna A. (2018) Energy tunnels: concept and design aspects. *Underground Space* **3**, 268-276.
- Bayer P., Attard G., Blum P. and Menberg K. (2019) The geothermal potential of cities. *Renewable and Sustainable Energy Reviews* **106**, 17-30.
- Bayer P., Rivera J. A., Schweizer D., Schärli U., Blum P. and Rybach L. (2016) Extracting past atmospheric warming and urban heating effects from borehole temperature profiles. *Geothermics* **64**, 289-299.
- Bense V. and Kooi H. (2004) Temporal and spatial variations of shallow subsurface temperature as a record of lateral variations in groundwater flow. *Journal of geophysical research: Solid Earth* **109**.
- Bense V. and Beltrami H. (2007) Impact of horizontal groundwater flow and localized deforestation on the development of shallow temperature anomalies. *Journal of Geophysical Research: Earth Surface* **112**.
- Bense V., Kurylyk B., de Bruin J. and Visser P. (2020) Repeated subsurface thermal profiling to reveal temporal variability in deep groundwater flow conditions. *Water Resources Research* **56**, e2019WR026913.
- Bense V. F. and Kurylyk B. L. (2017) Tracking the subsurface signal of decadal climate warming to quantify vertical groundwater flow rates. *Geophysical Research Letters* **44**, 12,244-212,253.
- Bense V. F., Kurylyk B. L., van Daal J., van der Ploeg M. J. and Carey S. K. (2017) Interpreting repeated temperature-depth profiles for groundwater flow. *Water Resources Research* **53**, 8639-8647.
- Benz S. A. (2016) Human Impact on Groundwater Temperatures. *Bauingenieur, Geo- und Umweltwissenschaften, KIT, PhD thesis*.
- Benz S. A., Bayer P. and Blum P. (2017a) Global patterns of shallow groundwater temperatures. *Environmental Research Letters* **12**, 034005.
- Benz S. A., Bayer P. and Blum P. (2017b) Identifying anthropogenic anomalies in air, surface and groundwater temperatures in Germany. *Science of The Total Environment* **584**, 145-153.
- Benz S. A., Bayer P., Winkler G. and Blum P. (2018a) Recent trends of groundwater temperatures in Austria. *Hydrology and Earth System Sciences* **22**, 3143-3154.
- Benz S. A., Bayer P., Menberg K., Jung S. and Blum P. (2015) Spatial resolution of anthropogenic heat fluxes into urban aquifers. *Science of The Total Environment* **524**, 427-439.
- Benz S. A., Bayer P., Goettsche F. M., Olesen F. S. and Blum P. (2016) Linking Surface Urban Heat Islands with Groundwater Temperatures. *Environ Sci Technol* **50**, 70-78.
- Benz S. A., Bayer P., Blum P., Hamamoto H., Arimoto H. and Taniguchi M. (2018b) Comparing anthropogenic heat input and heat accumulation in the subsurface of Osaka, Japan. *Science of the total environment* **643**, 1127-1136.
- Beyer C., Popp S. and Bauer S. (2016) Simulation of temperature effects on groundwater flow, contaminant dissolution, transport and biodegradation due to shallow geothermal use. *Environmental Earth Sciences* **75**, 1244.
- Bidarmaghz A., Choudhary R., Soga K., Kessler H., Terrington R. L. and Thorpe S. (2019) Influence of geology and hydrogeology on heat rejection from residential basements in urban areas. *Tunnelling and Underground Space Technology* **92**, 103068.

- Bloomfield J. P., Jackson C. R. and Stuart M. E. (2013) Changes in groundwater levels, temperature and quality in the UK over the 20th century: an assessment of evidence of impacts from climate change.
- Bloomfield J. P., Marchant B. P. and McKenzie A. A. (2019) Changes in groundwater drought associated with anthropogenic warming. *Hydrology and Earth System Sciences* **23**, 1393-1408.
- Blum P., Menberg K., Koch F., Benz S. A., Tissen C., Hemmerle H. and Bayer P. (2021) Is thermal use of groundwater a pollution? *Journal of Contaminant Hydrology*, 103791.
- BMWi (2020) Energieeffizienz in Zahlen - Entwicklungen und Trends in Deutschland 2020, in: B. f. W. u. E. (BMWi) (Ed.). Bundesministerium für Wirtschaft und Energie (BMWi), p. 102.
- Bodri L. and Cermak V. (2011) *Borehole climatology: a new method how to reconstruct climate*. Elsevier.
- Bonte M., van Breukelen B. M. and Stuyfzand P. J. (2013) Temperature-induced impacts on groundwater quality and arsenic mobility in anoxic aquifer sediments used for both drinking water and shallow geothermal energy production. *Water research* **47**, 5088-5100.
- Böttcher F. and Zosseder K. (2022) Thermal influences on groundwater in urban environments—A multivariate statistical analysis of the subsurface heat island effect in Munich. *Science of the Total Environment* **810**, 152193.
- Bredehoeft J. and Papaopulos I. (1965) Rates of vertical groundwater movement estimated from the Earth's thermal profile. *Water Resources Research* **1**, 325-328.
- Brielmann H., Griebler C., Schmidt S. I., Michel R. and Lueders T. (2009) Effects of thermal energy discharge on shallow groundwater ecosystems. *FEMS microbiology ecology* **68**, 273-286.
- Brielmann H., Lueders T., Schreglmann K., Ferraro F., Avramov M., Hammerl V., Blum P., Bayer P. and Griebler C. (2011) Shallow geothermal energy usage and its potential impacts on groundwater ecosystems. *Grundwasser* **16**, 77-91.
- Bucci A., Barbero D., Lasagna M., Forno M. G. and De Luca D. A. (2017) Shallow groundwater temperature in the Turin area (NW Italy): vertical distribution and anthropogenic effects. *Environmental Earth Sciences* **76**, 221.
- Buday T., Buday-Bódi E., Csákberényi-Nagy G. and Kovács T. Subsurface urban heat island investigation in Debrecen, Hungary based on archive and recently measured data. *European Geothermal Congress 2019*.
- Burns E. R., Ingebritsen S. E., Manga M. and Williams C. F. (2016) Evaluating geothermal and hydrogeologic controls on regional groundwater temperature distribution. *Water Resources Research* **52**, 1328-1344.
- Burns E. R., Zhu Y., Zhan H., Manga M., Williams C. F., Ingebritsen S. E. and Dunham J. B. (2017) Thermal effect of climate change on groundwater-fed ecosystems. *Water Resources Research* **53**, 3341-3351.
- Cantat O. (2004) L'îlot de chaleur urbain parisien selon les types de temps. *Norois. Environnement, aménagement, société*, 75-102.
- CDC (2021) Climate Data Center (CDC). opendata.dwd.de.
- Cermak V., Bodri L., Safanda J., Kresl M. and Ddcecek P. (2014) Ground-air temperature tracking and multi-year cycles in the subsurface temperature time series at geothermal climate-change observatory. *Studia Geophysica et Geodaetica* **58**, 403.

-
- Cermak V., Bodri L., Kresl M., Dedecek P. and Safanda J. (2017) Eleven years of ground–air temperature tracking over different land cover types. *International Journal of Climatology* **37**, 1084-1099.
- Changnon S. A. (1999) A rare long record of deep soil temperatures defines temporal temperature changes and an urban heat island. *Climatic Change* **42**, 531-538.
- Chaussé C., Leroyer C., Girardclos O., Allenet G., Pion P. and Raymond P. (2008) Holocene history of the River Seine, Paris, France: bio-chronostratigraphic and geomorphological evidence from the Quai-Branly. *The Holocene* **18**, 967-980.
- Colombani N., Giambastiani B. M. S. and Mastrociccio M. (2016) Use of shallow groundwater temperature profiles to infer climate and land use change: interpretation and measurement challenges. *Hydrological Processes* **30**, 2512-2524.
- Coluccio K. and Morgan L. K. (2019) A review of methods for measuring groundwater–surface water exchange in braided rivers. *Hydrology and Earth System Sciences* **23**, 4397-4417.
- Constantz J. (2008) Heat as a tracer to determine streambed water exchanges. *Water Resources Research* **44**.
- Couderc E. (2017) Geothermal energy: Underground urban scene. *Nature Energy* **2**, 16212.
- DABO (2020) Borehole Database (Bohrungsdatenbank DABO) maintained by the Geological Survey of North Rhine-Westphalia (GD NRW). www.bohrungen.nrw.de.
- Davies J. H. (2013) Global map of solid Earth surface heat flow. *Geochemistry, Geophysics, Geosystems* **14**, 4608-4622.
- Deroubaix A., Labuhn I., Camredon M., Gaubert B., Monerie P.-A., Popp M., Ramarohetra J., Ruprich-Robert Y., Silvers L. G. and Siour G. (2021) Large uncertainties in trends of energy demand for heating and cooling under climate change. *Nature communications* **12**, 5197.
- Dettwiller J. (1970) Deep soil temperature trends and urban effects at Paris. *Journal of Applied Meteorology* **9**, 178-180.
- Diffre P., Marquet G. and Richard M. (1977) Étude de la température des nappes peu profondes a Paris et dans la banlieue nord. *BRGM report 77 SGN 320 BDP, Bureau de Recherches Géologiques et Minières*.
- Djebebe-Ndjiguim C.-L., Huneau F., Denis A., Foto E., Moloto-a-Kenguemba G., Celle-Jeanton H., Garel E., Jaunat J., Mabingui J. and Le Coustumer P. (2013) Characterization of the aquifers of the Bangui urban area, Central African Republic, as an alternative drinking water supply resource. *Hydrological sciences journal* **58**, 1760-1778.
- Dohr F. (1989) Die Grundwassertemperatur in dem oberflächennahen Grundwasserstockwerk des Stadtgebiet Münchens. PhD Ludwig-Maximilians-Universität München.
- Domenico P. A. and Schwartz F. W. (1998) Physical and chemical hydrogeology, John Wiley and Sons. *Inc., New York*.
- Earman S. and Dettinger M. (2011) Potential impacts of climate change on groundwater resources—a global review. *Journal of Water and Climate Change* **2**, 213-229.
- Ebert M. and Voigtländer C. (2019) Aktuelle Zahlen zur Energieversorgung in Bayern - Prognose für das Jahr 2017. *Bayerisches Staatsministerium für Wirtschaft, Landesentwicklung und Energie*.

- Eggleston J. and McCoy K. J. (2015) Assessing the magnitude and timing of anthropogenic warming of a shallow aquifer: example from Virginia Beach, USA. *Hydrogeology Journal* **23**, 105-120.
- Egidio E., Mancini S., De Luca D. A. and Lasagna M. (2022) The impact of climate change on groundwater temperature of the Piedmont Po plain (NW Italy). *Water* **14**, 2797.
- ELWAS (2013) Electronic water management network for water management authorities in North Rhine-Westphalia www.elwasweb.nrw.de.
- Epting J. and Huggenberger P. (2013) Unraveling the heat island effect observed in urban groundwater bodies—Definition of a potential natural state. *Journal of hydrology* **501**, 193-204.
- Epting J., Händel F. and Huggenberger P. (2013) Thermal management of an unconsolidated shallow urban groundwater body. *Hydrol. Earth Syst. Sci.* **17**, 1851-1869.
- Epting J., Müller M. H., Genske D. and Huggenberger P. (2018) Relating groundwater heat-potential to city-scale heat-demand: a theoretical consideration for urban groundwater resource management. *Applied energy* **228**, 1499-1505.
- Epting J., García-Gil A., Huggenberger P., Vázquez-Suñe E. and Mueller M. H. (2017a) Development of concepts for the management of thermal resources in urban areas—Assessment of transferability from the Basel (Switzerland) and Zaragoza (Spain) case studies. *Journal of hydrology* **548**, 697-715.
- Epting J., Scheidler S., Affolter A., Borer P., Mueller M. H., Egli L., García-Gil A. and Huggenberger P. (2017b) The thermal impact of subsurface building structures on urban groundwater resources—A paradigmatic example. *Science of The Total Environment* **596**, 87-96.
- Escourrou G. (1990) La spécificité du climat de l'agglomération parisienne/The unique character of the Paris urban area's climate. *Géocarrefour* **65**, 85-89.
- ESRI R. (2011) ArcGIS desktop: release 10. *Environmental Systems Research Institute, CA*.
- EUROSTAT (2021) Energy statistics - cooling and heating degree days. ec.europa.eu/eurostat.
- Farr G., Patton A., Boon D., James D., Williams B. and Schofield D. (2017) Mapping shallow urban groundwater temperatures, a case study from Cardiff, UK. *Quarterly Journal of Engineering Geology and Hydrogeology* **50**, 187-198.
- Ferguson G. and Woodbury A. D. (2004) Subsurface heat flow in an urban environment. *Journal of Geophysical Research: Solid Earth* **109**.
- Ferguson G. and Woodbury A. D. (2007) Urban heat island in the subsurface. *Geophysical research letters* **34**.
- Figura S., Livingstone D. M., Hoehn E. and Kipfer R. (2011) Regime shift in groundwater temperature triggered by the Arctic Oscillation. *Geophysical Research Letters* **38**.
- Ford M. and Tellam J. (1994) Source, type and extent of inorganic contamination within the Birmingham urban aquifer system, UK. *Journal of Hydrology* **156**, 101-135.
- Forster P., Storelvmo T., Armour K., Collins W., Dufresne J.-L., Frame D., Lunt D., Mauritsen T., Palmer M. and Watanabe M. (2021) The Earth's energy budget, climate feedbacks, and climate sensitivity.
- Gallo K., Hale R., Tarpley D. and Yu Y. (2011) Evaluation of the relationship between air and land surface temperature under clear-and cloudy-sky conditions. *Journal of applied meteorology and climatology* **50**, 767-775.

-
- García-Gil A., Vázquez-Suñe E., Schneider E. G., Sánchez-Navarro J. Á. and Mateo-Lázaro J. (2014) The thermal consequences of river-level variations in an urban groundwater body highly affected by groundwater heat pumps. *Science of the total Environment* **485**, 575-587.
- García-Gil A., Epting J., Garrido E., Vázquez-Suñe E., Lázaro J. M., Navarro J. Á. S., Huggenberger P. and Calvo M. Á. M. (2016) A city scale study on the effects of intensive groundwater heat pump systems on heavy metal contents in groundwater. *Science of the Total Environment* **572**, 1047-1058.
- González-Rouco J. F., Beltrami H., Zorita E. and Stevens M. (2009) Borehole climatology: a discussion based on contributions from climate modeling. *Climate of the Past* **5**, 97-127.
- Green T. R., Taniguchi M., Kooi H., Gurdak J. J., Allen D. M., Hiscock K. M., Treidel H. and Aureli A. (2011) Beneath the surface of global change: Impacts of climate change on groundwater. *Journal of Hydrology* **405**, 532-560.
- Griebler C., Avramov M. and Hose G. (2019) Groundwater ecosystems and their services: current status and potential risks. In *Atlas of Ecosystem Services*. Springer. pp. 197-203.
- Griebler C., Brielmann H., Haberer C. M., Kaschuba S., Kellermann C., Stumpp C., Hegler F., Kuntz D., Walker-Hertkorn S. and Lueders T. (2016) Potential impacts of geothermal energy use and storage of heat on groundwater quality, biodiversity, and ecosystem processes. *Environmental Earth Sciences* **75**, 1391.
- Gunawardhana L. N. and Kazama S. (2011) Climate change impacts on groundwater temperature change in the Sendai plain, Japan. *Hydrological Processes* **25**, 2665-2678.
- Gunawardhana L. N., Kazama S. and Kawagoe S. (2011) Impact of urbanization and climate change on aquifer thermal regimes. *Water resources management* **25**, 3247-3276.
- Hafner J. and Kidder S. Q. (1999) Urban heat island modeling in conjunction with satellite-derived surface/soil parameters. *Journal of applied meteorology* **38**, 448-465.
- Hall D. and Riggs G. (2016) MODIS/Terra Snow Cover Daily L3 Global 0.05 Deg CMG, Version 6, Boulder, Colorado USA, NASA National Snow and Ice Data Center Distributed Active Archive Center.
- Headon J., Banks D., Waters A. and Robinson V. (2009) Regional distribution of ground temperature in the Chalk aquifer of London, UK. *Quarterly Journal of Engineering Geology and Hydrogeology* **42**, 313-323.
- Heitfeld K. H., Krapp L. and Weiler A. (1981) Temperaturanomalien im Stadtgebiet von Duisburg und deren Auswirkungen auf Baumaßnahmen der Stadtbahn. *Zeitschrift der Deutschen Gesellschaft für Geowissenschaften – Journal of Applied and Regional Geology (ZDGG)* **32**, 779-797.
- Hemmerle H. and Bayer P. (2020) Climate Change Yields Groundwater Warming in Bavaria, Germany. *Frontiers in Earth Science* **8**.
- Hemmerle H., May J.-H. and Preusser F. (2016) Übersicht über die pleistozänen Vergletscherungen des Schwarzwaldes. *Ber. Naturf. Ges. Freiburg i. Br.* **106**, 31-67.
- Hemmerle H., Ferguson G., Blum P. and Bayer P. Development of the geothermal potential of an urban aquifer over half a century. *European Geothermal Congress 2022*.

- Hemmerle H., Ferguson G., Blum P. and Bayer P. (2022b) The evolution of the geothermal potential of a subsurface urban heat island. *Environmental Research Letters* **17**, 084018.
- Hemmerle H., Dressel I., Blum P., Menberg K., Benz S. A. and Bayer P. Benefits from Subsurface Urban Heat Islands to Shallow Geothermal Applications – an Example from the City of Cologne, Germany. *World Geothermal Congress 2020+1*.
- Hemmerle H., Hale S., Dressel I., Benz S. A., Attard G., Blum P. and Bayer P. (2019) Estimation of Groundwater Temperatures in Paris, France. *Geofluids* **2019**.
- Henry A., Prasher R. and Majumdar A. (2020) Five thermal energy grand challenges for decarbonization. *Nature Energy* **5**, 635-637.
- Hilden H. (1988) Geology of the Lower Rhine (Geologie am Niederrhein). *Krefeld (Geol. L.-Amt Nordrhein-Westfalen)*, 142.
- Höllein K., Sutter K. and Wirth H. (1983) Grundwassertemperaturen München. *Bayern / Landesamt für Wasserwirtschaft: Informationsberichte des Bayerischen Landesamtes für Wasserwirtschaft* **6**, 26.
- Howard L. (1818) *The climate of London: deduced from meteorological observations, made at different places in the neighbourhood of the metropolis*. W. Phillips, George Yard, Lombard Street, sold also by J. and A. Arch ...
- Hsu A., Sheriff G., Chakraborty T. and Manya D. (2021) Disproportionate exposure to urban heat island intensity across major US cities. *Nature Communications* **12**, 2721.
- Huang F., Zhan W., Wang Z.-H., Voogt J., Hu L., Quan J., Liu C., Zhang N. and Lai J. (2020) Satellite identification of atmospheric-surface-subsurface urban heat islands under clear sky. *Remote Sensing of Environment* **250**, 112039.
- Huang S., Taniguchi M., Yamano M. and Wang C. H. (2009) Detecting urbanization effects on surface and subsurface thermal environment -- A case study of Osaka. *Science of The Total Environment* **407**, 3142-3152.
- Ichinose T. and Liu K. (2018) Modeling the relationship between the urban development and subsurface warming in seven Asian megacities. *Sustainable Cities and Society* **38**, 560-570.
- IEA (2018) The Future of Cooling IEA, Paris.
- InfoTerre (2018) Dossier du sous-sol, <http://infoterre.brgm.fr/>, accessed on 05.09.2018.
- ISO U. (2007) Thermal performance of buildings—Heat transfer via the ground—Calculation methods.
- IT.NRW (2021) Statistics and IT Services: Population in North Rhine-Westphalia (Statistik und IT-Dienstleistungen: Bevölkerung in Nordrhein-Westfalen). www.it.nrw.
- Jago-on K. A. B., Kaneko S., Fujikura R., Fujiwara A., Imai T., Matsumoto T., Zhang J., Tanikawa H., Tanaka K., Lee B. and Taniguchi M. (2009) Urbanization and subsurface environmental issues: An attempt at DPSIR model application in Asian cities. *Science of The Total Environment* **407**, 3089-3104.
- Jarsjö J., Andersson-Sköld Y., Fröberg M., Pietroń J., Borgström R., Löf Å. and Kleja D. B. (2020) Projecting impacts of climate change on metal mobilization at contaminated sites: Controls by the groundwater level. *Science of The Total Environment* **712**, 135560.
- Jiang J. and Tian G. (2010) Analysis of the impact of land use/land cover change on land surface temperature with remote sensing. *Procedia environmental sciences* **2**, 571-575.

-
- Jyväsjärvi J., Marttila H., Rossi P. M., Ala-Aho P., Olofsson B., Nisell J., Backman B., Ilmonen J., Virtanen R. and Paasivirta L. (2015) Climate-induced warming imposes a threat to north European spring ecosystems. *Global Change Biology* **21**, 4561-4569.
- Kaandorp V. P., Doornenbal P. J., Kooi H., Broers H. P. and de Louw P. G. (2019) Temperature buffering by groundwater in ecologically valuable lowland streams under current and future climate conditions. *Journal of Hydrology* **3**, 100031.
- Kammen D. M. and Sunter D. A. (2016) City-integrated renewable energy for urban sustainability. *Science* **352**, 922-928.
- Kappelmeyer O. and Haenel R. (1974) Geothermics with special reference to application. *Berlin gebrueder borntraeger geoexploration monographs series* **4**, 31.
- Kazemi G. A. (2011) Impacts of urbanization on the groundwater resources in Shahrood, Northeastern Iran: Comparison with other Iranian and Asian cities. *Physics and Chemistry of the Earth, Parts A/B/C* **36**, 150-159.
- Klene A., Hinkel K. and Nelson F. The Barrow Urban Heat Island Study: soil temperatures and active-layer thickness. *Proceedings of the Eighth International Conference on Permafrost*. Lisse: AA Balkema.
- Klostermann J. (1992) The Quaternary of the Lower Rhenish Bight (Das Quartär der Niederrheinischen Bucht). *Geologisches Landesamt Nordrhein-Westfalen, Krefeld*, 200.
- Kløve B., Ala-Aho P., Bertrand G., Gurdak J. J., Kupfersberger H., Kværner J., Muotka T., Mykrä H., Preda E. and Rossi P. (2014) Climate change impacts on groundwater and dependent ecosystems. *Journal of Hydrology* **518**, 250-266.
- Kobus H. and Söll T. (1987) Der Wärmehaushalt des Grundwassers und seine Nutzung. *Wasserkalender* **21**, 63-91.
- Kollet S. J., Cvijanovic I., Schüttemeyer D., Maxwell R. M., Moene A. F. and Bayer P. (2009) The influence of rain sensible heat and subsurface energy transport on the energy balance at the land surface. *Vadose zone journal* **8**, 846-857.
- Kounkou-Arnaud R., Desplat J., Lemonsu A. and Salagnac J.-L. (2014) Epicea: étude des impacts du changement climatique à Paris. *Rubrique: Changement climatique*.
- Kurylyk B. L. and Irvine D. J. (2019) Heat: An overlooked tool in the practicing hydrogeologist's toolbox. *Groundwater* **57**, 517-524.
- Kurylyk B. L., Bourque C. and MacQuarrie K. T. (2013) Potential surface temperature and shallow groundwater temperature response to climate change: an example from a small forested catchment in east-central New Brunswick (Canada). *Hydrology and Earth System Sciences*.
- Kurylyk B. L., MacQuarrie K. T. and McKenzie J. M. (2014) Climate change impacts on groundwater and soil temperatures in cold and temperate regions: Implications, mathematical theory, and emerging simulation tools. *Earth-Science Reviews* **138**, 313-334.
- Kurylyk B. L., Irvine D. J. and Bense V. F. (2019) Theory, tools, and multidisciplinary applications for tracing groundwater fluxes from temperature profiles. *Wiley Interdisciplinary Reviews: Water* **6**, e1329.
- Lee J.-Y. (2006) Characteristics of ground and groundwater temperatures in a metropolitan city, Korea: considerations for geothermal heat pumps. *Geosciences Journal* **10**, 165-175.

- Lee J.-Y. and Han J. (2013) Evaluation of groundwater monitoring data in four megacities of Korea: Implication for sustainable use. *Natural resources research* **22**, 103-121.
- Leonhardt G., Seifert L., Gerecke R., Müller J., Hotzy R. and Lotz A. Springs in the Bavarian National Parks as indicators for climate change. *6th Symposium for Research in Protected Areas*.
- Li S., Dong L., Chen J., Li R., Yang Z. and Liang Z. (2019) Vertical groundwater flux estimation from borehole temperature profiles by a numerical model, RFLUX. *Hydrological Processes* **33**, 1542-1552.
- Limberger J., Boxem T., Pluymaekers M., Bruhn D., Manzella A., Calcagno P., Beekman F., Cloetingh S. and van Wees J.-D. (2018) Geothermal energy in deep aquifers: A global assessment of the resource base for direct heat utilization. *Renewable and Sustainable Energy Reviews* **82**, 961-975.
- Lo Y. T. E., Mitchell D. M., Gasparrini A., Vicedo-Cabrera A. M., Ebi K. L., Frumhoff P. C., Millar R. J., Roberts W., Sera F., Sparrow S., Uhe P. and Williams G. (2019) Increasing mitigation ambition to meet the Paris Agreement's temperature goal avoids substantial heat-related mortality in U.S. cities. *Science Advances* **5**, eaau4373.
- Lofi W. (1977) Grundwassererwärmung im Stadtgebiet von Karlsruhe und ihre Ursachen. Diploma Universität Karlsruhe.
- Lokoshchenko M. and Korneva I. (2015) Underground urban heat island below Moscow city. *Urban Climate* **13**, 1-13.
- Lucazeau F. (2019) Analysis and Mapping of an Updated Terrestrial Heat Flow Data Set. *Geochemistry, Geophysics, Geosystems* **20**, 4001-4024.
- Makasis N., Kreitmair M., Bidarmaghz A., Farr G., Scheidegger J. and Choudhary R. (2021) Impact of simplifications on numerical modelling of the shallow subsurface at city-scale and implications for shallow geothermal potential. *Science of The Total Environment*, 148236.
- Mammola S., Piano E., Cardoso P., Vernon P., Domínguez-Villar D., Culver D. C., Pipan T. and Isaia M. (2019) Climate change going deep: the effects of global climatic alterations on cave ecosystems. *The Anthropocene Review* **6**, 98-116.
- Mann M. E. and Schmidt G. A. (2003) Ground vs. surface air temperature trends: Implications for borehole surface temperature reconstructions. *Geophysical Research Letters* **30**.
- Marschalko M., Krčmář D., Yilmaz I., Fláková R. and Ženišová Z. (2018) Heat contamination in groundwater sourced from heat pump for heating in Bratislava (Slovakia)'s historic centre. *Environmental earth sciences* **77**, 1-12.
- Maxwell R. M. and Kollet S. J. (2008) Interdependence of groundwater dynamics and land-energy feedbacks under climate change. *Nature Geoscience* **1**, 665-669.
- Melo-Aguilar C., González-Rouco J. F., García-Bustamante E., Navarro-Montesinos J. and Steinert N. (2018) Influence of radiative forcing factors on ground-air temperature coupling during the last millennium: implications for borehole climatology. *Climate of the Past* **14**, 1583-1606.
- Menberg K., Blum P., Schaffitel A. and Bayer P. (2013a) Long-term evolution of anthropogenic heat fluxes into a subsurface urban heat island. *Environmental science & technology* **47**, 9747-9755.
- Menberg K., Blum P., Kurylyk B. L. and Bayer P. (2014) Observed groundwater temperature response to recent climate change. *Hydrology and Earth System Sciences* **18**, 4453-4466.

-
- Menberg K., Bayer P., Zosseder K., Rumohr S. and Blum P. (2013b) Subsurface urban heat islands in German cities. *Science of the total environment* **442**, 123-133.
- Meng B., Vienken T., Kolditz O. and Shao H. (2019) Evaluating the thermal impacts and sustainability of intensive shallow geothermal utilization on a neighborhood scale: Lessons learned from a case study. *Energy Conversion and Management* **199**, 111913.
- Merheb F. (1984) Modele de Gestion des Echanges Hydrothermiques dans les Nappes Souterraines: Application a la Region de Strasbourg.
- MODIS (2018) LP DAAC data pool. https://lpdaac.usgs.gov/data_access/data_pool.
- Molina-Giraldo N., Bayer P., Blum P. and Cirpka O. A. (2011) Propagation of seasonal temperature signals into an aquifer upon bank infiltration. *Groundwater* **49**, 491-502.
- Molnar P. (2022) Differences between soil and air temperatures: Implications for geological reconstructions of past climate. *Geosphere* **18**, 800-824.
- Morris B. L., Darling W. G., Gooddy D. C., Litvak R. G., Neumann I., Nemaltseva E. J. and Poddubnaia I. (2006) Assessing the extent of induced leakage to an urban aquifer using environmental tracers: an example from Bishkek, capital of Kyrgyzstan, Central Asia. *Hydrogeology Journal* **14**, 225-243.
- Mount H. R. and Hernandez L. (2002) Soil Temperature and Anthropogenic Soils Soil Temperature Study for New York City. In *Anthropogenic soils. ICOMANTH Report No. 1. CD-ROM*. (eds. J. M. Galbraith, H. R. Mount and J. M. Scheyer). p. 9.
- Müller N., Kuttler W. and Barlag A.-B. (2014) Analysis of the subsurface urban heat island in Oberhausen, Germany. *Climate research* **58**, 247-256.
- Noethen M., Hemmerle H. and Bayer P. (2022) Sources, intensities, and implications of subsurface warming in times of climate change. *Critical Reviews in Environmental Science and Technology* 10.1080/10643389.2022.2083899, 1-23.
- Oke T. R. (1982) The energetic basis of the urban heat island. *Quarterly Journal of the Royal Meteorological Society* **108**, 1-24.
- Öngen A. S., ÖNGEN A. S. and ERGÜLER Z. A. (2021) The effect of urban heat island on groundwater located in shallow aquifers of Kutahya city center and shallow geothermal energy potential of the region. *Bull. Miner. Res. Explor.* **165**, 217-234.
- OpenGeoDataNRW (2021) Digital Elevation Model - grid width 1m. State of North Rhine-Westphalia, Cologne District Government, Geobasis NRW. www.opengeodata.nrw.de.
- OpenStreetMap (2018) www.openstreetmap.org/copyright, accessed on 03.04.2018.
- Pal S., Xueref-Remy I., Ammoura L., Chazette P., Gibert F., Royer P., Dieudonné E., Dupont J.-C., Haeffelin M. and Lac C. (2012) Spatio-temporal variability of the atmospheric boundary layer depth over the Paris agglomeration: An assessment of the impact of the urban heat island intensity. *Atmospheric environment* **63**, 261-275.
- Parsons M. L. (1970) Groundwater thermal regime in a glacial complex. *Water Resources Research* **6**, 1701-1720.
- Peppler A. (1929) Das Auto als Hilfsmittel der meteorologischen Forschung. *Zeitschrift für angewandte Meteorologie* **46**, 305-308.
- Perrier F., Le Mouel J. L., Poirier J. P. and Shnirman M. G. (2005) Long-term climate change and surface versus underground temperature measurements in Paris. *International Journal of Climatology* **25**, 1619-1631.

- Pollack H. N. and Chapman D. S. (1993) Underground records of changing climate. *Scientific American* **268**, 44-50.
- Pollack H. N., Hurter S. J. and Johnson J. R. (1993) Heat flow from the Earth's interior: analysis of the global data set. *Reviews of Geophysics* **31**, 267-280.
- Previati A. and Crosta G. B. (2021) Characterization of the subsurface urban heat island and its sources in the Milan city area, Italy. *Hydrogeology Journal*, 1-14.
- Rau G. C., Andersen M. S., McCallum A. M. and Acworth R. I. (2010) Analytical methods that use natural heat as a tracer to quantify surface water–groundwater exchange, evaluated using field temperature records. *Hydrogeology journal* **18**, 1093-1110.
- Reiter M. (2007) Variability of recent ground surface temperature changes in the Albuquerque basin, central New Mexico. *Journal of Geophysical Research: Atmospheres (1984–2012)* **112**.
- Riedel T. (2019) Temperature-associated changes in groundwater quality. *Journal of Hydrology* **572**, 206-212.
- Ritchie H. and Roser M. (2018) Urbanization. *Our world in data*.
- Rivera J. A., Blum P. and Bayer P. (2017) Increased ground temperatures in urban areas: Estimation of the technical geothermal potential. *Renewable energy* **103**, 388-400.
- Rotta Loria A. F., Thota A., Thomas A. M., Friedle N., Lautenberg J. M. and Song E. C. (2022) Subsurface heat island across the Chicago Loop district: Analysis of localized drivers. *Urban Climate* **44**, 101211.
- Saar M. O. (2011) Geothermal heat as a tracer of large-scale groundwater flow and as a means to determine permeability fields. *Hydrogeology Journal* **19**, 31-52.
- Salem Z., Sakura Y. and Aslam M. M. (2004) The use of temperature, stable isotopes and water quality to determine the pattern and spatial extent of groundwater flow: Nagaoka area, Japan. *Hydrogeology Journal* **12**, 563-575.
- Sarkar A. and De Ridder K. (2011) The urban heat island intensity of Paris: a case study based on a simple urban surface parametrization. *Boundary-layer meteorology* **138**, 511-520.
- Savva Y., Szlavecz K., Pouyat R. V., Groffman P. M. and Heisler G. (2010) Effects of land use and vegetation cover on soil temperature in an urban ecosystem. *Soil Science Society of America Journal* **74**, 469-480.
- Schmidt W. (1927) Die Verteilung der Minimumtemperaturen in derl Frostnacht des 12. 5.19. 27 im Gemeindegebiet von Wien. *Fortschritte der Landwirtschaft*.
- Schneider E. A. G., García-Gil A., Vázquez-Suñe E. and Sánchez-Navarro J. Á. (2016) Geochemical impacts of groundwater heat pump systems in an urban alluvial aquifer with evaporitic bedrock. *Science of the Total Environment* **544**, 354-368.
- Schweighofer J. A., Wehrl M., Baumgärtel S. and Rohn J. (2021a) Calculating Energy and Its Spatial Distribution for a Subsurface Urban Heat Island Using a GIS-Approach. *Geosciences* **11**, 24.
- Schweighofer J. A., Wehrl M., Baumgärtel S. and Rohn J. (2021b) Detecting Groundwater Temperature Shifts of a Subsurface Urban Heat Island in SE Germany. *Water* **13**, 1417.
- Shi B., Tang C.-S., Gao L., Liu C. and Wang B.-J. (2012) Observation and analysis of the urban heat island effect on soil in Nanjing, China. *Environmental Earth Sciences* **67**, 215-229.
- Smerdon B. D. (2017) A synopsis of climate change effects on groundwater recharge. *Journal of Hydrology* **555**, 125-128.

-
- Sorey M. L. (1971) Measurement of vertical groundwater velocity from temperature profiles in wells. *Water Resources Research* **7**, 963-970.
- StadtKöln (2021) Cologne district information Population 2020 (Kölner Stadtteilinformationen Bevölkerung 2020). www.stadt-koeln.de.
- Stauffer F., Bayer P., Blum P., Giraldo N. M. and Kinzelbach W. (2013) *Thermal use of shallow groundwater*. CRC Press.
- Stemmler R., Hammer V., Blum P. and Menberg K. (2022) Potential of low-temperature aquifer thermal energy storage (LT-ATES) in Germany. *Geothermal Energy* **10**, 1-25.
- Stewart I. D. (2019) Why should urban heat island researchers study history? *Urban Climate* **30**, 100484.
- Stoll S., Hendricks Franssen H.-J., Butts M. and Kinzelbach W. K. (2011) Analysis of the impact of climate change on groundwater related hydrological fluxes: a multi-model approach including different downscaling methods. *Hydrology and Earth System Sciences* **15**, 21-38.
- Tang C.-S., Shi B., Gao L., Daniels J. L., Jiang H.-T. and Liu C. (2011) Urbanization effect on soil temperature in Nanjing, China. *Energy and Buildings* **43**, 3090-3098.
- Taniguchi M. (1993) Evaluation of vertical groundwater fluxes and thermal properties of aquifers based on transient temperature-depth profiles. *Water Resources Research* **29**, 2021-2026.
- Taniguchi M., Uemura T. and Sakura Y. (2005) Effects of urbanization and groundwater flow on subsurface temperature in three megacities in Japan. *Journal of Geophysics and Engineering* **2**, 320-325.
- Taniguchi M., Uemura T. and Jago-on K. (2007) Combined effects of urbanization and global warming on subsurface temperature in four Asian cities. *Vadose Zone Journal* **6**, 591-596.
- Taniguchi M., Shimada J., Fukuda Y., Yamano M., Onodera S.-i., Kaneko S. and Yoshikoshi A. (2009) Anthropogenic effects on the subsurface thermal and groundwater environments in Osaka, Japan and Bangkok, Thailand. *Science of the Total Environment* **407**, 3153-3164.
- Taniguchi M., Shimada J., Tanaka T., Kayane I., Sakura Y., Shimano Y., Dapaah-Siakwan S. and Kawashima S. (1999) Disturbances of temperature-depth profiles due to surface climate change and subsurface water flow: 1. An effect of linear increase in surface temperature caused by global warming and urbanization in the Tokyo Metropolitan Area, Japan. *Water Resources Research* **35**, 1507-1517.
- Taylor C. A. and Stefan H. G. (2009) Shallow groundwater temperature response to climate change and urbanization. *Journal of Hydrology* **375**, 601-612.
- Thierry P., Prunier-Leparmentier A.-M., Lembezat C., Vanoudheusden E. and Vernoux J.-F. (2009) 3D geological modelling at urban scale and mapping of ground movement susceptibility from gypsum dissolution: The Paris example (France). *Engineering Geology* **105**, 51-64.
- Tissen C., Benz S. A., Menberg K., Bayer P. and Blum P. (2019) Groundwater temperature anomalies in central Europe. *Environmental Research Letters* **14**, 104012.
- Tissen C., Menberg K., Benz S. A., Bayer P., Steiner C., Götzl G. and Blum P. (2021) Identifying key locations for shallow geothermal use in Vienna. *Renewable Energy* **167**, 1-19.

- Tran H., Uchiyama D., Ochi S. and Yasuoka Y. (2006) Assessment with satellite data of the urban heat island effects in Asian mega cities. *International Journal of Applied Earth Observation and Geoinformation* **8**, 34-48.
- Turkoglu N. (2010) Analysis of urban effects on soil temperature in Ankara. *Environmental Monitoring and Assessment* **169**, 439-450.
- United Nations D. o. E. and Social Affairs P. D. (2018) World urbanization prospects: The 2018 revision, online edition. Department of Economic and Social Affairs PD New York, NY.
- van Ruijven B. J., De Cian E. and Wing I. S. (2019) Amplification of future energy demand growth due to climate change. *Nature communications* **10**, 1-12.
- Vienken T., Kreck M. and Dietrich P. (2019) Monitoring the impact of intensive shallow geothermal energy use on groundwater temperatures in a residential neighborhood. *Geothermal Energy* **7**, 1-14.
- Visser P. W., Kooi H., Bense V. and Boerma E. (2020) Impacts of progressive urban expansion on subsurface temperatures in the city of Amsterdam (The Netherlands). *Hydrogeology Journal* **28**, 1755-1772.
- Vranjes A., Milenic D. and Dokmanovic P. (2015) Geothermal concept for energy efficient improvement of space heating and cooling in highly urbanized area. *Thermal Science* **19**, 857-864.
- Wang K. and Lewis T. J. (1992) Geothermal evidence from Canada for a cold period before recent climatic warming. *Science* **256**, 1003-1005.
- Watson S. M. and Westaway R. (2020) Borehole temperature log from the Glasgow Geothermal Energy Research Field Site: a record of past changes to ground surface temperature caused by urban development. *Scottish Journal of Geology* **56**, 134-152.
- Westaway R. and Younger P. L. (2016) Unravelling the relative contributions of climate change and ground disturbance to subsurface temperature perturbations: Case studies from Tyneside, UK. *Geothermics* **64**, 490-515.
- World Meteorological Organization (2017) WMO guidelines on the calculation of climate normals. World Meteorological Organization Geneva, Switzerland.
- Wunsch A., Liesch T. and Broda S. (2022) Deep learning shows declining groundwater levels in Germany until 2100 due to climate change. *Nature communications* **13**, 1221.
- Yalcin T. and Yetemen O. (2009) Local warming of groundwaters caused by the urban heat island effect in Istanbul, Turkey. *Hydrogeology Journal* **17**, 1247-1255.
- Yalew S. G., van Vliet M. T., Gernaat D. E., Ludwig F., Miara A., Park C., Byers E., De Cian E., Piontek F. and Iyer G. (2020) Impacts of climate change on energy systems in global and regional scenarios. *Nature Energy* **5**, 794-802.
- Yamano M., Goto S., Miyakoshi A., Hamamoto H., Lubis R. F., Monyrath V. and Taniguchi M. (2009) Reconstruction of the thermal environment evolution in urban areas from underground temperature distribution. *Science of the Total Environment* **407**, 3120-3128.
- Yusuf K. (2007) Evaluation of groundwater quality characteristics in Lagos-City. *Journal of Applied Sciences* **7**, 1780-1784.
- Zhan W., Ju W., Hai S., Ferguson G., Quan J., Tang C., Guo Z. and Kong F. (2014) Satellite-derived subsurface urban heat island. *Environmental Science & Technology* **48**, 12134-12140.
- Zhang Z., Li Y., Barlage M., Chen F., Miguez-Macho G., Ireson A. and Li Z. (2020) Modeling groundwater responses to climate change in the Prairie Pothole Region. *Hydrol. Earth Syst. Sci.* **24**, 655-672.

-
- Zhu K., Bayer P., Grathwohl P. and Blum P. (2015) Groundwater temperature evolution in the subsurface urban heat island of Cologne, Germany. *Hydrological Processes* **29**, 965-978.
- Zhu K., Blum P., Ferguson G., Balke K.-D. and Bayer P. (2010) The geothermal potential of urban heat islands. *Environmental Research Letters* **5**, 044002.

Curriculum Vitae

Work Experience

since 2019	Research Associate	<i>Martin-Luther-Universität Halle-Wittenberg</i>
2018 – 2019	Research Associate	<i>Technische Hochschule Ingolstadt</i>

Education

2015 – 2017	M.Sc. Geowissenschaften	<i>FAU Erlangen-Nürnberg</i>
2012 – 2015	B.Sc. Geowissenschaften	<i>Universität Freiburg</i>

List of peer-reviewed publications

- Noethen, M., Hemmerle, H., Menberg, K., Epting, J., Benz, S. A., Blum, P., & Bayer, P. (2023). Thermal impact of underground car parks on urban groundwater. *Science of The Total Environment*, 166572.
- Noethen, M., Hemmerle, H., Bayer, P. (2022). Sources, intensities, and implications of subsurface warming in times of climate change. *Critical Reviews in Environmental Science and Technology*, 53(5), 700-722.
- Hemmerle H., Ferguson G., Blum P. and Bayer P. (2022) The evolution of the geothermal potential of a subsurface urban heat island. *Environmental Research Letters* **17**, 084018.
- Blum P., Menberg K., Koch F., Benz S. A., Tissen C., Hemmerle H. and Bayer P. (2021) Is thermal use of groundwater a pollution? *Journal of Contaminant Hydrology*, 103791.
- Hemmerle H., van Geldern R., Juhlke T., Huneau F., Garel E., Santoni S. and Barth J. (2021) Altitude isotope effects in Mediterranean high-relief terrains: a correction method to utilize stream water data. *Hydrological Sciences Journal* **66**, 1409-1418.
- Hemmerle H. and Bayer P. (2020) Climate Change Yields Groundwater Warming in Bavaria, Germany. *Frontiers in Earth Science* **8**.
- Hemmerle H., Hale S., Dressel I., Benz S. A., Attard G., Blum P. and Bayer P. (2019) Estimation of Groundwater Temperatures in Paris, France. *Geofluids* **2019**.
- Juhlke T., Van Geldern R., Huneau F., Garel E., Santoni S., Hemmerle H. and Barth J. (2019) Riverine carbon dioxide evasion along a high-relief watercourse derived from seasonal dynamics of the water-atmosphere gas exchange. *Science of the Total Environment* **657**, 1311-1322.

List of non-peer-reviewed publications and conference papers

- Hemmerle H., Ferguson G., Blum P. and Bayer P. (2022) Development of the geothermal potential of an urban aquifer over half a century. *European Geothermal Congress 2022*, Berlin, Germany.
- Hemmerle H., Dressel I., Blum P., Menberg K., Benz S. A. and Bayer P. (2021) Benefits from Subsurface Urban Heat Islands to Shallow Geothermal Applications – an Example from the City of Cologne, Germany. *World Geothermal Congress 2020+1*. Reykjavik, Iceland.
- Hemmerle H., May J.-H. and Preusser F. (2016) Übersicht über die pleistozänen Vergletscherungen des Schwarzwaldes. *Ber. Naturf. Ges. Freiburg i. Br.* **106**, 31-67.

Declaration

Ich erkläre an Eides statt, dass ich die Arbeit selbstständig und ohne fremde Hilfe verfasst, keine anderen als die von mir angegebenen Quellen und Hilfsmittel benutzt und die den benutzten Werken wörtlich oder inhaltlich entnommenen Stellen als solche kenntlich gemacht habe.

I declare under penalty of perjury that this thesis is my own work entirely and has been written without any help from other people. I used only the sources mentioned and included all the citations correctly both in word or content.

Datum / Date

Hannes Hemmerle